TURN-TO-TURN FAULT PROTECTION FOR AIR CORE SHUNT REACTORS

A Thesis

Presented in Partial Fulfillment of the Requirements for the

Degree of Master of Science

with a

Major in Electrical Engineering

in the

College of Graduate Studies

University of Idaho

by

Asad Iqbal Mohammad

Major Professor: Brian K. Johnson, Ph.D., P.E
Committee Members: James F. Frenzel, Ph.D., P.E.;
Yacine Chakhchoukh, Ph.D.
Department Administrator: Mohsen Guizani, Ph.D.

August 2017

AUTHORIZATION TO SUBMIT THESIS

This thesis of Asad Iqbal Mohammad, submitted for the degree of Master of Science with a major in Electrical Engineering and titled "**Turn-to-turn fault protection for Air Core Shunt Reactors**," has been reviewed in final form. Permission, as indicated by the signatures and dates given below, is now granted to submit final copies to the College of Graduate Studies for approval.

Major Professor: _____ Date: _____
Brian K. Johnson, Ph.D., P.E

Committee Members: _____ Date: _____
James Frenzel, Ph.D., P.E

_____ Date: _____
Yacine Chakhchoukh, Ph.D.

Department Administrator:
_____ Date: _____
Mohsen Guizani, Ph.D.

ABSTRACT

The demand for installation of air core reactors to provide shunt compensation to nullify the capacitance effect created by high voltage long transmission lines or cables has increased in recent years. Air-core reactors consist of bulk coils of copper or aluminum with many turns that can be prone to inter-turn faults on the windings as the insulation ages. These faults are hard to detect for cases with a small number of windings shorted due to small current changes visible at the terminal. Current protection elements have trouble reliably detecting these faults. Inter-turn faults on a winding can lead to high localized currents which can further damage surrounding insulation due to overheating and cascade to more severe faults. This research seeks to develop a sensitive fault detection scheme to allow isolation of the circuit. Two solutions are proposed based on the design of a reactor installation at a local utility and partially validated through computer simulation and a lab scale hardware demonstration. The proposed solution can be applied in the field to protect dry type air core reactors for turn-to-turn faults.

ACKNOWLEDGEMENTS

I would like to thank my major professor Dr. Brian Johnson for all the knowledge he has imparted, also to mention the time and support he has given to me making this thesis become a reality. I would also like to thank the committee members Dr. James Frenzel and Dr. Yacine Chakhchoukh for taking time off their busy schedule to review this thesis and provide their valuable suggestions.

I would like to thank Kevin Damron of Avista in supporting this research with field visit and field inputs, Dr. Normann Fischer of SEL for sponsoring the project and the senior design team of ECE department – Tanner Mort, Andrew Hoth, Justin Jeter and Lyn England for supporting me by building the hardware for this project.

I would like to thank the engineers at SEL who assisted me with valuable suggestions on tackling the problem and most importantly my graduate students who have stood by me with assistance and their knowledge.

DEDICATION

To my family and all those who matter to me

TABLE OF CONTENTS

LIST OF FIGURES

LIST OF TABLES

ACRONYMS

AWG – American Wire Guage

EHV – Extra High Voltage

HV- High Voltage

IEC – International Electrotechincal Commission

IEEE – Institute of Electrical and Electronic Engineers

SEL – Schweitzer Engineering Laboratories

TRV- Transient Recovery Voltage

CT- Current Transformer

PT- Potential transformer

IED- Intelligent Electronic Device

SLG – Single Line to Ground

REF – Restricted Earth Fault

NOMENCLATURE

V_R – Receiving end voltage

V_S – Sending end voltage

X_L – Inductive reactance

X_C – Capacitive reactance

I_L – Line Current

SIL – Surge Impedance Loading

V_{rated} – Rated Voltage

Z_C – Characcteristic impedance

L – Self inductance of reactor coil

N – Number of turns of reactor coil

μ_0 – Permeability of free space or air

μ_r – relative permeability of free space or air

A – Area of coil

l – Length of coil

Ln – Self inductance of nth layer

m – Number of layers in a multi-layer coil

n – Select layer of coil

inter turn – turn-to-turn

ANSI protection element numbers

49 – Thermal

50 – Instantaneous Overcurrent

51 – Inverse Time Overcurrent

63 – Pressure switch

67 – Directional Overcurrent

71 – Liquid Level Switch

80 – Flow Switch

87 – Current Differential

1. INTRODUCTION

1.1. Background

The introduction of AC transmission of power facilitated flexible transmission of energy following the DC era. It allowed power distribution at reduced losses by increasing the transmission voltages using transformers, allowing load centers to be situated farther from generating stations. High voltage transmission lines have a capacitance effect between the conductors or between the conductors to ground. For steady-state analysis, this capacitance can be represented for modeling through the short line model, the medium line model and the long line model where the impact of capacitance on circuit behavior is subject to the length of the line or its construction. If the transmission of power is done through underground or underwater cables the effect of the capacitance between the conductors or the conductors to the insulation can be as high as 20 times as that observed on overhead transmission line of the same voltage and length. Some other factors which effect line capacitance are conductor size, distances between conductors and proximity with nearby conductors.

One consequence of this capacitance is the Ferranti effect [1]. This describes the impact of capacitance where the voltage at the receiving end raises in comparison to the sending end voltage. This can be formulized using a simple network equation.

$$Vr = Vs - I * \left(j * X_L - \frac{j}{X_C}\right) \tag{1.1}$$

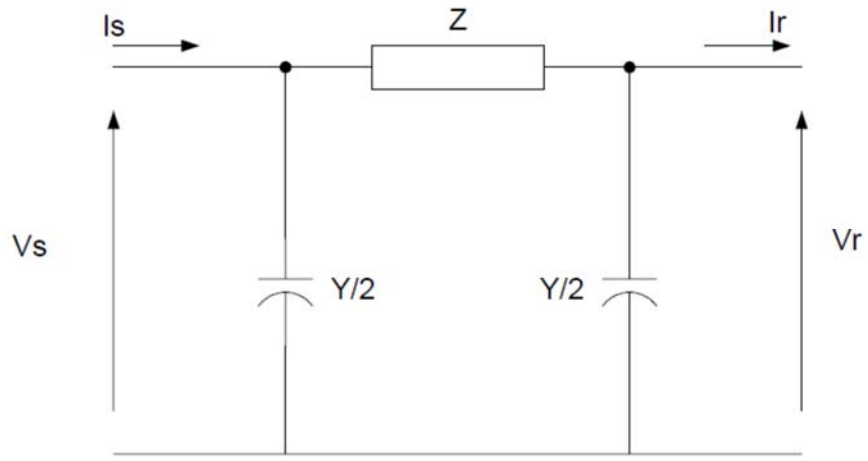

Figure 1.1: Circuit model of medium length transmission line

Figure 1.1 shows the circuit model for a medium length transmission length from which equation (1.1) is derived. Under light or no load conditions the current is capacitive. As the capacitance increases, the product of capacitive current and the inductive impedance is a negative number, which in turn adds to the voltage, causing the receiving voltage to observe a voltage higher than the sending end. This overvoltage can be on the order of about 1.5 pu with potential to damage critical equipment and cause faults if the equipment insulation is not designed to that voltage. The Ferranti effect usually can be observed in light loading or no load conditions, where the net current in the line can be highly capacitive in nature.

The Surge Impedance Loading (SIL) is the power delivered by a lossless line to a load resistance equal to the surge impedance Z_C. When loaded at the SIL, the voltage profile over the length of the line is flat, that is the voltage magnitudes at all point along a lossless line at SIL are the same. SIL is given by

$$SIL = \frac{V_{rated}^2}{Z_c} \tag{1.2}$$

In practice, power lines are not terminated by their surge impedance. Instead loadings can vary from a small fraction of SIL during light load conditions up to multiples of SIL, depending on the line length and on line compensation during heavy load conditions. If a line is not terminated by its surge impedance, the voltage profile at SIL is not flat. Figure 1.2 shows the voltage profile behavior based on the loading conditions of a transmission line feeding only a passive load.

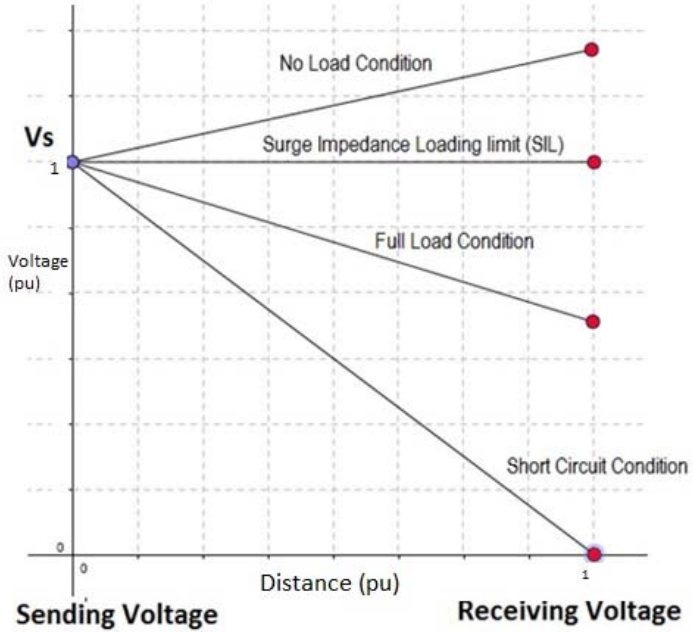

Figure 1.2: Voltage profiles of a transmission system under different loading conditions

Shunt reactors are installed to reduce the overvoltages under light loading conditions by cancelling part of the capacitive impedance. The shunt reactors installed for this application are typically designed to cancel about 70% of the

capacitance. This rating is to ensure that the power factor doesn't become too inductive under full load conditions, although the reactors are generally switched out when the transmission line is loaded closer to its rated ampacity. Shunt reactors can reduce line loadability if they are not removed under full load conditions. Given the system design and load conditions, a shunt reactor can be switched in and out more than once a day. In other cases, they are designed to be connected permanently to the bus or line where full line loadability isn't foreseen until the distant future.

The construction of a shunt reactor resembles the construction of a transformer in most cases. Reactors can be constructed around an air core or around an iron core. Depending on the location, application and size, these could be dry type or oil immersed, although iron core reactors are often oil immersed. The dry type air core shunt reactor is probably the simplest and the oldest design for a shunt reactor. In simple terms, it is a cylindrical coil creating an inductance as required for the application. The reactance of the coil is dependent on the material, radius, length, installation geometry and the number of turns of the coil itself [2] [3].

Dry-type air core reactors have several advantages over iron core reactors such as lower cost and maintenance needs, shipping flexibility, more environmentally friendly operation (oil free) and no inrush current at startup. They are usually preferred for installations where space is not an issue. Compared to an iron core reactor, the air core reactor consumes more space in the substation which poses a disadvantage along with more extensive radiated

magnetic fields and higher heating. Manufacturers today also provide flexibility in construction of the reactors based on space considerations for shipping and installation.

One factor driving the increased demand for dry type shunt reactors is the increased generation from renewable power sources such as solar and wind. Wind generation is often installed in environmentally sensitive areas where the installation of dry type reactors is preferred [4]. Dry-type air core reactors can be installed in several applications, such as series reactors in lines, harmonic filters and detuning reactors for capacitor banks.

This thesis will look primarily at shunt reactors which are used in high voltage transmission lines with a focus on protective devices for shunt reactors. The neutral connection for the three phases of the reactor serves as a crucial point of information for protection which will later be discussed in Chapter 3.

Air core reactors used for shunt compensation were earlier restricted installations directly to the bus of up to 138 kV, or to the tertiary bus of a transmission level transformer for voltage up to 138 kV [5]. This however has changed with improved insulation materials and designs of air core reactors with present bus connected installations going up to 345 kV [4]. In this project, the reference application is a substation in Noxon (MT), where the rated voltage of the installed reactor is 230 kV. The reactors were sized to decrease overvoltages observed on the system by about 5 kV with two banks and each bank contributing 2.5 kV in compensation. A total of 100 MVAr of reactance is installed directly on the bus.

The construction of oil immersed iron core reactors resembles the construction of a regular transformer. They come with all supporting accessories and are usually installed where space is a constraint. That type of reactor is not part of the research at hand.

The protection schemes for air core reactors are usually the same as the protection applied to oil filled iron core reactors. However, the protection on the turn-to-turn faults can be made more sensitive for an oil filled shunt reactors due to the ability to use mechanical protection elements which cannot be installed for an air core reactor, as will be discussed in Chapter 2. The objective for this thesis is to develop a solution to find a turn-to-turn fault protection solution for an air core reactor with sensitivity similar to that for protection of an oil filled reactor.

1.2. Overview

Chapter 2 an introduction to protection practices as recommended by standards and industry personnel in various publications. The chapter will serve as guidance for the protection studies in this thesis and highlight shortcomings observed in protecting an air core reactor from turn-to-turn faults.

Chapter 3 will introduce the basic concepts of air core reactors and discuss the equations relevant to their design and construction. The chapter will discuss modelling shunt reactor across different software tools as well as protection design issues considered in this study. The simulation models developed for the circuit design in RTDS, ATP and Matlab will be introduced to observe faults

on the reactor. The cross-platform verification is helpful to solidify the observations made.

Chapter 4 will discuss the protection schemes which are proposed in this thesis to identify turn-to-turn faults and the measured quantities required.

Chapter 5 will illustrate the simulation results of the system model on which the turn-to-turn faults were produced and evaluate the performance of the protection schemes. The chapter will serve as a guide on what is expected from the protection scheme when faults are induced on the hardware test bed.

Chapter 6 will introduce a hardware test setup for the project made with the help of a senior design team. The chapter will discuss the specifics of the construction of the reactor windings for the testing turn-to-turn faults as well as the relay used for measurements to test the protection scheme and event recording.

Chapter 7 presents and evaluates the test results obtained from the hardware setup and the ATP simulation for the two different relays with different sampling rates. The chapter discusses the results of both testing methods and validates the proposed protection design.

Chapter 8 will discuss conclusions on the thesis and suggest possible future work on this subject.

2. CURRENT PRACTICES AND RECOMMENDATION ON PROTECTION SCHEME OF SHUNT REACTOR

This chapter will delve into the recommendations put forth and practiced by professionals in the field for protection of shunt reactors. IEEE standards and some well cited technical papers have been referenced in this thesis.

Observing the recommendations across several references, the application of protection of shunt reactor is observed to be similar for both the air core type and the iron core type equipment. The iron core reactors usually have high current ratings at high voltages and are installed in oil filled tanks like transformers, which permits installation of mechanical protective devices and gas monitoring which make the detection of turn-to-turn faults easier.

First, the different types of faults that can occur in an outdoor type dry type reactor need to be discussed. The reactor can be built from one or two sections, which are supported or mounted on insulators high above the ground. Figure 2.1 shows the typical installation of high voltage air core reactors on pedestals. The proximity and arrangement of the phases is decided by the ratings and manufacturer recommendations. The most common faults which can occur in this type of reactor are phase-to-phase faults, phase-to-ground faults, high voltage bushing to ground faults and turn-to-turn faults [5].

Figure 2.1: 20kV, 45MVAr air core reactors mounted on insulators and pedestals [4].

2.1. Recommendations in IEEE standards

The IEEE guide for protection of shunt reactors [5] provides detailed recommendations on the protection of air core reactors including turn-to-turn fault protection. The suggestions provided are specifically for shunt reactors connected to the tertiary of a transmission level transformer and compare the neutral to ground voltages of the shunt reactor and of the grounding transformer. System unbalance can be seen on both, but a turn-to-turn fault on the shunt reactor will not be reflected on the grounding transformer. The

standard also gives valuable suggestions on the protection of an oil filled shunt reactor connected directly to the bus. It lists different options to implement turn-to-turn fault protection such as sequence directional overcurrent elements (67N and 67Q), distance protection (21) and a split phase reactor overcurrent relay (50N or 51N).

Based on suggestions for oil filled shunt reactors from the IEEE standard [5], the possible protection elements that can be used for air core reactors include a sequence directional overcurrent element. The directional overcurrent element will need to be blocked during breaker closing and opening times because, in case of single pole breakers, the timing of the closing operation will be skewed which can cause momentary flow of negative and zero sequence currents.

2.2. Shunt Reactor Protection Recommendations in Literature

The authors of [4], who are with one of the leading air core reactor manufacturers, shed light on reactor design and protection options. The writers point out that to detect turn-to-turn faults in an air core reactor, it will be necessary to monitor the voltage at the neutral point in the reactor through a potential transformer (PT) in cases where the neutral is ungrounded. In cases where the neutral is grounded, the current flowing through it (3I0) can be used to detect faults. The paper goes on to describe the construction of the reactor coils and the magnetic fields generated around the reactors. The main design parameter for dry-type reactors is the steady-state voltage drop along the surface of the reactor. The length of the winding is chosen to provide abundant

creepage distance along the winding surface to cope with the continuous voltage stress. The paper further goes on to describe the implications of reactor switching and design on CTs and circuit breakers.

The authors in [7] discuss the basics of shunt reactor implementation and the calculations for sizing of reactors. The paper discusses the use of transmission line ABCD parameters in estimating the size of the shunt reactor to provide about 70%-80% of the compensation as required. The paper also discusses shunt reactor switching implications, CT saturation and effect CT saturation has on protection schemes implemented on the reactor. The paper also discusses turn-to-turn faults and simulations depicting the behavior of the phenomenon. The paper, through its simulations, points out that a small rise in current is observed in the neutral path of the reactor and this flow of current due to the fault is not sufficient to create a voltage imbalance. The simulation results show that a fault incorporating 1% of the active turns is detected by observing zero sequence current through the neutral. A similar simulation is done as part of this thesis to validate the models developed.

The authors in [6] also discuss the basics of shunt reactor design and implementation. The paper further delves into possible faults occurring in shunt reactors and ways to protect the equipment. The paper provides detailed recommendations for the protection of iron core and coreless (air core) reactors with suggestions for turn-to-turn fault protection. The authors point out that the most common cause of turn-to-turn faults is breaker restrikes causing Transient Recovery Voltage (TRV), usually resulting in faults at the supply

side of the reactor where the higher transient recovery voltages (TRV) are observed. The insulating material is damaged during due to these TRVs if not designed properly. The authors of [6] note that increased neutral currents can be observed during a turn-to-turn fault. The sensitive overcurrent setting recommended in this case is about 10-15% current used to rate the CTs and relay for the ground overcurrent protection. Sufficient margin should be considered for measurement errors the tolerance of the reactor impedance.

Figure 2.2 is an extract from [6] showing suggestions for shunt reactor protection. Note that this scheme also includes the mechanical protection found in an oil filled reactor which cannot be used in a dry type air core reactor since there isn't an oil filled tank.

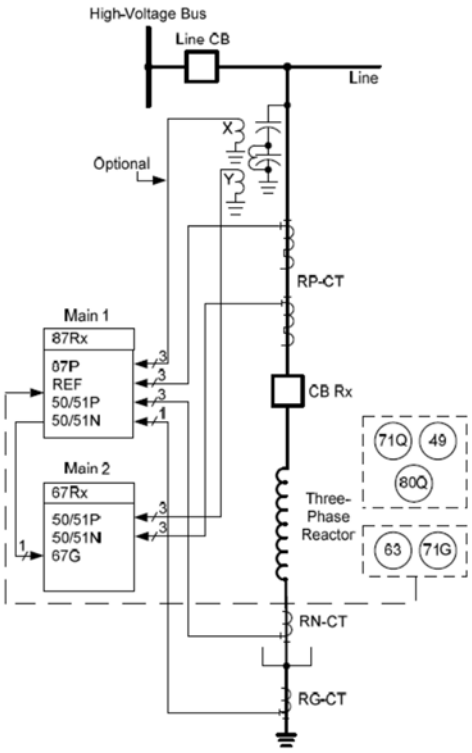

Figure 2.2: Overall protection scheme for oil filled shunt reactor [6]

The authors of [8] discuss an installation of an EHV air core shunt reactor at a utility and the practical considerations to be taken for such installations. The paper starts out discussing the installation, CT selection, protection design and switching studies and observations of the reactor operation. The hardware test bed discussed in Chapter 6 of this thesis was sponsored by the utility which installed the air core reactors in [8]. The paper gives valuable information on switching studies with field measurements validating the author's simulation model. The paper mentions that a ground overcurrent relay with setting of 10%-15% sensitivity pick up was installed to detect turn-to-turn faults on the reactor. This level of sensitivity can only detect faults when approximately 400 turns have been shorted.

The goal of this research is to find methods to detect such faults with much better sensitivity and possibly detect even a single shorted turn.

2.3 Summary

This chapter has discussed the recommended practices and technical opinions of standards and industry personnel to better understand the protection of shunt reactors in general. This chapter included a literature review, pointing out the limitations of existing protection practices for high sensitivity in fault detection. Further it suggests the possible solution of observing the current in the reactor neutral path for signature as a turn-to-turn faults in the reactor.

3. MODELLING OF SHUNT REACTORS

The air core reactor is probably one of the simplest of constructions in power engineering. As the name suggests, it has no iron core and the magnetic flux created by the coil is free to flow naturally in air. The coil winding is usually made from aluminum for light weight construction and reduced costs with losses at a comparable level with copper. Although copper is preferred in some cases for higher X/R.

The simple construction of the air core reactor used at the transmission level consists of a few parts which are illustrated in the Figure 3.1. The coil is wound based on the design around a circular frame known as the spider with the winding spaced evenly in layers to get the required number of turns for the desired reactance. The coil sits on insulators and in some cases, based on the capacity of the reactor, is split in two parts for easier logistics and installation.

The reactors are independently made per phase and can be installed in different arrangements as suggested by the manufacturer. The three phases of the reactors are either stacked on top of each other, arranged in a straight line or in a triangle. Each arrangement effects the mutual inductance between the different phases. The terminals for the reactors are usually provided at the top and the bottom.

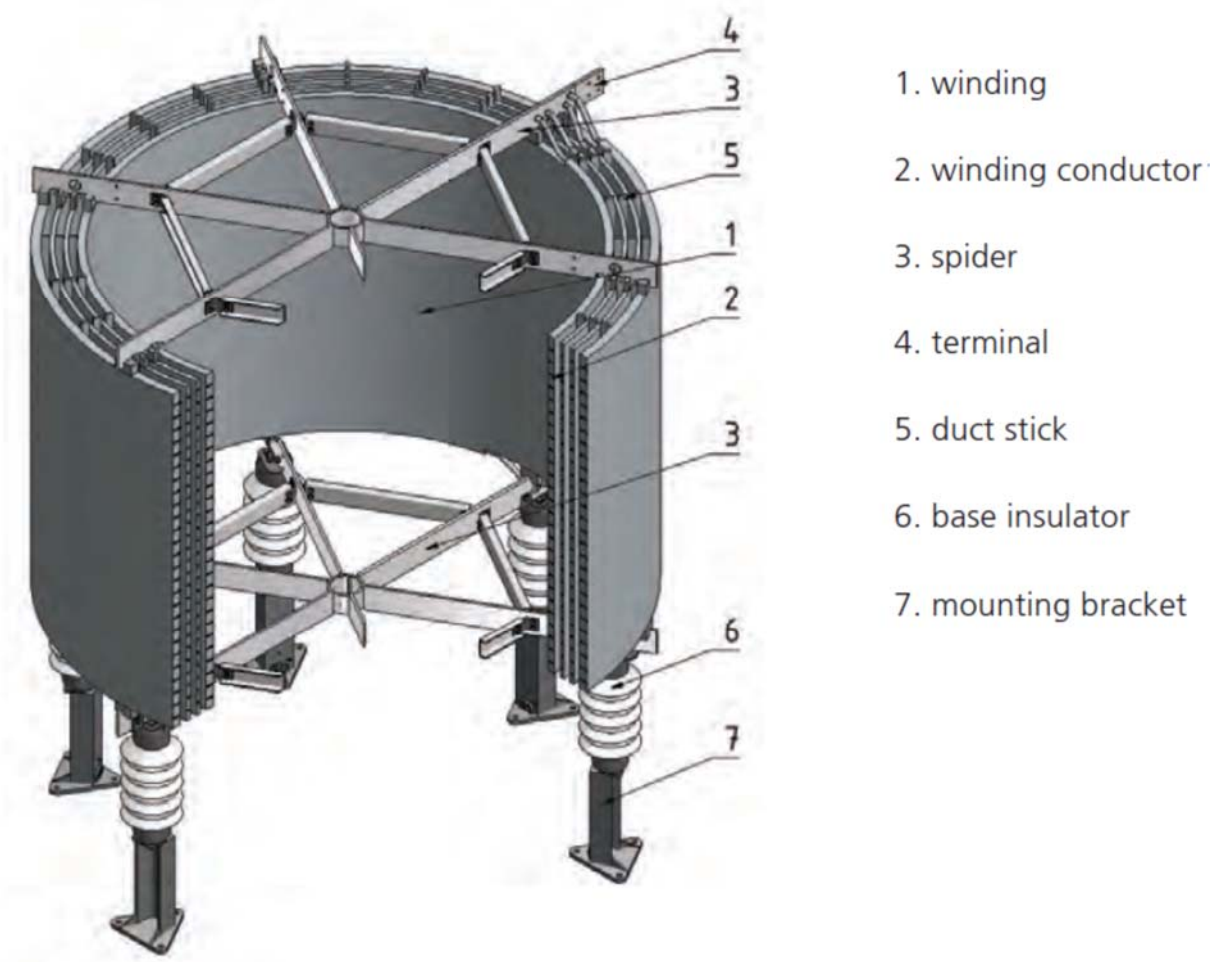

Figure 3.1: Construction of outdoor type shunt air core reactor. Trench dry type air core shunt reactor catalogue [4]

The most preferred construction of coils in most transformers, reactors and generators is of a rectangular cross section. This construction is the best solution to reduce resistance in the circuit, which is desired for reducing heating losses and increased X/R ratio. The air core reactors are also of similar construction with aluminum as the conductor [2].

The inductance of a coil is generally the combination of the self-inductance and the mutual inductance. The self-inductance is dominant in contributing to

the reactance and can be found using Ampere's circuit law which can be represented in (3.1).

$$\oint H * dl = I_{enc} \tag{3.1}$$

The paper written by W.B. Brooks [2] gives more equations to calculate accurately the inductance of the coil based on its geometry, but this research considers (3.2) for approximate calculations as complete accuracy is not mandatory.

The shape of the reactor itself is in the form of a cylindrical toroid with multiple layers of coils and sufficient empty space in the center. As the paper by Brooks describes it, there are infinite possible ways to create the coil of required inductance. The design needs to be optimum in balancing the number of turns and the radius of the coil.

3.1. Air Core Reactor Design

3.1.1. Basic theory

The design of the reactor stems from the basic laws of electromagnetics. The inductance of a circular coil is given by equation (3.1)

$$L = \frac{N^2 * \mu_r * \mu_0 * A}{l} \tag{3.2}$$

The relative permeability (μ_r) for the air core case is 1.0, whereas for iron core μ_r ranges on the order of 6000-10000. Hence to obtain the same amount of

inductance with an air core, the inductor should be designed by varying the area of coil, length of coil or the number of turns.

The magnetic flux generated by the inductor is strongest in the central axis of the inductor. Stacking sections of the reactor coil or independently connecting multiple reactor coils in series increases the inductance of the coil. The reactors installed in the Noxon substation have four sections per phase with two sets of sections stacked on top of each other as shown in Figure 3.2.

Figure 3.2: Reactor banks at Noxon substation with one bank in the foreground and the second bank in the background

3.1.2. Parallel Connected Multi-layer Reactor Coil

Commercial air core reactor coils are designed as parallel connections of multiple branches. Each branch has a DC resistance, self-inductance and mutual inductance with neighboring branches [9]. The circuit model shown in Figure 3.3 has N parallel branches.

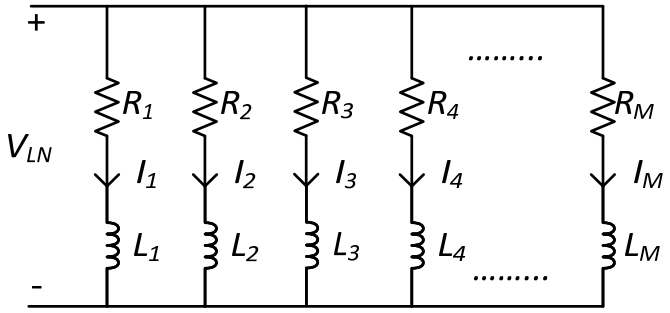

Figure 3.3: Multi-layer air core reactor model [9] with R_M, L_M and I_M indicated as the resistance, inductance and current in M^{th} layer.

The construction of the reactors in the Noxon switchyard is similar, with parallel branches influencing mutual inductance between the layers and the split reactance through the coils. Further understanding to estimate the amount of current that would flow through shorted turns. The current will differ for shorted turns at different points in the coil. The individual layers are configured such that the radial voltage stress is virtually nil and the remaining axial voltage stress is small enough that surface stress values are less than those on porcelain insulators and turn-to-turn steady state operating voltages are well below the level at which partial discharge can occur [4]. Taking these considerations into account, the reactors at Noxon have 985 turns per single layer per section. The key point of interest however for reactor protection is

the current observed at available measurement points to detect turn-to-turn faults.

The construction of the commercial reactors is further discussed in [10]. The authors provide detailed circuit designs for reactors with multiple layers.

Figure 3.4 illustrates the connections for a high voltage multi-layer tapped reactor [10], where an algorithm is used to calculate weight, power loss, height and the number of coils required for a given inductance. The tapped reactor design is shown here for better understanding of the construction of the multi-layer reactor. Taps are not applicable in this study since they are not used as intermediate measurement points.

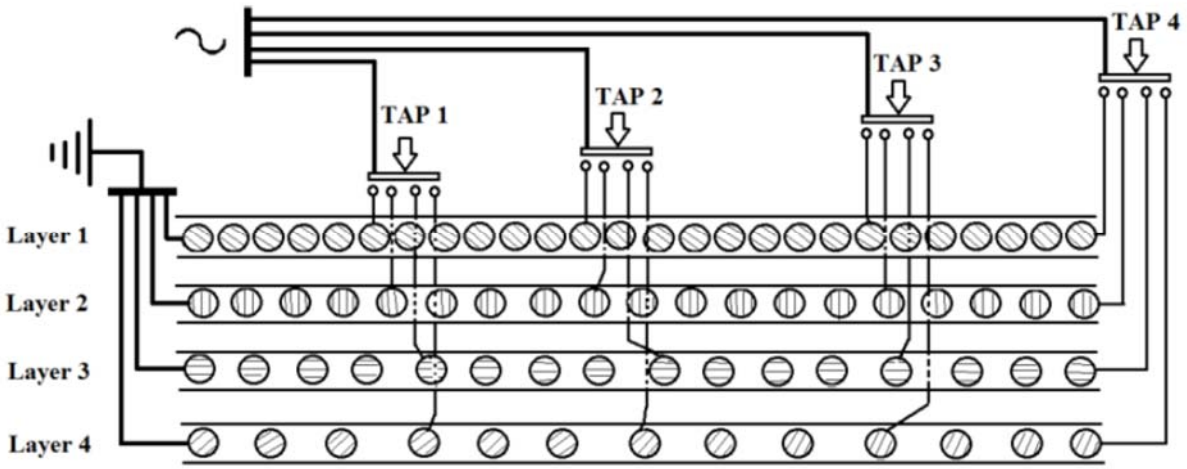

Figure 3.4: Illustration of multi-layer air core reactor showing distribution of turns per layer [10].

3.1.3. Calculation of Inductance of Parallel Connected Multilayer Coils

Information on the number of the turns on the outermost and the innermost layer of the coils was provided by Avista, which they received from the reactor manufacturer. Using this information, the inductance was estimated following the formula in (3.3). Since, the information of each layer of the coil was not available, using the difference in turns between the outer and inner layers, turns per layer was approximated to have an addition of 44 turns/layer counting out from the innermost layer. The inductance of each layer of coil was calculated using (3.3) approximating the mutual inductance by a scaling factor per the layer number in the coil. Equation (3.3) shows the typical equation used to calculate the effective self-inductance of each layer of coil, where N^{th} layer inductance is calculated out of a reactor coil with m layers. The calculated overall inductance of one section of the coil is 661.931µH, whereas the actual inductance of one section of the coil in Noxon is 695µH according to the reactor test report. The calculation yielded results with an accuracy of 5%. Appendix-C has the complete calculation.

$$L_n = \frac{N^2 * (m - n + 1) * \mu_0 * A}{l} \tag{3.3}$$

To validate the calculation, a simple coil with parallel branches was constructed similar to the commercial reactor coil. The coil is shown in Figure 3.5. The coil has three layers wound concentrically. The individual inductances of each coil are 115µH, 148µH and 250µH respectively going from the

innermost to the outermost coil. When connected in parallel, the resulting effective inductance was measured at 120µH. The calculated inductance using the approximate method is 97µH (see Appendix B). The error in this case is higher than the calculation for the Noxon reactor, but understand that this calculation is an approximation using several assumptions in the construction of the coil. This method of inductance calculation can be used to make a rough estimate on the fault currents which can be observed in faulted turns and then in setting protection elements.

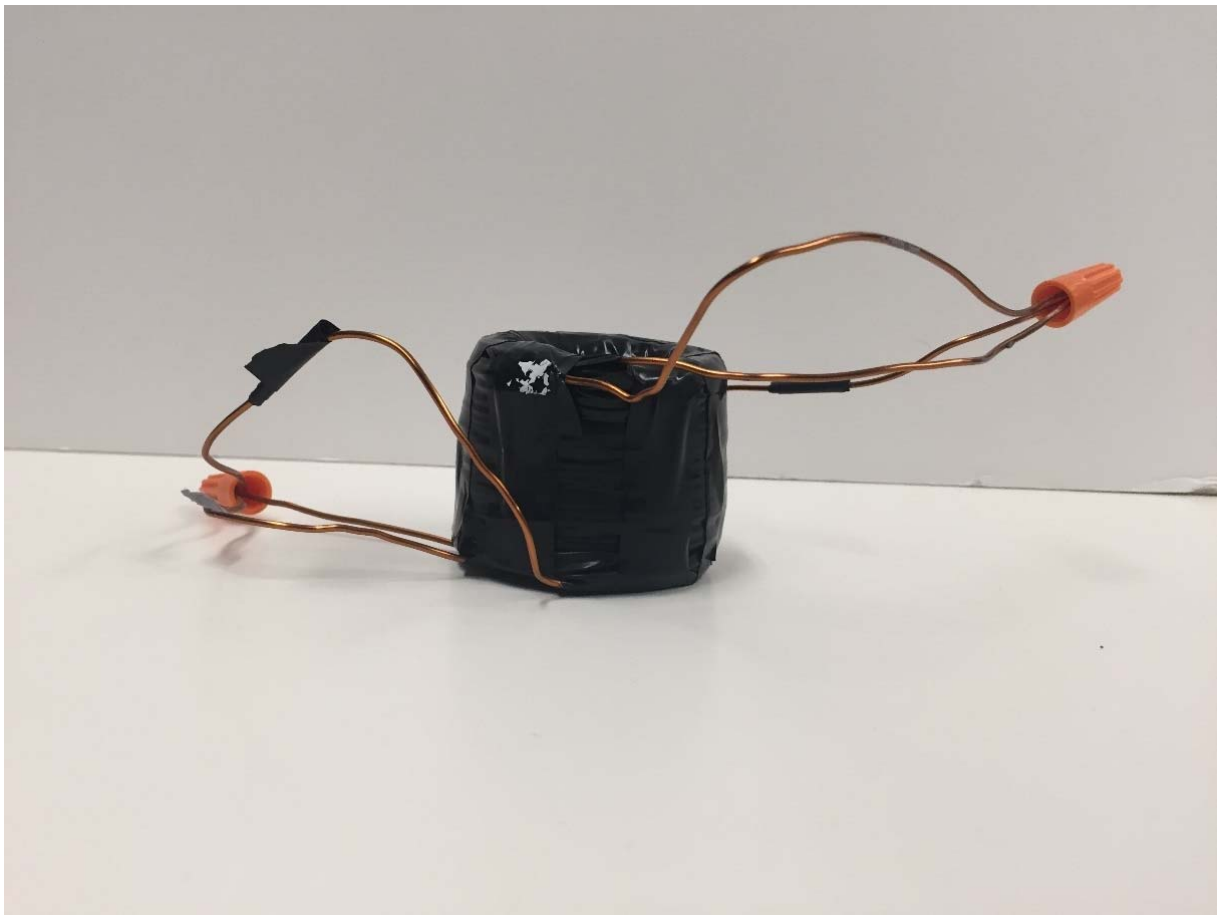

Figure 3.5: Hand wound three-layer coil, connected in parallel.

3.2. Simulation Models

Two software tools were primary used for modelling turn-to-turn faults on the reactor. When the fault occurs, the current flowing through the coil skips the shorted windings to follow the shorted path. As mentioned in several technical papers such as [6], the turn-to-turn fault is effectively a reduced inductance which can create an imbalance in the three-phase symmetry of the terminal currents. The circuit was designed in ATPdraw (graphical interface for ATP) and RSCAD (graphical interface for RTDS) as a series of small inductances. When the fault occurs a small part of the inductance is bypassed.

A three phase circuit was designed in both software tools to observe the impact of faults on the symmetrical components of the circuit. Since the reactor is connected in shunt to the bus, there is no other equipment in the path between the bus and the ground. The star point of the circuit is grounded in the circuit, as is the case at Noxon. The model includes a switch that can be opened to observe the circuit in an ungrounded condition as suggested by some authors on reactor protection [5].

In most reactor installations, a very high X/R ratio is desired as the main purpose of the reactor is to provide pure inductive reactance. Based on the current installation at Noxon, MT, an X/R ratio of 55 was used to select the resistance in the circuit.

Current measurements need to be made at both ends of the reactor and in the neutral to ground path in the circuit. Hence, measuring instruments are located

at the reactor terminals, neutral ends of windings, and in neutral path to represent readings for all forms of protection implemented. The bus voltage was the best choice for voltage measurement, which is consistent with field installations. Figure 3.6 shows the typical current transformer locations installed for measurements to protection devices for shunt reactor protection. A combination of CT1, CT2 and CTN are used for current differential protection. The case modeled in this thesis uses CTs at these locations.

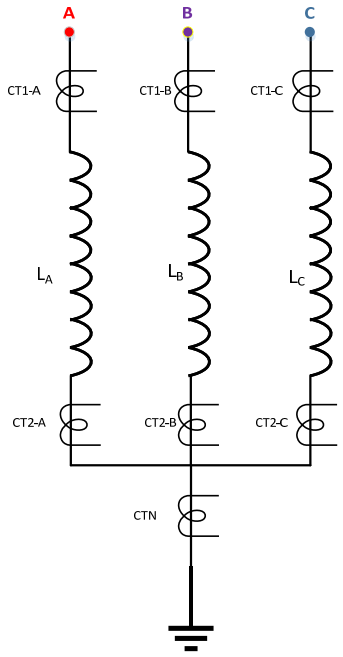

Figure 3.6: Three phase reactor with typical current transformer arrangement.

The ATPdraw model uses parameter information available in the reactor model obtained from the project sponsor. Each section has an impedance of 283 ohm (0.75 H) and the stack of four sections had an inductance of about 3 H per phase. One section of the final model in ATPdraw is shown in Figure 3.7. It is

a representation of the coil section as seen from a terminal, and doesn't account for mutual coupling between sections or between phases. The distance between the phases is sufficient to neglect mutual coupling and the section mutual coupling is not significant to affect transient studies. The complete model system is attached as Appendix-A.

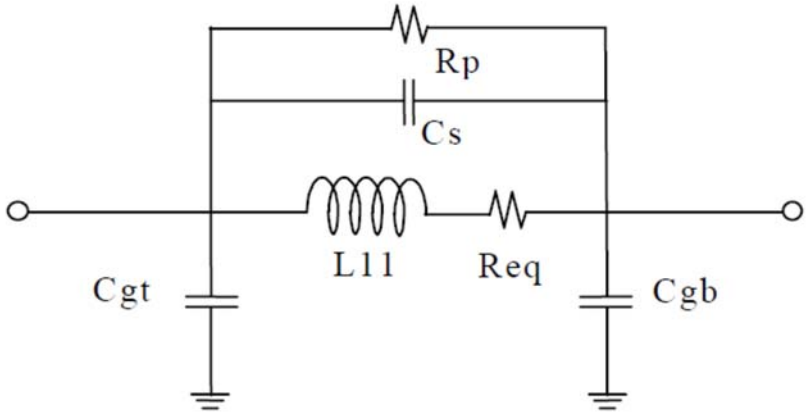

Figure 3.7: One phase section of the reactor model implemented in ATPdraw

The coil model includes the main inductance (L11), the equivalent series resistance (Req), the insulation resistance (Rp), and parasitic capacitances (Cgt, Cgb and Cs). Four sections were connected in series per phase.

The study system one line diagram is shown in Figure 3.7. Appendix A has the full model in more detail. The system has some power flow on the bus between generator and the load at the far end. The impact of system disturbances can also be modeled to see the effect of the external disturbances on the turn-to-turn fault protection element in order to prevent misoperation. The parameters of the shunt reactor used in the ATP model are shown in Table 3.1.

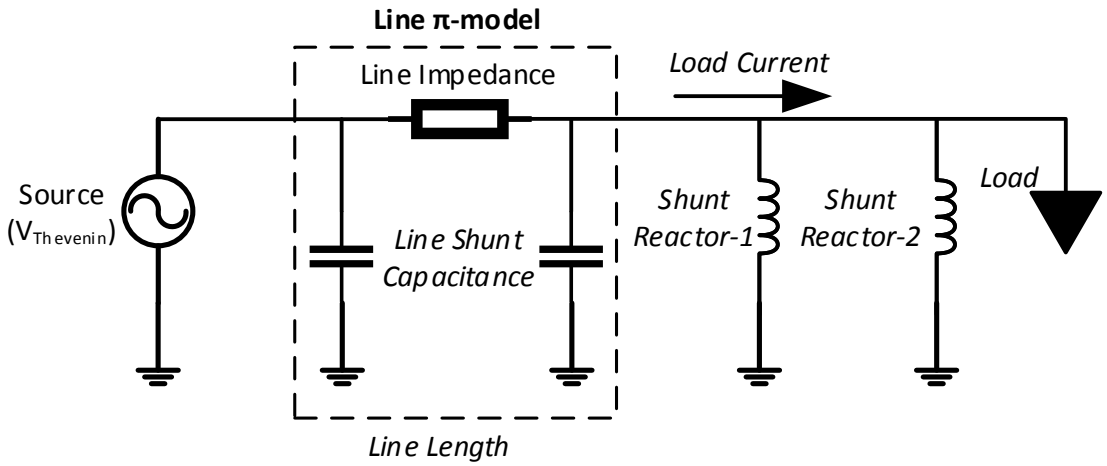

Figure 3.8: One line diagram of the system model under study

Table 3.1: Reactor section parameters from the Noxon Reactor

Rp	Cs	L11	Req	Cgt	Cgb
20MΩ	125pF	751.25mH	30Ω	101.27pF	85.6pF

3.3. Summary

This chapter outlined the basic design and construction of the air core reactor and explained the circuit design which was used in software for simulations. Equations used for calculations were also developed to show how the estimate of the effective inductance of the reactor was made both in single layer and multi-layer coils.

4. PROPOSED PROTECTION SCHEMES

4.1. Study Considerations for Protection Scheme Development

The protection element design for sensitive turn-to-turn fault detection on an air core reactor is challenging, especially in the absence of mechanical pressure relays and other sensitive protection which can be used in oil filled reactors or transformers. Observing the known industry recommendations and applications for transformer protection, the neutral current or the zero sequence current measured at the reactor will be key factors to detect inter-turn faults when developing a scheme. Similar observations can be seen from the ATP simulation results on the reactor. However, a comparative concept is utilized to further improve a technique for the detection of these faults.

Using the system data from Noxon, the model described in Chapter 3 was created in ATPdraw to aid in the search for new solutions. One concept that can be applied to a case with multiple three phase reactor banks is to compare the neutral current of one reactor bank against the neutral current of the other reactors. The neutral current of a faulted reactor bank is different from the neutral current of the unfaulted reactor, which can be used to differentiate internal faults from external imbalances. This method also requires both the reactors to be connected to the bus for detection. Two possible solutions based on this concept are described below:

1. **Ideal comparison case**: In an ideal case the reactors have zero error on their phase impedances and there should be no current flowing through

the neutral when there is no external source imbalance. In case of a turn-to-turn fault in a phase of one of the reactors, the difference in the currents through the neutral can be used as a potential trigger for fault detection. This is for an ideal condition, hence there are no errors to be considered in measuring instruments, reactor design and source voltage. The difference in the currents can be observed at the relay through two methods:

a. Calculating sequence quantities on each reactor using a protection IED, or on measurements communicated to the IED through DNP3, IEC61850 GOOSE messages, sampled values, vendor specific propriety communication interfaces such as Mirrored Bits or Network Global Variable List (NGVL).
b. Physical connection of the differential CTs in anti-parallel in the neutrals of the two reactors and observing the difference in currents at the relay.

2. **Actual condition**: In actual conditions, there are several sources of error including current transformer error, reactor design tolerance, system unbalances and unequal cable lengths. All this data needs to be considered to determine the settings. Calibration of the element is required before energization for implementing a correct protection scheme.

The steps for developing the protection scheme are as follows:

a. Find a solution allowing clear identification of a turn-to-turn fault.
b. Implement the scheme for calculations using measured field data from reactors in normal operating conditions, including slight imbalances in phase reactances.
c. Verify proper operation of scheme in external system voltage unbalance conditions.
d. Verify correct operation of scheme during faults on the system external to protection zone.
e. Identify response of scheme for a faulted reactor.

4.2. Proposed Detection Methods

The currents seen on the neutral CT primary when a small number of turns are shorted is on the order of a few amps, primary. This raises concern about the ability of the relay to pickup the current using CT secondary current. This is because the current transformers in these applications are usually designed with high ratios to avoid saturation due to the long-lasting DC offset for external faults because of the high X/R ratio of the reactor impedance. Given a ratio CT ratio of 80, a neutral current of 3A primary has a secondary current of 0.0375A. Small currents such as that falls below the relay A/D converter minimum pickup and are within CT measuring error. A better solution is to directly measure this current by the protection relay or an intermediate relay since there is no danger of high voltages observed during normal operation. However, a surge protection device should be connected across the relay for added protection during ground faults with large currents. Another option is to add a low ratio isolating

transformer for any surge in current due to external or internal ground faults. The connection design can be made as shown in Figure 4.1, where I_{N1} is the primary neutral current in reactor 1 and I_{N2} is the primary neutral current in reactor 2. This method of fault detection can be highly effective and should be preferred for accurate detection of turn-to-turn fault in a reactor in the case with two three phase reactors on the same bus.

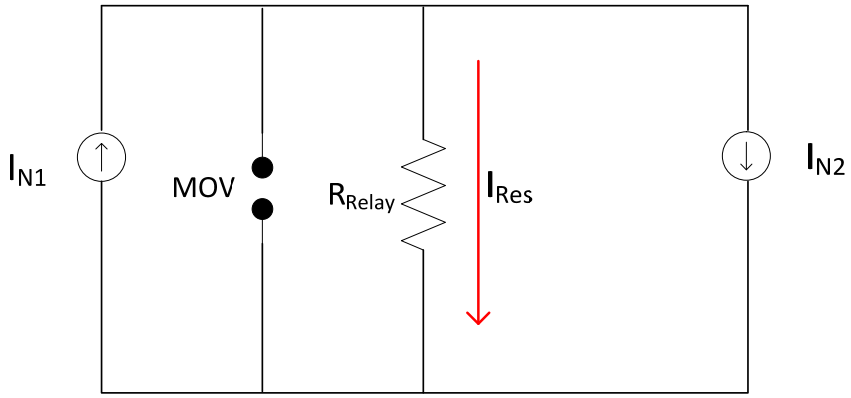

Figure 4.1: Neutral current differential current with reactor 1 and reactor 2 neutral currents.

This neutral current differential comparison can be used only in a condition where the both reactors are operational when the fault occurs. It can't be applied for free standing reactors where there isn't another reactor neutral to measure against. The current I_{Res} is the difference in the reactor neutral currents which can be formulated as in (4.1).

$$I_{Res} = I0_{Diff} = I_{N1} - I_{N2} \tag{4.1}$$

A more general option that can work for a single reactor is to use the bus VT to measure the bus zero sequence voltage, which will have a very small change

during internal faults when compared to an external fault on the system. The change in 3V0 during a turn-to-turn fault is usually not noticeable and can be solid reference to compare against the change in neutral current of the reactor. Some other options are using core flux summing CT at the terminals or a neutral current on the bus CTs, neither of which is possible in many cases.

The broken delta arrangement of the bus VTs shown in Figure 4.2(a) will readily provide the system 3V0. Figure 4.2(a) shows a hypothetical arrangement to effectively implement a relay pick up element for any air core reactor. The comparison between the terminal 3V0 and the neutral current can be used as for fault detection. Converting the 3I0 to a voltage can ease the comparison. The voltage across the relay resistance or an intermediate resistor will be the deciding quantity for this protection element. A large resistance, sized based on the system voltage level, is placed in series with the measuring resistance to protect the relay from system unbalances and to sensitize the circuit for this scheme. The potential across the relay resistance will allow an effective quantity for making a decision.

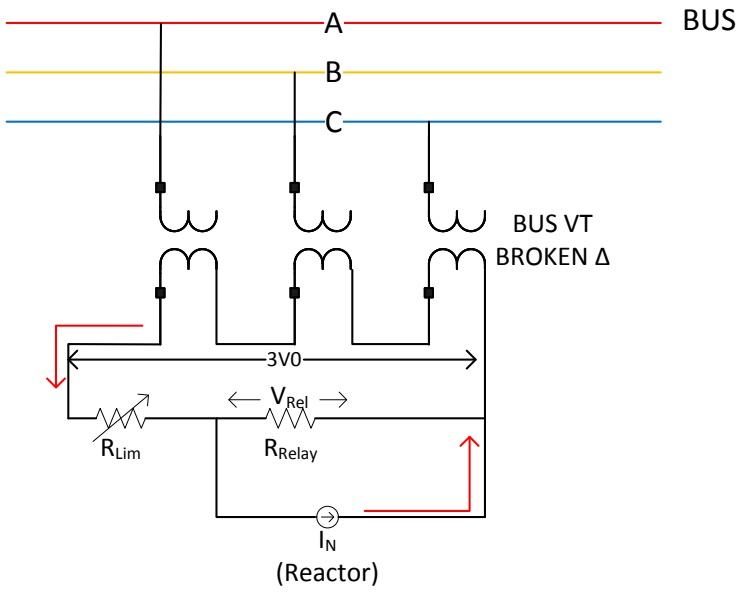

Figure 4.2 (a): Bus zero sequence voltage differential measurement with reactor neutral current.

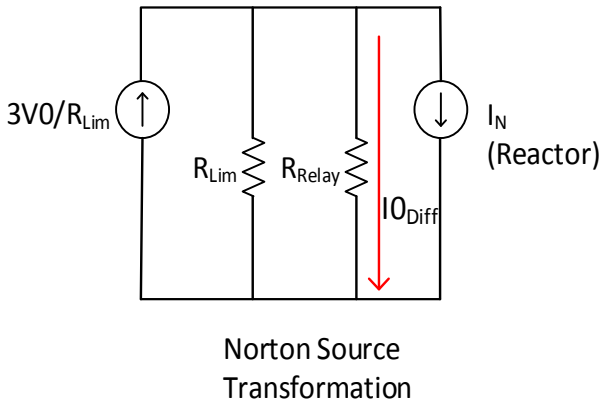

Figure 4.2 (b): Bus zero sequence voltage differential with reactor neutral current after source transformation

The hypothetical illustration in Figure 4.2 (a) is a simple visualization of the concept and cannot be implemented since it violates Kirchoff's laws. For the scheme to be implemented, the source transformation for the zero sequence voltage should be made using a resistor R_{Lim}. R_{Lim} cannot be implemented as a

real resistance as it needs to be dynamic responding to changing bus zero sequence voltage but it can be calculated term in a relay. The calculation and application of the variable resistance R_{Lim} is explained in the following sections.

4.3. Polarizing Quantity for Turn-To-Turn Faults

The zone of protection can be defined using the phase angle relationship of the zero sequence voltage (V0) and zero sequence current (I0). Reference [11] discusses methods to identify a turn-to-turn fault in a shunt reactor and differentiate it from an external fault. Two possible ways for polarizing the protection element and defining the zone of protection are:

a. Direction of zero sequence power flow:

   Compare the phase relationship of V0 to I0 to differentiate based on the direction of zero sequence fault current flow.

b. Magnitude and sign of measured amplitude of zero sequence impedance:

   Measuring zero sequence impedance clearly differentiates an internal fault from an external one. The zero sequence impedance (Z0) is equal to the effective system zero sequence impedance for an internal fault in the reactor whereas the measured effective impedance is the negative of the zero sequence of the reactor for an external fault.

This research applies the concept of zero sequence power flow direction to identify a fault as internal and provide a polarizing reference. In the case of an external ground fault V0 leads I0 by 90 degrees, whereas for an internal fault

such as turn-to-turn or turn-to-ground I0 leads V0 by 90 deg. The known polarity of the neutral CT can be used for identifying this difference as shown in the one line diagram in Figure 4.3. Reference [11] also provides two solutions for configuring the ground overcurrent protection element (50G) with a zero sequence directional element (67N) and a negative sequence directional element (67Q) to effectively differentiate the turn-to-turn fault from the phase-to-ground fault.

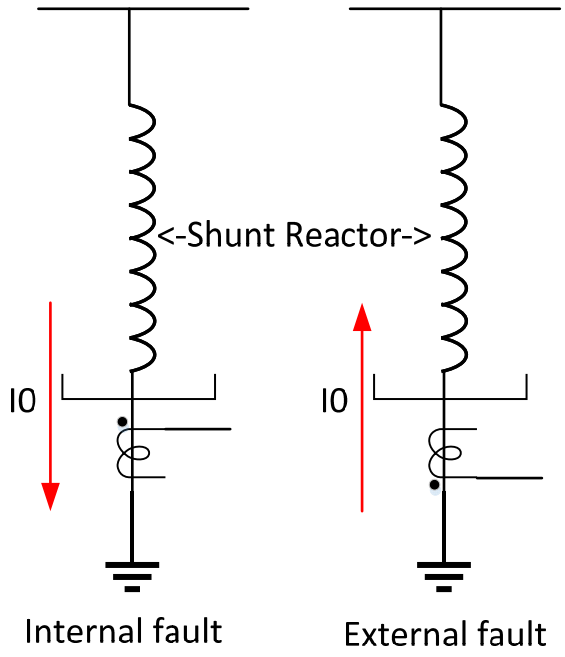

Figure 4.3: Differentiation of internal fault versus external fault using neutral current polarity

4.4. Calculations for Detecting the Turn-To-Turn Fault

The previous sections of this chapter described the scheme and logic required to identify a turn-to-turn fault in the reactor. Appendix-D has the complete set of MathCAD calculations for the settings for the detection of turn-to-turn

faults. In these calculations, the parameters of the substation are considered and tested through simulation for an imbalance caused in the reactor due to a turn-to-turn fault. This section will describe the procedure to perform calculation to determine the existence of such a type of fault from measured quantities.

In an ideal condition, i.e. when the system voltage is perfectly balanced and the coils of each phase are of the same inductance, the zero sequence current would be the only determining factor needed to identify a turn-to-turn fault condition. However, if there is a disturbance on the power system, or unmatched inductances of the individual coils, or standing unbalances in the power system, a zero sequence current detection element needs a dynamic comparison to confirm a fault condition. To utilize the zero sequence voltage comparison scheme, the zero sequence voltage needs to be scaled to be compared to the zero sequence current. Since the voltage unbalances are dynamic, the scaling factor (R_{Lim}), which acts as a limiting resistor in Figure 4.2 (a), needs to be pre-calculated with respect to a reference bus zero sequence voltage and a predetermined zero sequence current in the reactor neutral for an unfaulted reference case.

In part A of the calculation in Appendix-D, the limiting resistor is calibrated such that the measured differential current $I0_{diff}$ is zero. The voltage unbalance is varied over a range of -10% to +10% where the voltages are calculated as a factor of the unbalance K_{un} in equation (4.2). The unbalance factor is predominantly a real number and the unbalance is an artifact of the magnitude

alone. The zero sequence current for reactor is calculated for the range of unbalance of voltage in (4.3).

$$V_{abc_{un}}(K_{un}) = \begin{bmatrix} K_{un} * V_a \\ V_b \\ V_c \end{bmatrix} \tag{4.2}$$

$$I_{abc_{un}}(K_{un}) = \frac{V_{abc_{un}}(K_{un})}{\sqrt{3} * Z_{ph}} \tag{4.3}$$

The scaling factor R_{lim} is calculated as a ratio of the magnitude of the zero sequence bus voltage and the magnitude of the zero sequence reactor current measured at the neutral.

$$R_{lim} = \frac{V0(K_{un})}{I0(K_{un})} \tag{4.4}$$

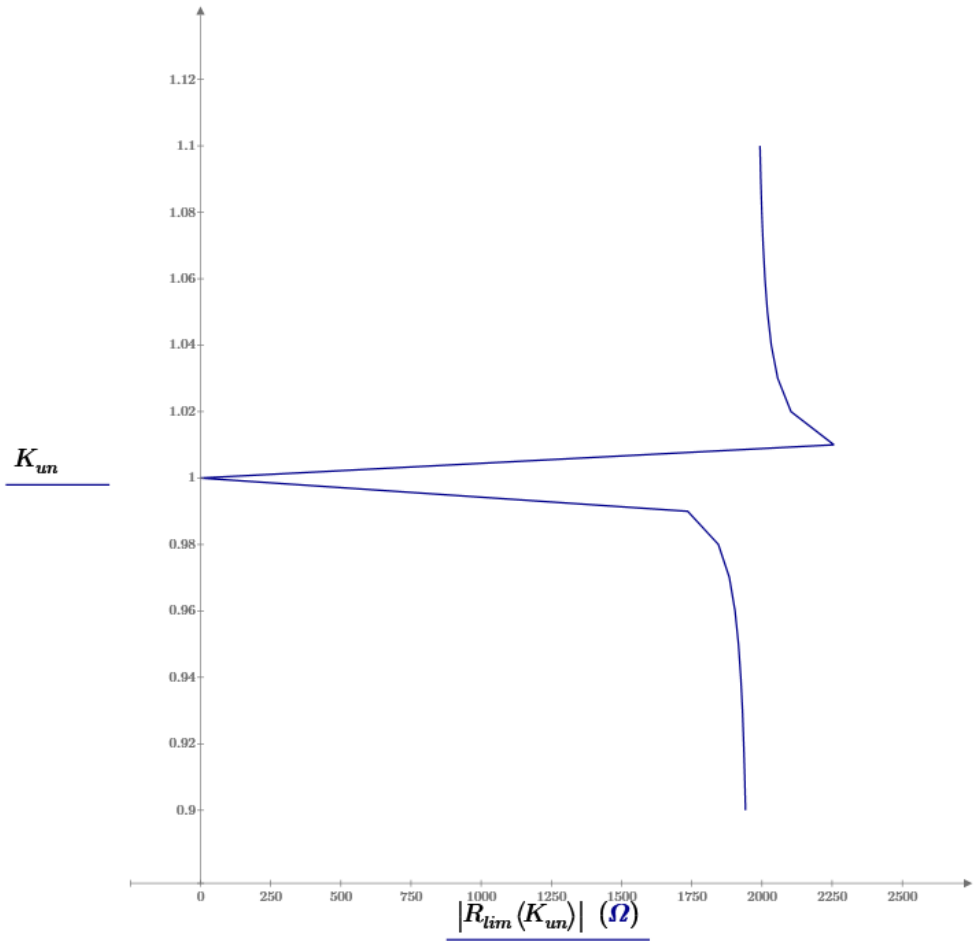

Figure 4.4: Variation of calculated limiting resistance magnitude with system voltage unbalance.

The variation of limiting resistance with voltage unbalance is demonstrated in Figure 4.4. The size of the limiting resistor R_{Lim} varies over a range of (0 - 2250Ω) over the range of system voltage unbalance from 0.85-1.1 (where 1 is no imbalance) considered in calculating it. Physical implementation of such a variable resistor in field is not possible as this is a sensitive protection element for which accuracy is important. For this reason, the proposed method using

this scaling factor needs to be limited to microprocessor relays or other IEDs, where it is a calculated parameter to use in an equation.

Part B of the calculations in Appendix-D shows the range of relay pickup currents required under different levels of unbalance on the system. It is observed that the pickup current lies with a narrow range simplifying the pickup limits. The pickup current ($I0_{diffa}$) is calculated as shown in equation (4.5), calculated with phase A referenced sequence quantities.

$$I0_{diffa}(K_{un}) = \frac{I_0(im)}{CTR} - \frac{V_0(K_{un})}{PTR * R_{lim}(K_{un})} \tag{4.5}$$

The pickup current, a differential current, is calculated using secondary measurements of the potential transformer and the current transformer. It is preferable that the current transformer in the neutral of the reactor have a small turns ratio, up to 50, for better accuracy. This is considering other neutral protection CT is available for primary protection functions. Figure 4.5 shows the variation of pick up current for a range of zero sequence voltage variation of ±10%. These calculations are done for a turn-to-turn fault with 2.5% of the inductance in one phase faulted.

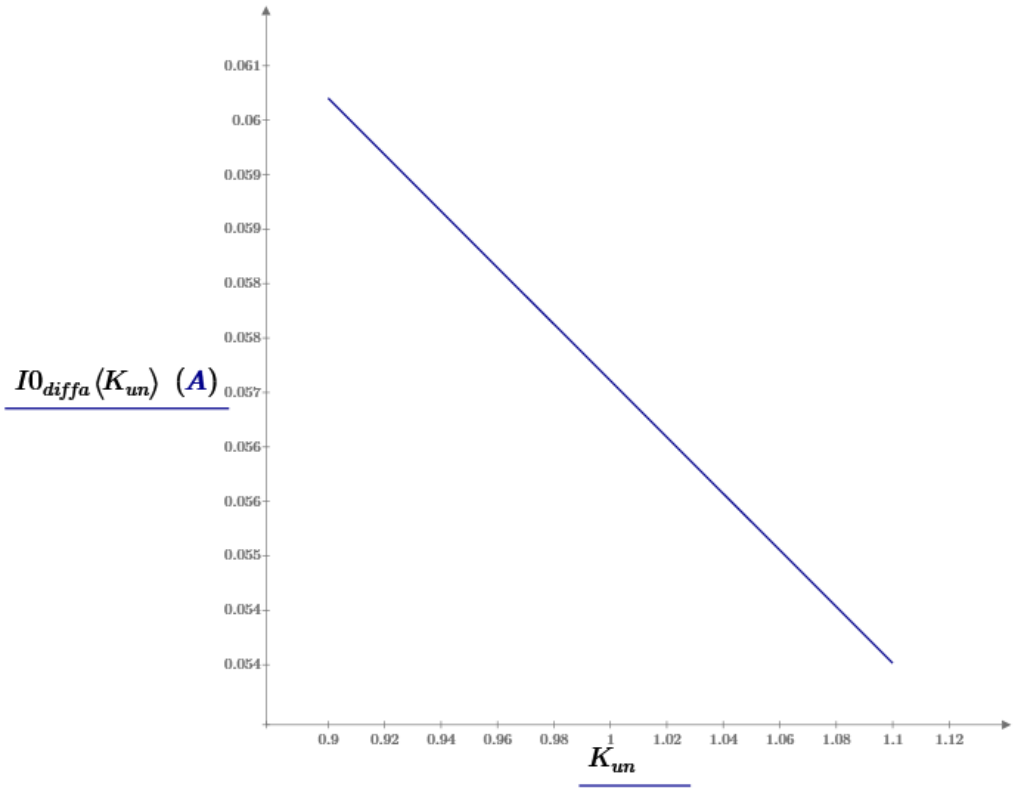

Figure 4.5: Variation of selected pick up current with system unbalance.

4.5. Faulted Phase Selection

It is also beneficial for the relay to identify the faulted phase in the reactor. One approach is to use the difference between the phase angle of the zero sequence current and the negative sequence current of the reactor to identify the faulted phase. Part C of the calculation in Appendix-D shows the identification of the faulted phase of the reactor. Since the fault is created on phase A in the example case and the phase of reference for the symmetrical components is phase A, the angle difference between I0 and I2 is close to 0 deg as calculated from equation (4.6).

$$\theta_{fault} = \theta_{I0} - \theta_{I2} \tag{4.6}$$

However, if the fault is on one of the other two phases, the angle difference is displaced by approximately plus or minus 120 deg based on the faulted phase. Figure 4.6 shows the difference in phase angles for a fault shorting 2.5% of the reactor turns on each of three phases using phase A referenced symmetrical components. The blue trace shows the angle for a fault on phase A. The red trace shows the angle is +120deg for a fault on phase C, and the black trace shows the angle is -120deg for a fault on phase B.

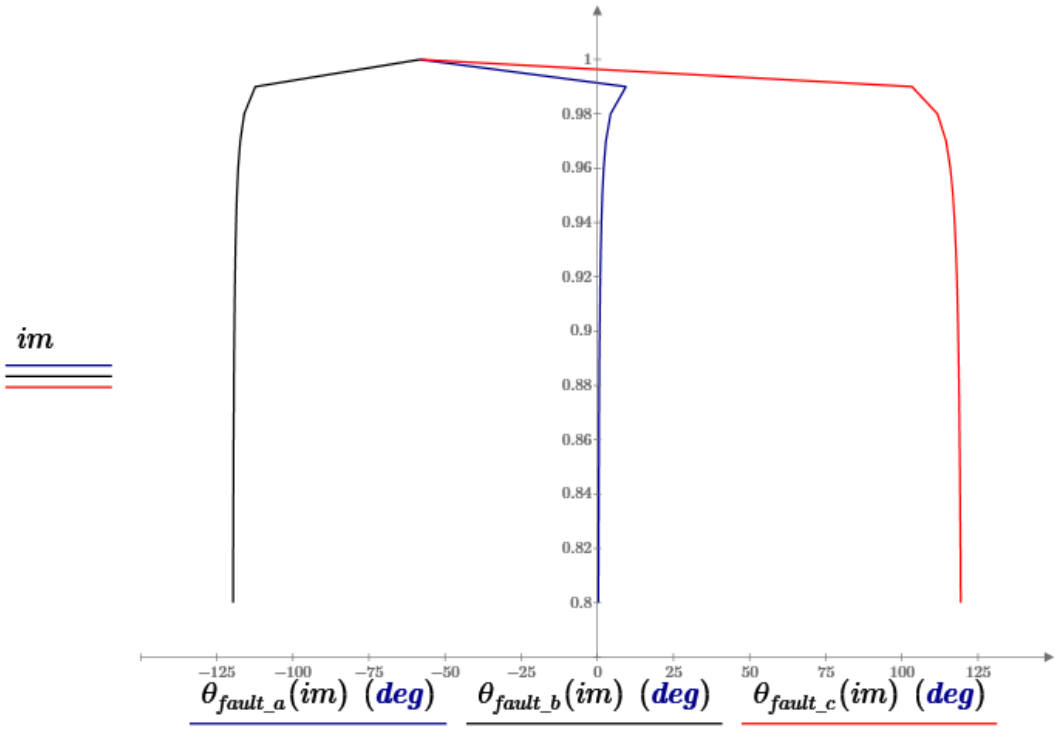

Figure 4.6: Angle difference between zero sequence current and negative sequence current using A referenced components with fault on phase A (blue), phase B (black) and phase C (red) as system voltage balance varies respectively.

4.5. Summary

This chapter introduced two methods to identify turn-turn faults in a reactor. The two-reactor method described to be a better choice to identify sensitive faults. The other method compares a reference bus voltage and a reference neutral current from an unfaulted condition against the measured $I0_{diff}$ which the relay calculates during a turn-to-turn fault. A scheme to differentiate an internal fault from an external fault using polarizing methods is discussed. The calculations in the chapter and Appendix-D show that the pickup current is not impacted for system imbalances or for faults external to the reactor. The scheme can detect turn-to-turn faults and identify the faulted phase. The following chapter tests the logic in a transient simulation program.

5. SIMULATION STUDY

Chapter 2 introduced the software used in this research and described the setup of the model used. This chapter will discuss the observations made from the simulations considered in this research. Based on real installations of protective equipment the measurement instruments, measurements from of currents and voltages taken at similar locations in the simulated system will be plotted.

The ATPdraw software provides free and comfortable design of circuit models and plotting for electromagnetic transient conditions. The design of the circuit was discussed in Chapter 2. Using this circuit design, we observe the currents and voltages at different points in the circuit and compare them with some normal operating conditions to determine signatures for faults. Each test condition is described separately.

5.1. Turn-To-Turn Fault in Balanced System Condition:

In an ideal condition with no system anomalies and balanced conditions, a turn-to-turn fault is created shorting 2.5% of the total impedance in phase A. The current flowing through the faulted turns is measured, although this is approximate as the accurate model of the reactor winding configuration is not available to model. The present model shorts a specified percentage of inductance on the reactor to match observable currents and voltages at measuring points. It does not take into account the effect of the mutual inductance the reactor coil has with the multiple layers on the same section, and the mutual inductance linked with other sections of the stack. Since the

design of sections and size of reactor is modular, a universal approach to measure circulating current is not possible since the currents aren't accessible in practice and are also not the primary concern for this research. Appendix C shows the calculations utilized to estimate the inductance of each coil section using the number of turns per layer. Chapter 3 described the model used for simulating the turn-to-turn faults in ATP, where the reactor coil is represented by section and not as per the actual multi-layered construction. The simulations observed in this chapter do not require the actual detailed model as current and voltage measurements are only seen from the terminals. Phase currents at the reactor terminals are plotted in Figure 5.1 for prefault conditions and Figure 5.2 for the faulted condition.

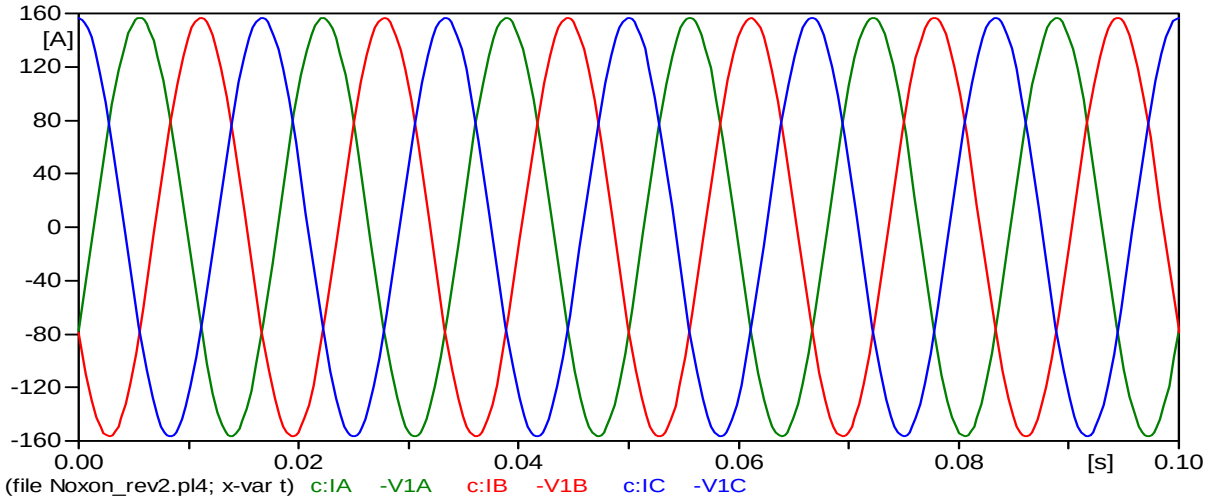

Figure 5.1: Prefault currents measured at reactor terminal

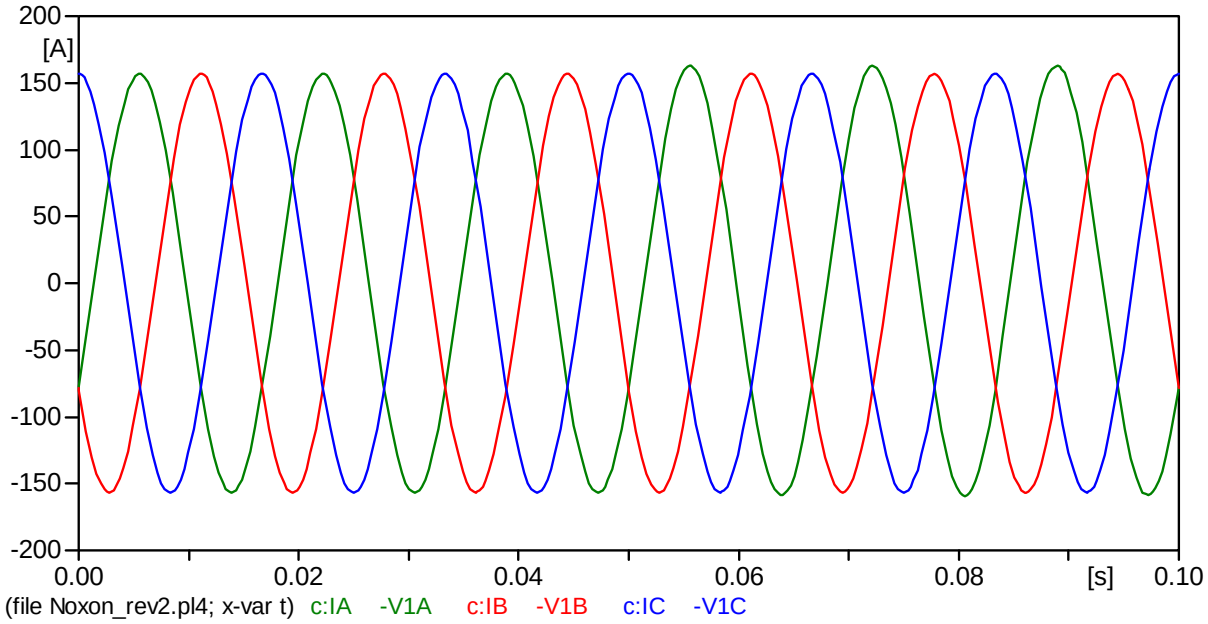

Figure 5.2: Faulted currents measured at reactor terminal with 2.5% of phase A the reactor shorted at 0.05s.

As observed, the change in the currents of the faulted phase is difficult to differentiate within the phase currents alone and is no different than system imbalance or reactor imbalance from manufacturing tolerances. The simulation study is to observe differences in steady state operation instead of transients as the relay is not intended to trip instantly. The neutral currents of the two parallel 3 phase reactors are plotted in Figure 5.3.

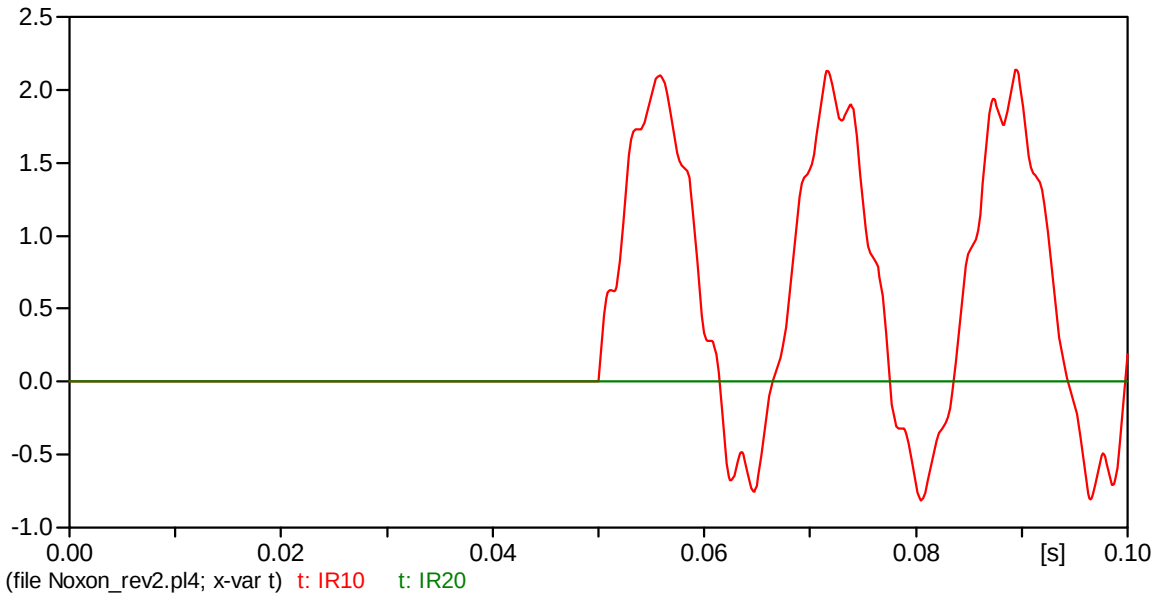

Figure 5.3: Zero sequence currents observed through the neutral of reactor 1 (Red) and reactor 2 (Green)

After fault is triggered at 0.05s, the difference in neutral current of reactor 1 (IR10) and reactor 2 (IR20) is observable. This demonstrates the advantage of using a differential current unit $I0_{diff}$ as defined in Chapter 4 to use the difference in currents between the neutrals, which is plotted in Figure 5.4, and is based on equation (4.1).

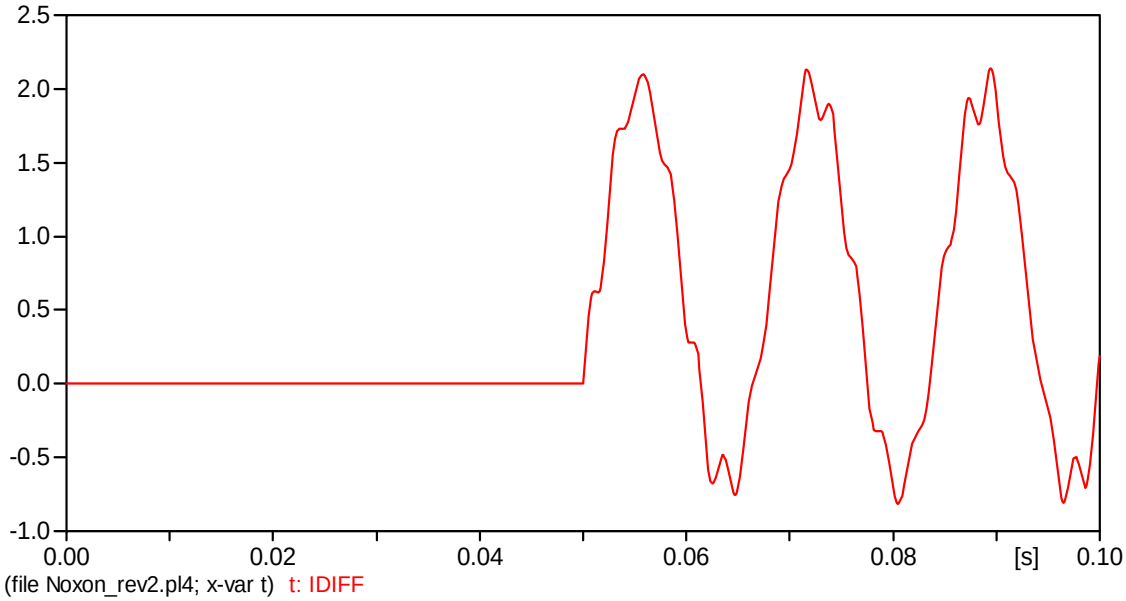

Figure 5.4: Zero sequence differential current, $I0_{diff}$

The RTDS simulations yield similar results and are not shown here.

5.2. System Imbalances

Earlier it was noticed that the drop in inductance due to the shorted turns increases the current flowing in the circuit. The same phenomena can be observed even when there is change in system voltage, which is a regular occurrence. A case with source voltage imbalance is simulated and the 3V0 measured at the terminals of both reactors is plotted in Figure 5.5.

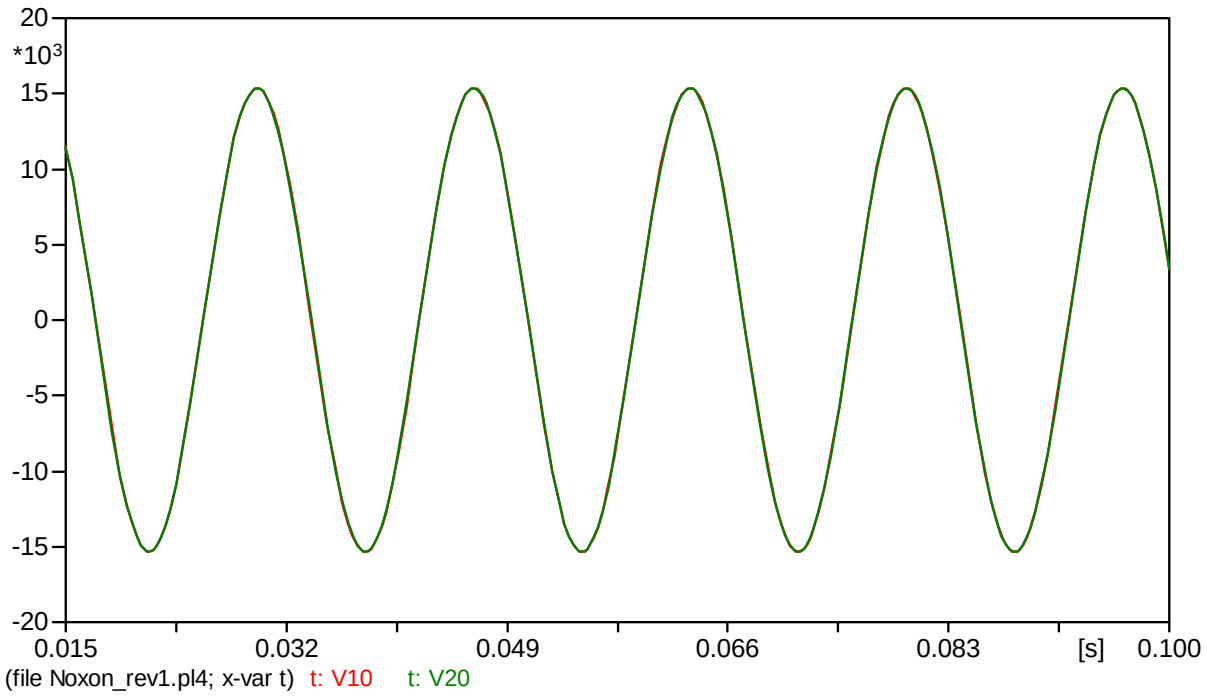

Figure 5.5: Zero sequence voltages recorded at each reactor terminal when the system voltage has a 3% imbalance. Reactor 1 (with turn-to-turn fault) in red and reactor 2 in green

Both the reactors seen the same imbalance in voltage. In the same simulation, a turn-to-turn fault was triggered at t=0.05s to observe the $I0_{diff}$ quantity. Figure 5.6 shows the neutral currents in each reactor where a change in magnitude due to the fault can be observed between them.

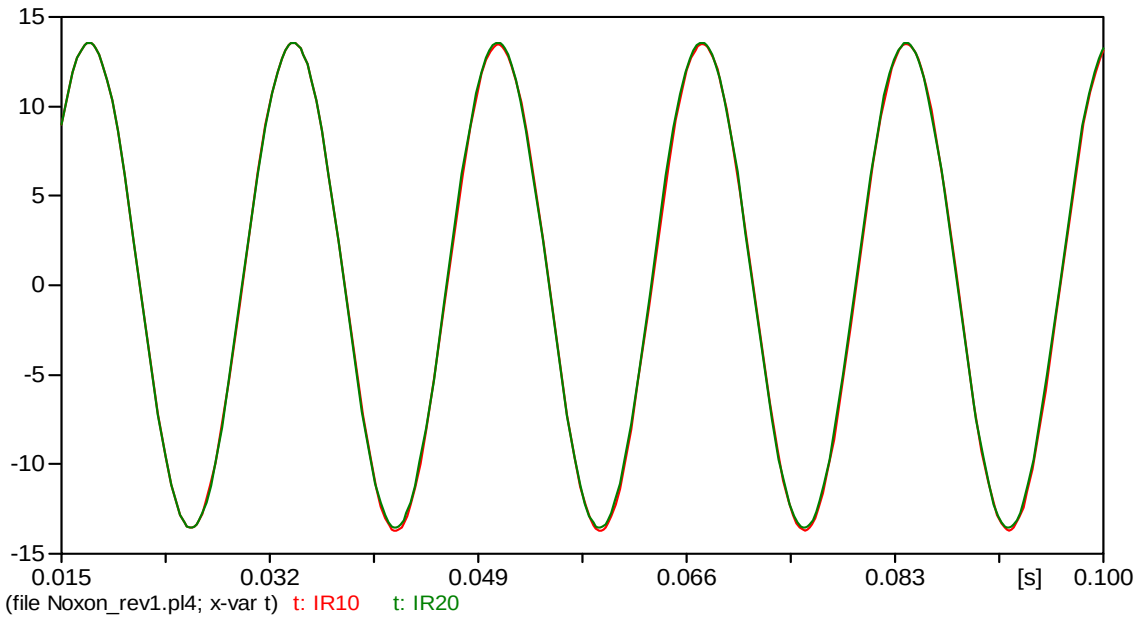

Figure 5.6: Zero sequence currents observed between the two reactors. Reactor 1 in red and reactor 2 in green.

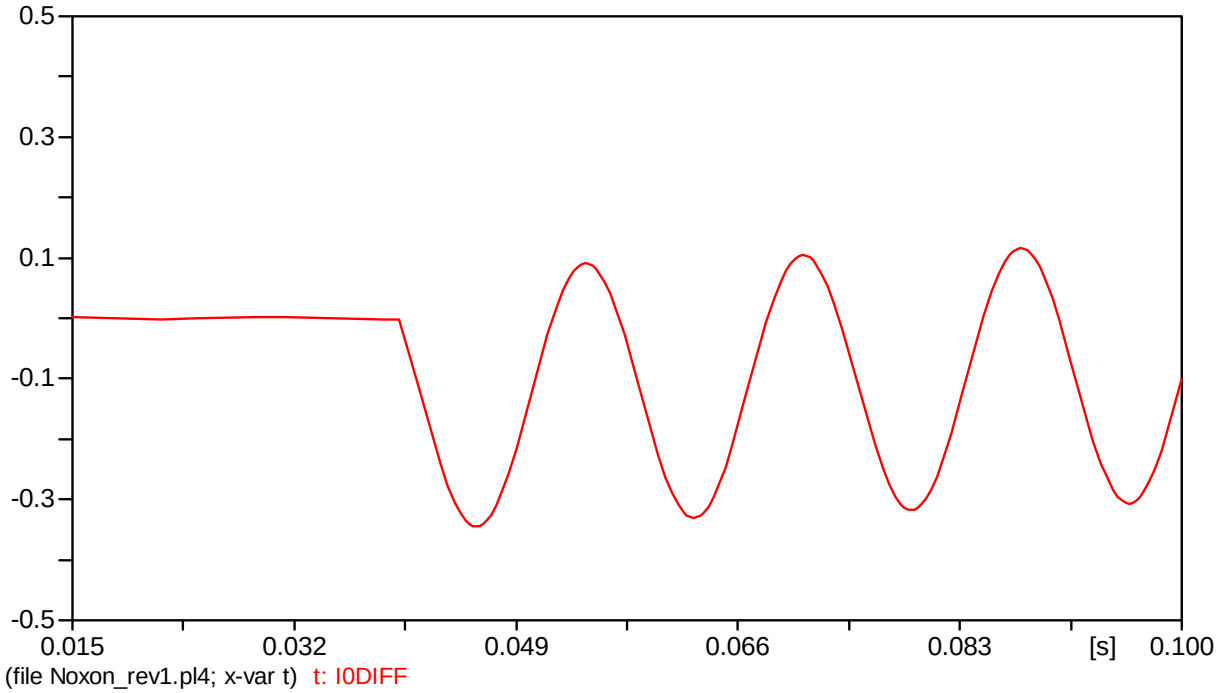

Figure 5.7: Differential zero sequence current $I0_{diff}$ for case with system imbalance and a turn-to-turn fault at 0.05 sec.

There is a noticeable change in $I0_{diff}$ when the fault occurs as seen in Figure 5.7. The pre-fault $I0_{diff}$ is 0A Peak, whereas the $I0_{diff}$ during the fault is at 0.3A peak which corresponds to 0.7% of the reactor shorted. This was a case with a perfectly balanced set of reactors, hence the standing zero sequence current difference is not noticed. The system imbalance does not impact $I0_{diff}$.

5.3. Fault External to Reactor

In this case a SLG fault is simulated at the bus to observe the response of the $I0_{diff}$ element. Since this is a system fault and not internal to the reactors, the fault effect should be the same on both reactors. Figure 5.8 shows the neutral currents in both reactors with a turn-to-turn fault. Note the dc offset with very slow decay. Figure 5.9 shows the differential current $I0_{diff}$.

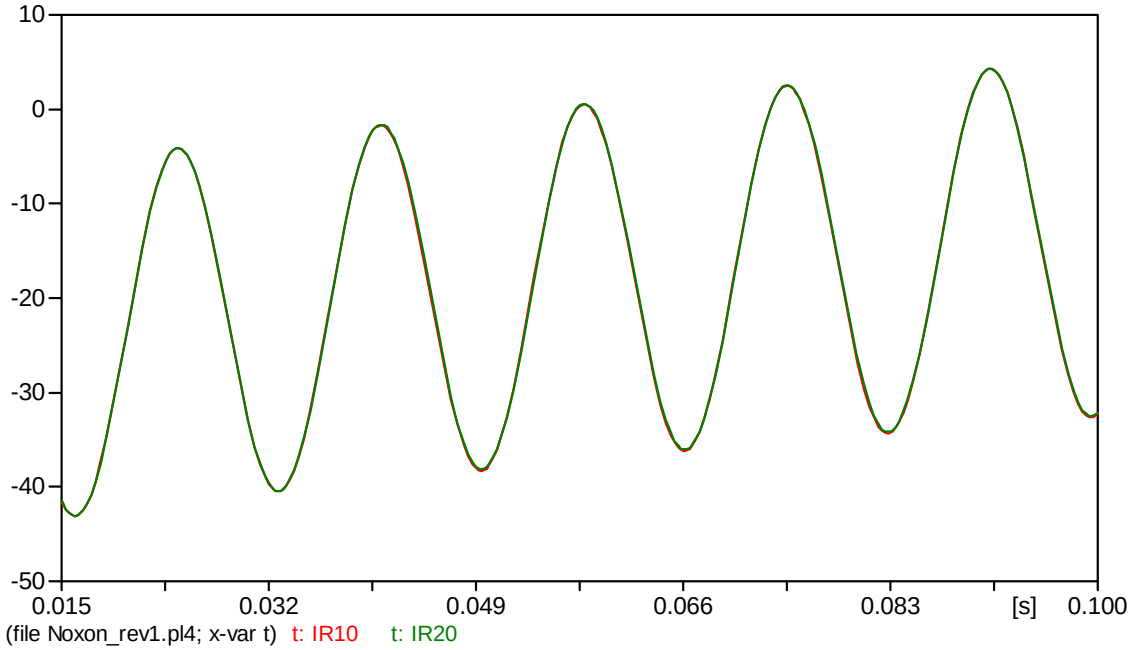

Figure 5.8: Zero sequence currents of reactors during ground fault on bus with reactor 1 current in red and reactor 2 current in green.

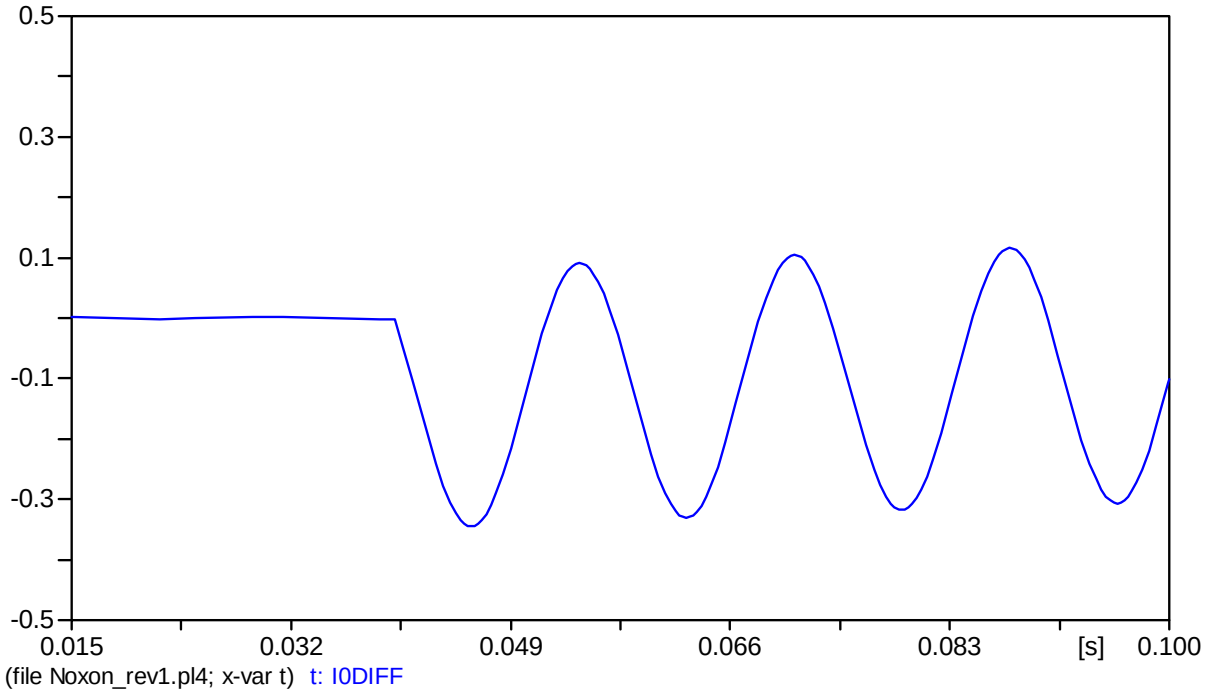

Figure 5.9: Zero sequence differential current of the two reactors with a ground fault on the bus.

The neutral current magnitudes are very high compared to the earlier turn-to-turn fault cases. The magnitude of the fundamental component of $I0_{diff}$ is 0.3A peak which is smaller than the current for the case of 0.7% of the winding shorted. This shows a limit of sensitivity. The relay will act on filtered fundamental component values. Comparing Figures 5.4, 5.7 and 5.9 notice that the $I0_{diff}$ current for the external fault has a direction opposite to the condition with turn-to-turn fault.

The trip response of turn-to-turn fault protection should be delayed by at least 30 cycles to allow external fault protection elements to take precedence. The external fault will be cleared, removing the $I0_{diff}$ current before the time delay expires. This is further explained later in the proposed logic diagram.

5.4. Identification of the Faulted Phase

In previous section, schemes were demonstrated to effectively identify turn-to-turn faults. However, the phase which has the fault is not identifiable with just the neutral current. As described in Chapter 4, a separate indication is needed to identify the faulted phase. It can be noted that in a faulted condition, the neutral current (or 3I0) is the same for a fault on any of the phases. However, the angle of the calculated negative sequence current will be different for a fault on each phase if calculated using the Phase A components. Comparing the phase angle of the negative sequence current with respect to the phase angle of the zero sequence current can indicate the faulted phase. The same can be viewed if the faulted phase doesn't change when the Phase B or Phase C referenced symmetrical components are used.

In Figure 5.10, A phase is faulted and the currents I0 and I2 are plotted using the Phase A referenced components. Figures 5.11 and 5.12 repeat using the Phase B and Phase C referenced components

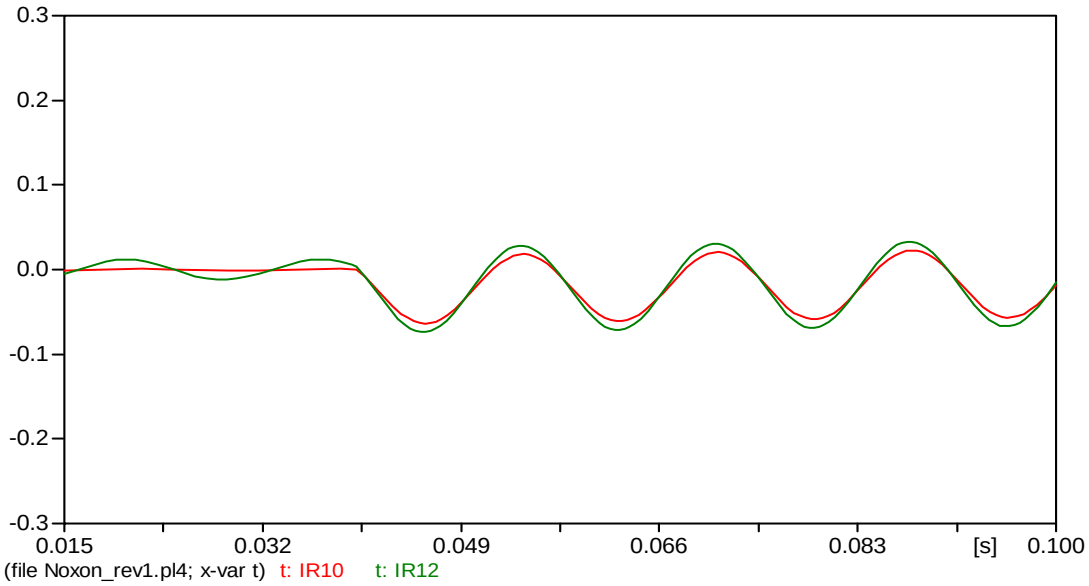

Figure 5.10: Plot of zero sequence current and the negative sequence current calculated using A reference components for a Phase A turn-to-turn fault.

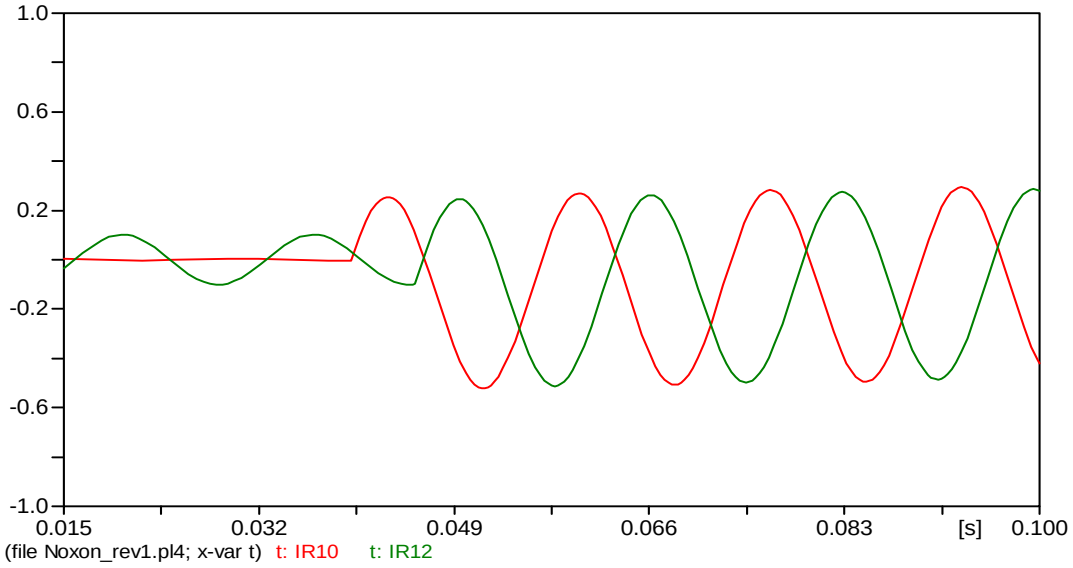

Figure 5.11: Plot of zero sequence current and the negative sequence current calculated using A reference components for a Phase B turn-to-turn fault.

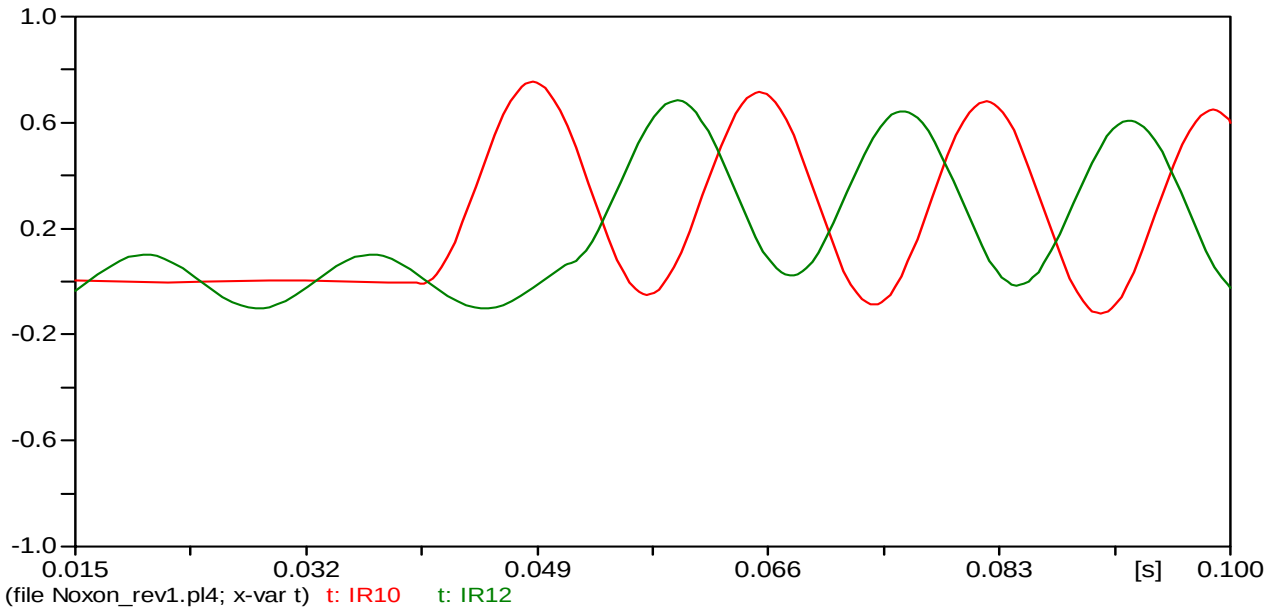

Figure 5.12: Plot of zero sequence current and the negative sequence current calculated using A reference components for a Phase C turn-to-turn fault.

Observing the contrast in the phase angle between the zero sequence currents and negative sequence currents in different reference frames we can identify the faulted phase. Simultaneous calculations can be performed in a microprocessor relay to identify the correct faulted phase or results from just one phase reference can be used to see all sections of the reactor.

5.5. Trip Logic

Based on derivations in Chapter 4 and the results shown in this chapter trip logic can be developed.

a. The turn-to-turn fault protection is to be active only for sensitive (low fault current) fault detections. Faults with a clear distinction in phase

currents can be picked up by a conventional current imbalance protection element.

b. A time delay is included to ensure other protection elements take precedence for cases with large neutral currents. A lockout relay (86) is used to block the turn-to-turn fault element for faults picked up by other elements.
c. The element will be blocked for a standby imbalance, 3V0, above a threshold range. In ideal conditions 3V0=0.
d. The phase angle difference between zero sequence current and Phase A referenced negative sequence current to identify the faulted phase winding.

Based on the conditions listed above, trip logic can be defied as shown in Figure 5.13.

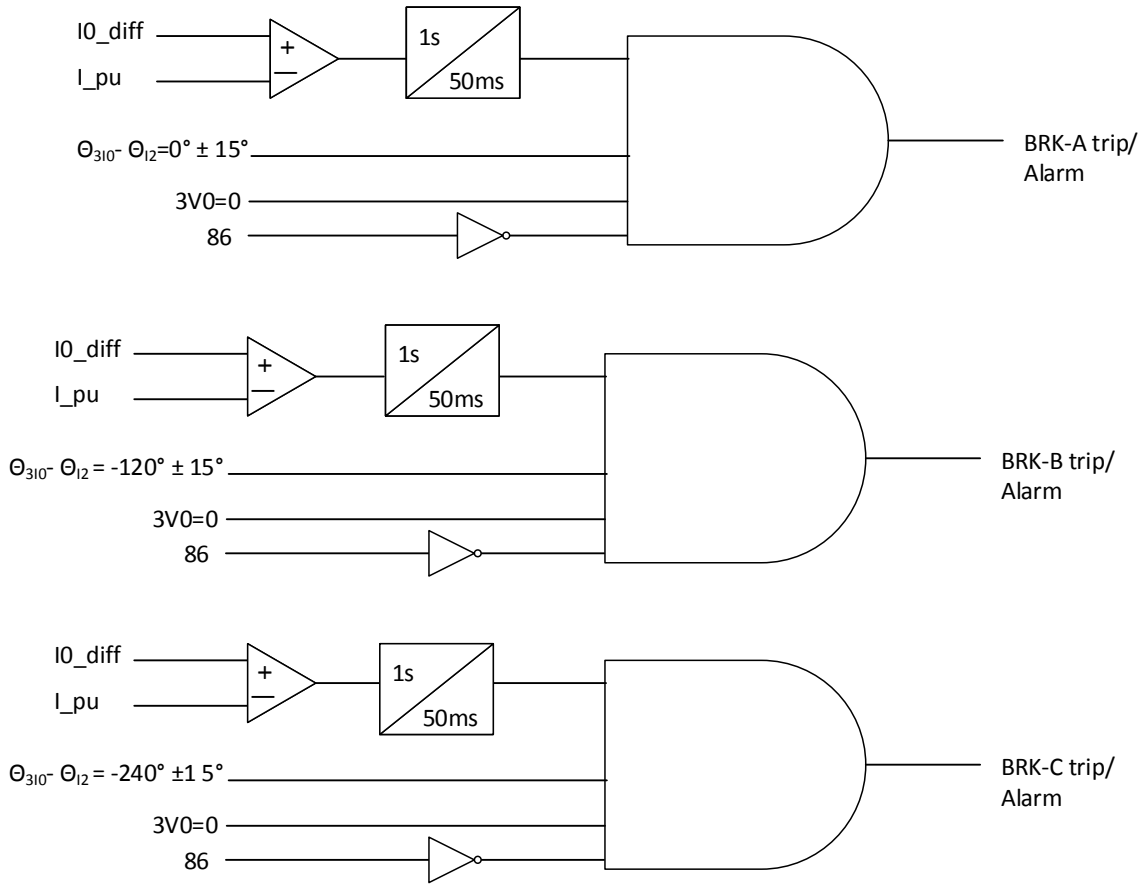

Figure 5.13: Trip logic to identify fault on a phase of the reactor

5.6. Summary

This chapter demonstrated the concept of comparative measurement of zero sequence currents between faulted and unfaulted reactors for providing information to discriminate shorted turn faults from system imbalances and external faults. Computer simulation with a limited runtime was used to benchmark the measurement performance for the change in neutral current, and the ability to discriminate faults and the identification of faulted phase**.**

6. HARDWARE TESTING

In this chapter, the hardware setup used to test and prove the protection scheme proposed earlier is will be discussed. The hardware setup uses simple reactor coils partly purchased and partly wound manually in the university. The calculations required to size the right impedance of the reactor bank is discussed followed by some observations made in the final setup.

6.1. Preliminary Calculation for Lab Test Setup

This project partly funded a hardware test setup built by a senior design team. The sizing of the reactor coils required for the setup was calculated, test coils of known inductance and similar material were hand wound and the circuit was constructed as shown in Figure 6.1.

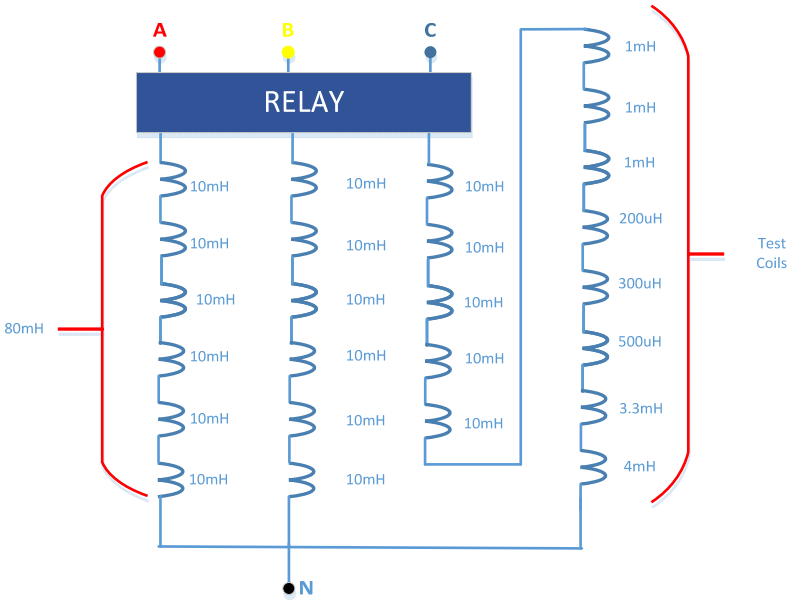

Figure 6.1: Circuit diagram of hardware test setup

The source voltage available in the lab is 110V (line to neutral) and the maximum secondary steady-state current read by the relay is limited to 5A. Therefore, the reactors in each phase were designed such that the current in the circuit is limited to less than 5A. Equations (6.1) and (6.2) calculate the inductance per phase at 60Hz system frequency for a wye connected reactor.

$$X_{star} = \frac{V_{an}}{I_{an}} = 22\Omega \tag{6.1}$$

$$L_{star} = \frac{Im(X_{star})}{\omega} = 58.357mH \tag{6.2}$$

The reactors used in the set up are copper wire with a 15AWG cross section. The set up consists of several coils connected in series on each phase, with one phase having a set of test coils of different inductances to allow varying percentages of the reactor to be shorted. Three coils on the test coil leg are hand wound to smaller inductances of 200µH, 300µH and 500µH respectively.

6.2. Hardware Setup and Observations

The final hardware test set up is constructed similar to circuit in Figure 6.1 and are shown in Figure 6.2. The setup has four legs, three of which are the three phases, and one has the set of test coils with shorting connections to imitate turn-to-turn fault conditions. A 411L relay is used for recording the phase voltages, currents and the neutral current for analysis in post-processing software.

The coils on two of the phases have six coils of 10mH connected in series for a total of 60mH. The phase where faults will be tested has five coils of 10mH

each and another leg dedicated for small test coils totaling to 10mH. The phase with 50mH is connected in series with the leg with the test coils for completing the inductance to match the other phases.

The inductance measured on each of the phases (80mH) was higher than the calculated inductance (60mH). This is because the coils were stacked on top of each other. The coils have a common axis and share a flux path where the flux from one coil links with the coil adjacent to it.

6.3. Test Procedure and Test Series Conducted

The test procedure involved simple connections of the test coils where a set test coils was bypassed while they were still magnetically coupled with the rest of the reactor to imitate shorted turns. The inductance of the faulted phase was reduced therefore raising the currents in that phase and generating residual current in the neutral. Events were recorded in steady state using a SEL 411L relay. The events were then exported as COMTRADE files to be analyzed in SEL Synchrowave and Mathcad.

The tests were done in increasing steps of bypassed inductance on the test coils. The first test was done in steady-state with no fault on the winding. This is done to calibrate the calculated limiting resistor, R_{Lim}, as discussed in Chapter 4.

Shunt reactors for high voltages in the field are monitored with protection elements such as current differential, overcurrent, restricted earth fault and voltage unbalance protection as mentioned in Chapter 1. Overcurrent protection

takes measurements of the flow of current in one direction and requires only one set of CTs, although voltage measurement from potential transformers is required to determine the direction of current. However, in the case of a current differential element the current transformers need to take measurements on either side of the reactor. The relay used in this project is like the one used in the field. The SEL 411L has multiple current inputs which simplifies the hardware set up to just one relay to take current measurements at the reactor terminals and at the neutral end of each phase as shown in Figures 2.2 and 3.6. Since the currents are limited to less than 5A, which is also a common current level on the secondary of most current transformers, the current input points are directly connected to the terminals of the relay. Current transformers are not utilized in this circuit. The picture in Figure 6.2 can be compared with the circuit design of the hardware in Figure 6.1.

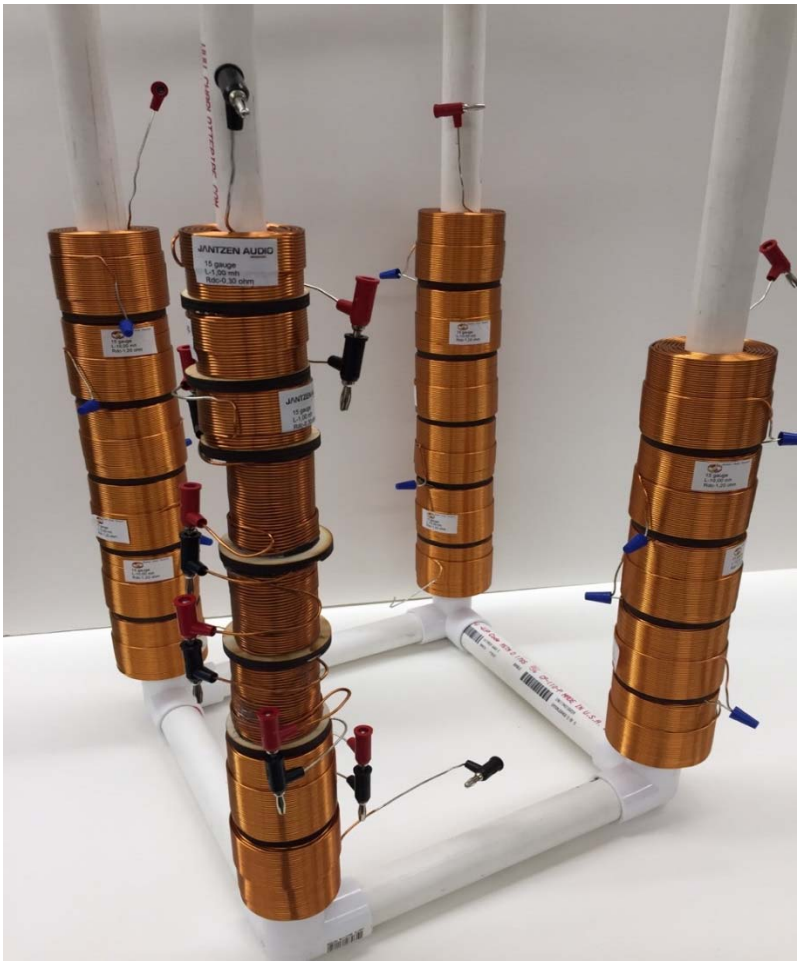

Figure 6.2: Reactor test set up with three phases and a leg with test coils for short circuit tests (front left)

6.4. Summary

This chapter introduced hardware used in this project to test the protection scheme, the calculations involved in estimating the components and the construction of the test setup. It also described the test procedure followed to achieve the results as discussed in chapter 7.

7. RESULTS AND VALIDATION

The behavior exhibited by the hardware test setup matched the simulation results to a good extent. Using the test coils on the independent leg, we could simulate turn-to-turn faults on the C phase of the reactor and record the voltages and currents seen by the relay. The tests were first done using a SEL 411L relay with a maximum sampling rate of 133 samples per cycle and then repeated with a SEL-735 power meter which offers a higher sampling rate of 512 samples per cycle. It was noticed that higher processing rate and sampling rate were beneficial in identifying the turn-to-turn fault on the reactor when there is a single reactor. In each case, the scaling factor (R_{Lim}) was first calibrated in the unfaulted condition and later utilized in every fault condition for comparing the zero sequence currents with the ratio of bus zero sequence voltage and R_{Lim}.

7.1. Test Results with SEL-400 Series Relay

Calibration of the R_{Lim} factor is necessary for calculation of the pickup current for the $I0_{diff}$ element described in Section 4.4. Figure 7.1 shows the three phase voltages and Figure 7.2 shows the currents for an unfaulted condition. It is observed that they are well balanced.

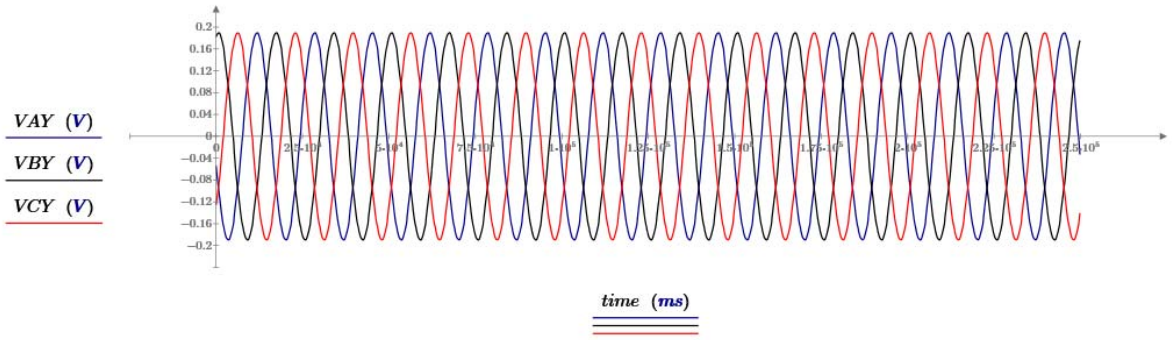

Figure 7.1: Phase voltages in unfaulted condition

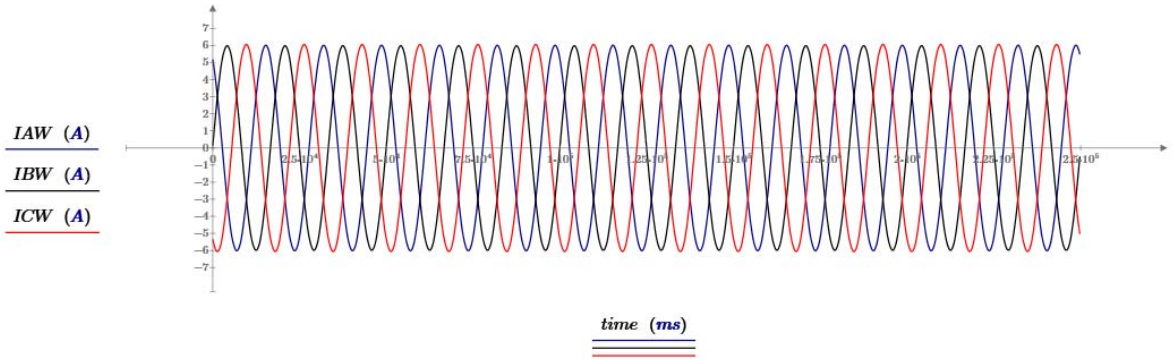

Figure 7.2: Currents in unfaulted condition

The zero sequence current ($I0W_{ref}$) and zero sequence voltage ($V0Y_{ref}$) were calculated by the relay and are plotted in Figures 7.3 and 7.4. The R_{Lim} factor is the ratio of the zero sequence voltage and zero sequence current shown in (7.1). R_{Lim} is not a fixed number as the voltage $V0Y_{ref}$ and current $I0W_{ref}$ are variable over a period.

$$R_{Lim} = \frac{V0Y_{ref}}{I0W_{ref}} \tag{7.1}$$

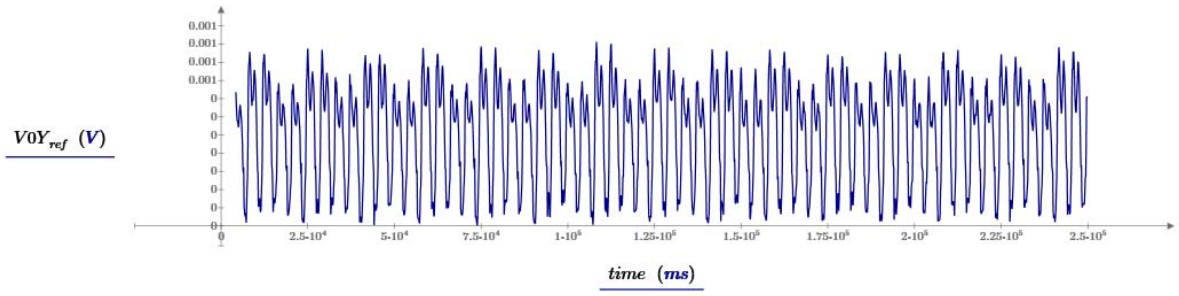

Figure 7.3: Zero sequence reference voltage ($V0Y_{ref}$)

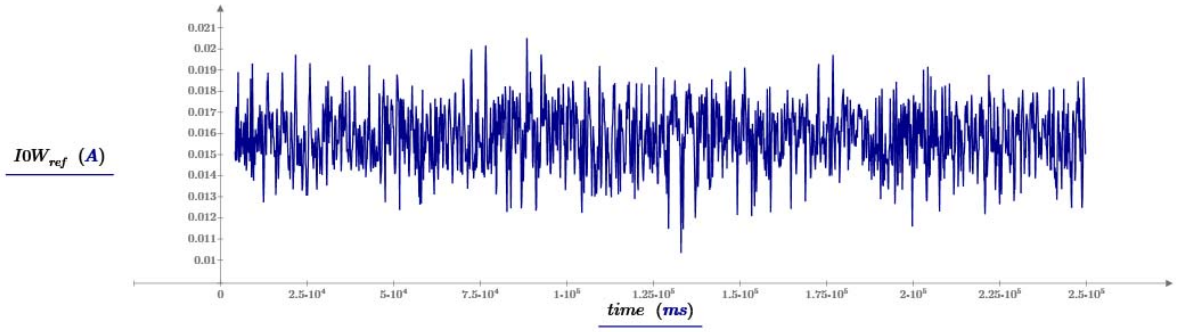

Figure 7.4: Zero sequence reference Current ($I0W_{ref}$)

Since the system is balanced, the zero sequence voltage in Figure 7.3 and current in Figure 7.4 are almost negligible. Based on these results, R_{Lim} was set based on a set of voltage data points and current data points. The pickup current ($I0_{diff}$) is defined as per Equation (7.2)

$$I0_{diff} = \left| \frac{V0Y}{R_{Lim}} - I0W \right| \tag{7.2}$$

A series of fault cases were conducted, in each case $I0_{diff}$ was calculated, and the results will later be used to set the pickup current for the turn-to-turn fault element.

Figures 7.5 to 7.10 show the pickup $I0_{diff}$ current calculated by the relay as the shorted inductance varied over 3 mH, 3.3 mH, 3.5 mH, 4 mH, 7.3 mH and 10 mH in steps. A combination of small (0.25 % for 3 mH) and large (12.5 % for 10 mH) inductances was shorted to observe change in the $I0_{diff}$ element. Notice the noise levels observed in the Figures 7.5 to 7.10, which is due to extraction of raw unfiltered sinusoidal quantities from the relay sampling at 133 samples/cycle.

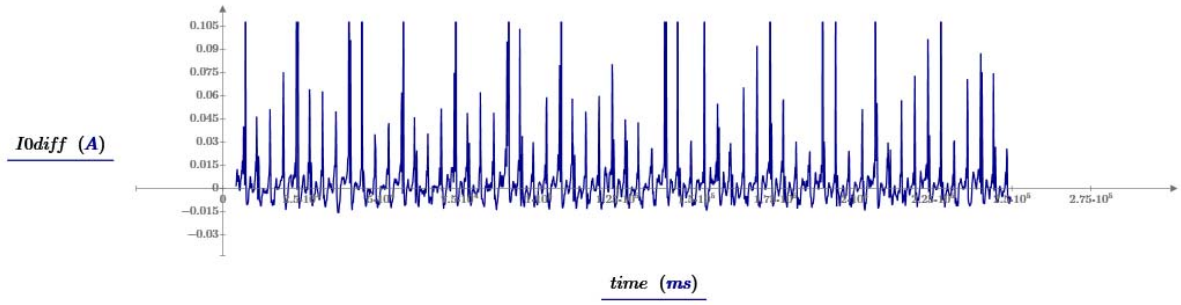

Figure 7.5: $I0_{diff}$ with fault shorting 3 mH of the inductance

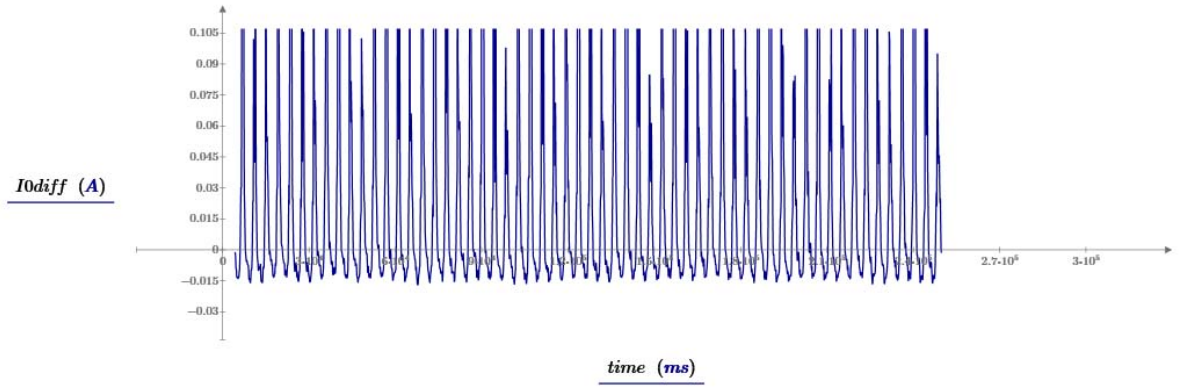

Figure 7.6: $I0_{diff}$ with fault shorting 3.3 mH of the inductance

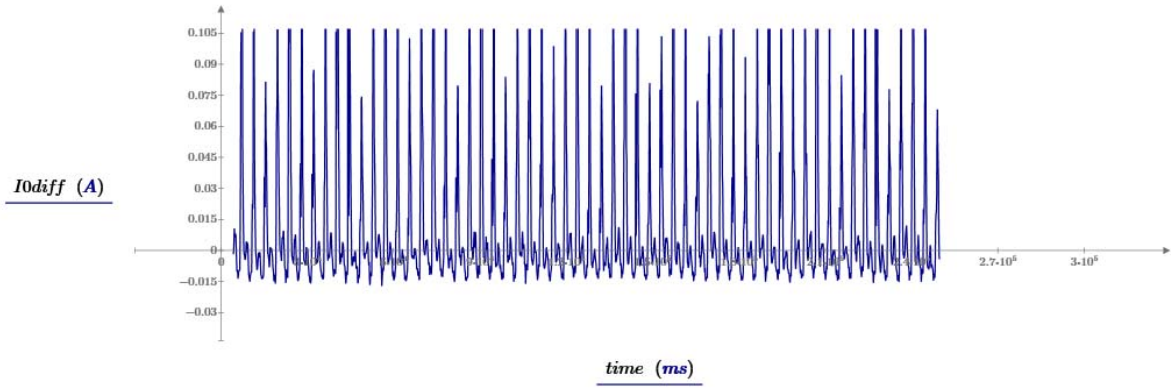

Figure 7.7: $I0_{diff}$ with fault shorting 3.5 mH of the inductance

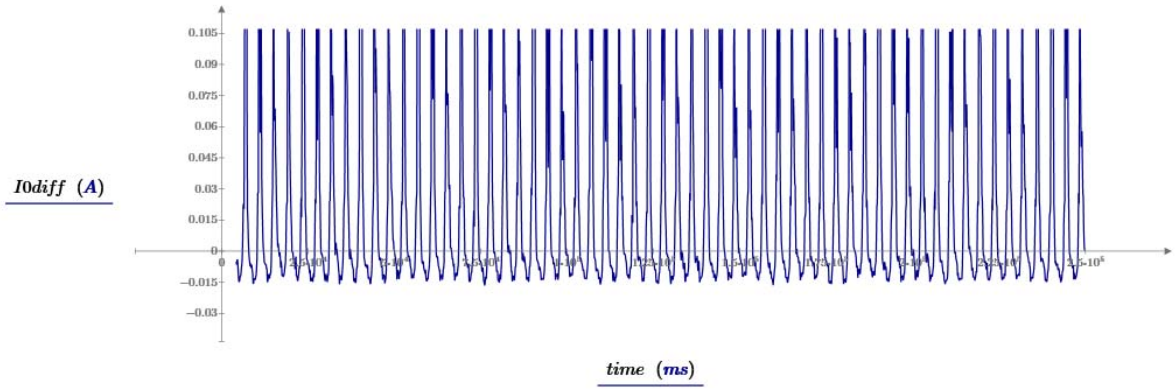

Figure 7.8: $I0_{diff}$ with fault shorting 4 mH of the inductance

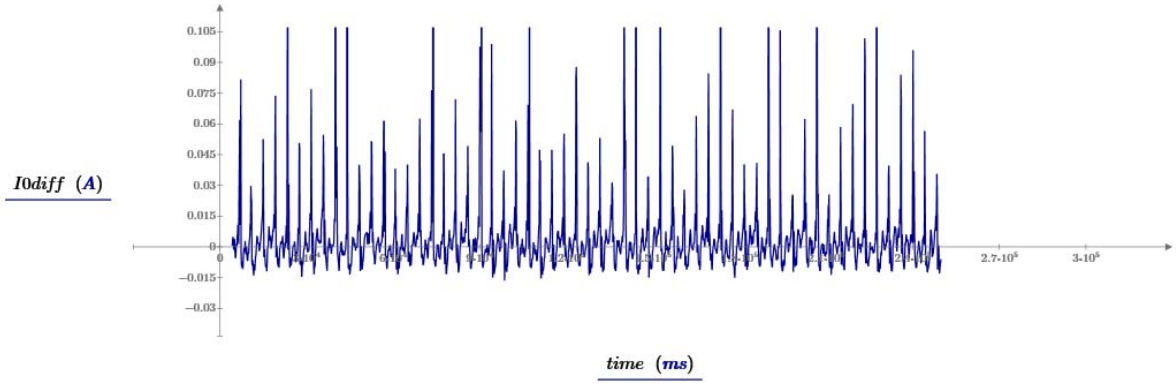

Figure 7.9: $I0_{diff}$ with fault shorting 7.3 mH of the inductance

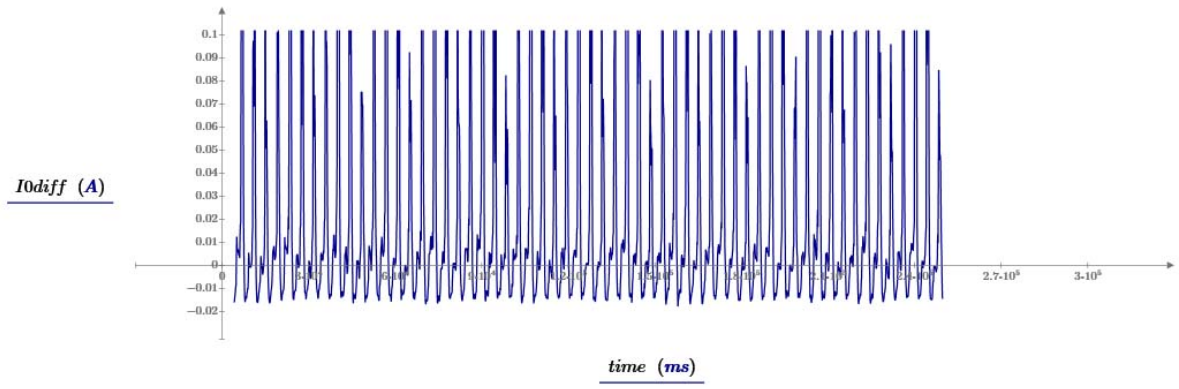

Figure 7.10: $I0_{diff}$ with fault shorting 10 mH of the inductance

Observing the figures, it can be noticed that no valuable information can be identified from the SEL-411L relay sampling data at 133 samples per cycle. This was not sufficient for sensitive turn-to-turn fault detection.

7.2. Test results with SEL-735 Power Meter

The SEL 735 IED is a power meter used specially in metering applications for revenue purposes. Accuracy of the meter is of high priority in revenue applications, hence this IED is provided with a higher sampling rate of 512 samples per cycle. Since this has a higher sampling device than the SEL-411L, it was used to repeat the tests mentioned in Section 7.1 to try to achieve better results.

Similar to the procedure in Section 7.1, the first test calibrates the R_{Lim} factor by observing the unfaulted condition on the reactor bank. Figure 7.11 shows the phase voltages and Figure 7.12 shows the phase currents for normal balanced operation.

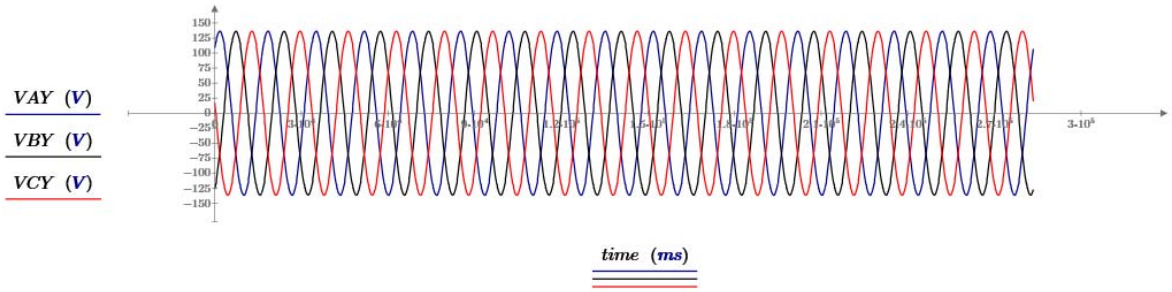

Figure 7.11: Phase voltages in pre-fault condition

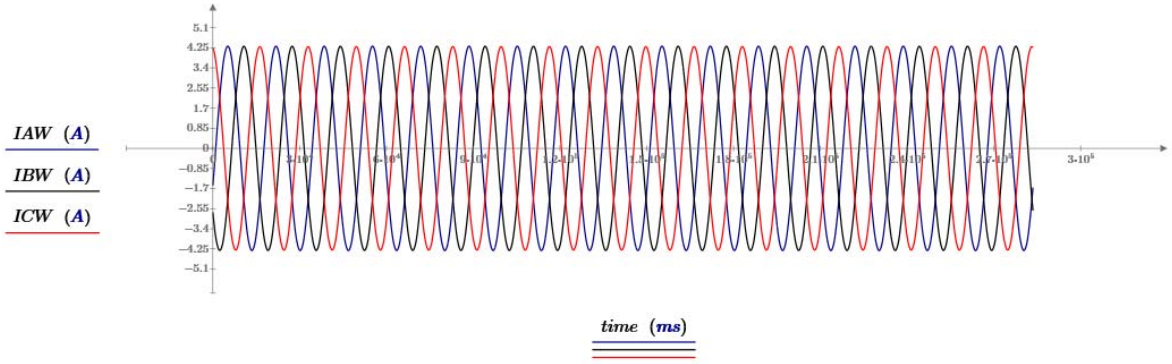

Figure 7.12: Phase currents in pre-fault condition

Figures 7.13 and 7.14 show the raw zero sequence voltage ($V0Y_{ref}$) and raw zero sequence current ($I0W_{ref}$) measured by the relay at the terminals of the reactor which will be used as reference quantities in unfaulted condition to calculate and compare $I0_{diff}$ in each fault condition. Figure 7.15 shows the R_{Lim} calculated with the available $V0Y_{ref}$ and $I0W_{ref}$. Figures 7.16 to 7.22 show the $I0_{diff}$ calculated in each fault case by shorting inductance in steps of 200µH, 1mH, 2 mH, 3 mH, 4 mH, 7.3 mH and 10 mH on the test leg of the hardware setup.

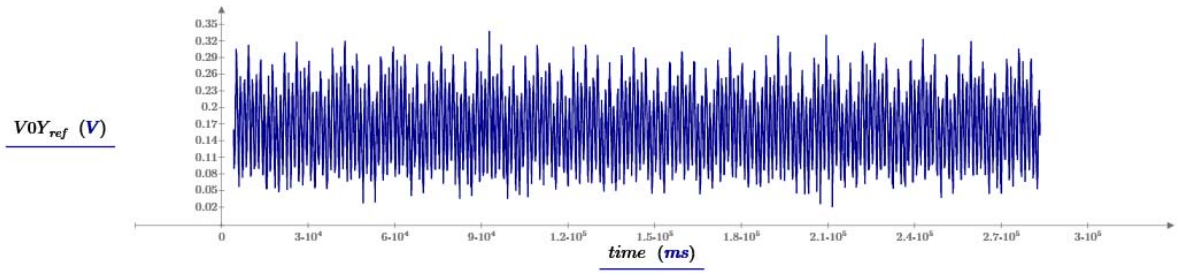

Figure 7.13: Zero Sequence reference voltage ($V0Y_{ref}$) in prefault condition

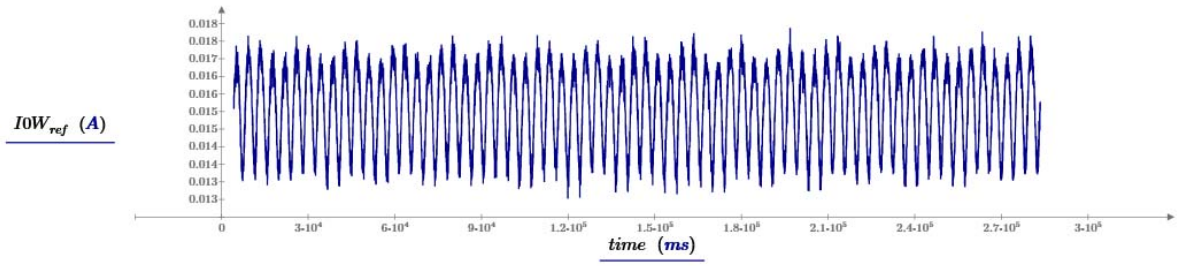

Figure 7.14: Zero sequence reference current ($I0W_{ref}$) in prefault condition

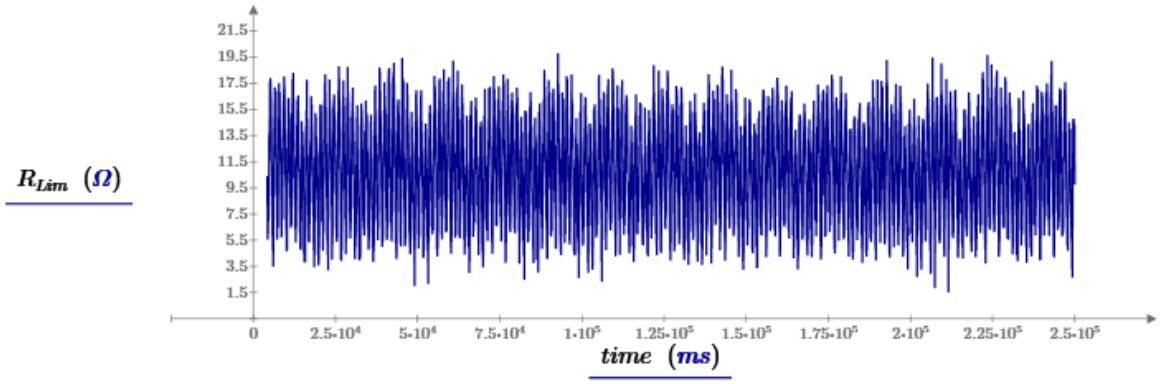

Figure 7.15: Reference factor R_{Lim} calculated using equation (7.1).

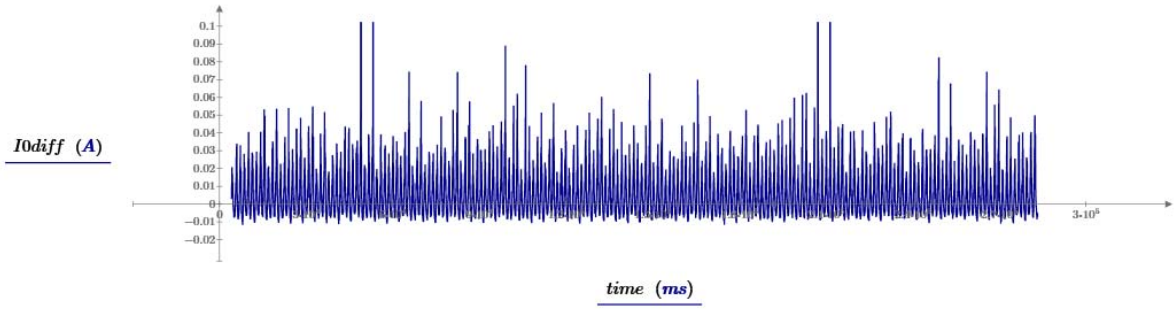

Figure 7.16: $I0_{diff}$ with fault shorting 200µH of the inductance

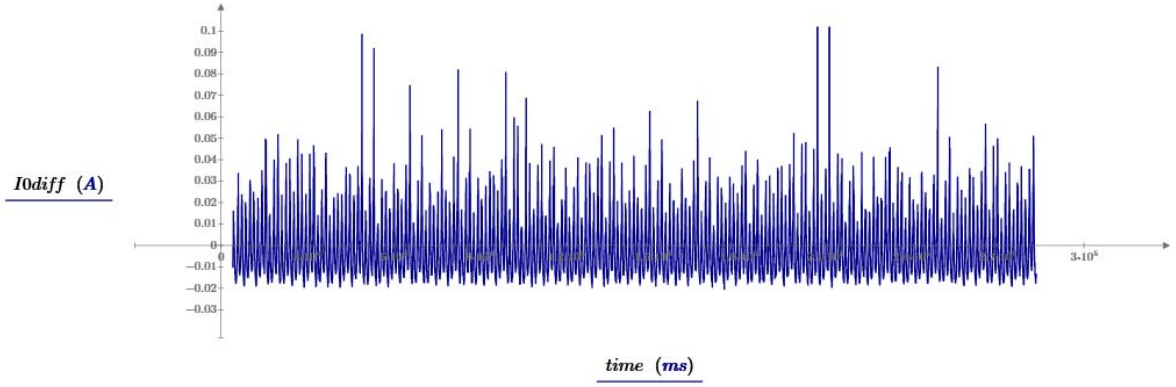

Figure 7.17: $I0_{diff}$ with fault shorting 1mH of the inductance

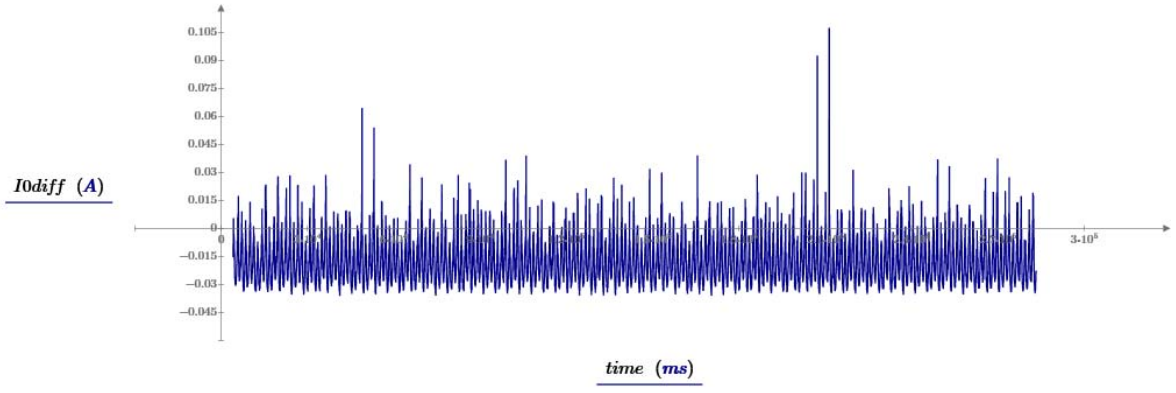

Figure 7.18: $I0_{diff}$ with fault shorting 2mH of the inductance

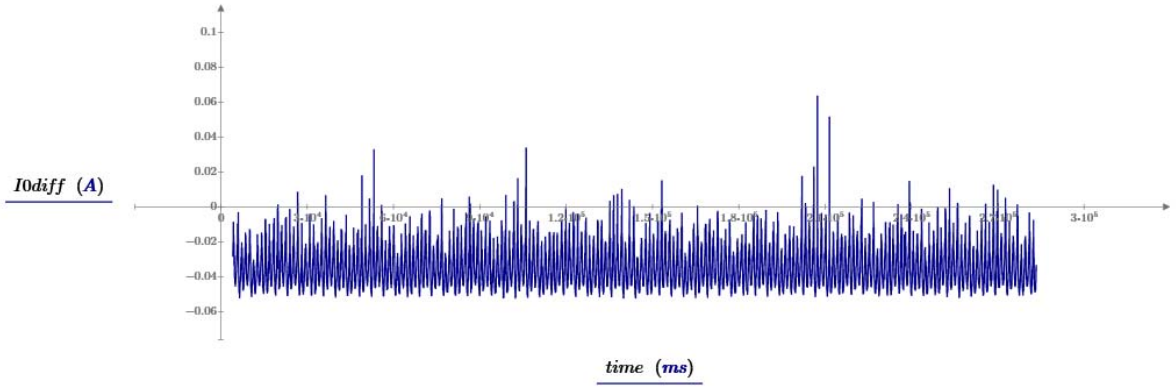

Figure 7.19: $I0_{diff}$ with fault shorting 3mH of the inductance

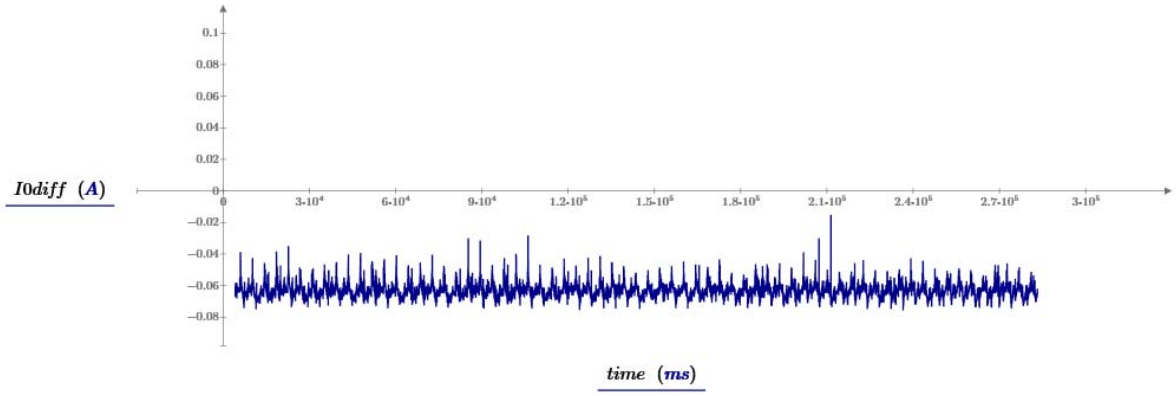

Figure 7.20: $I0_{diff}$ with fault shorting 4mH of the inductance

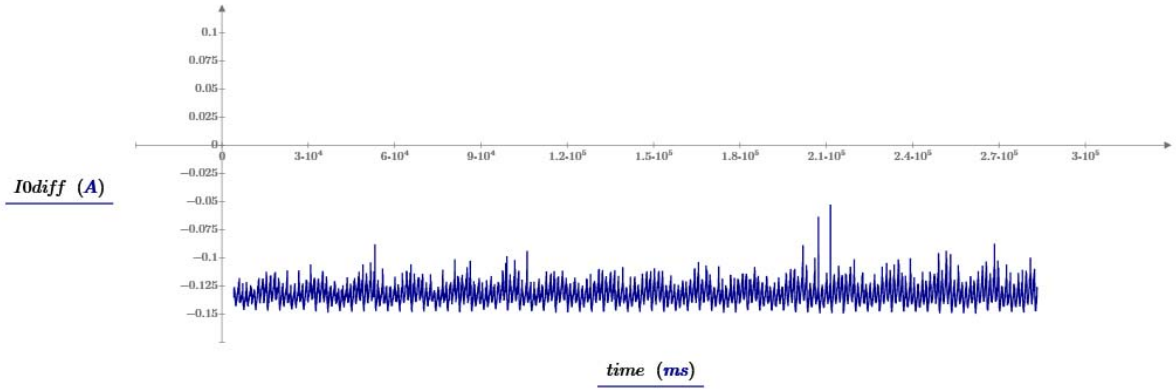

Figure 7.21: $I0_{diff}$ with fault shorting 7.3mH of the inductance

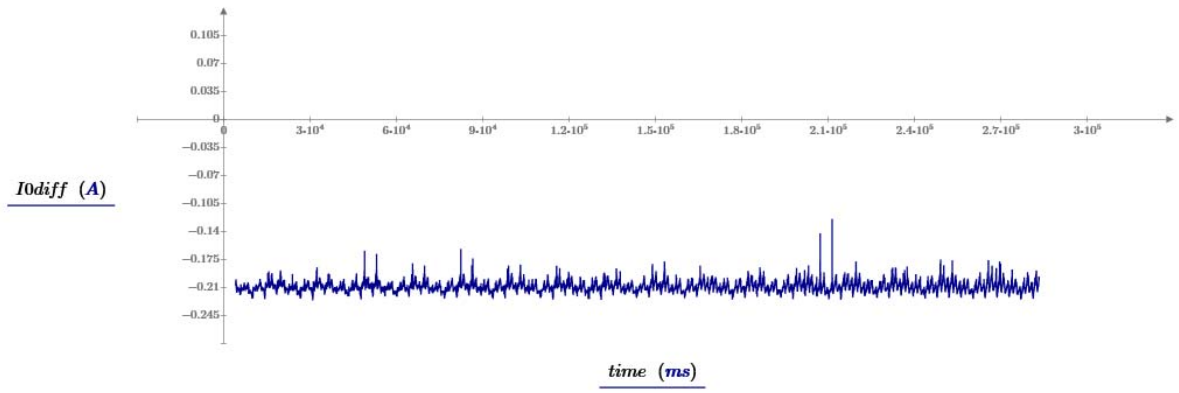

Figure 7.22. $I0_{diff}$ with fault shorting 10mH of the inductance

It can be observed from Figures 7.16 to 7.22 that the $I0_{diff}$ is offset from the origin based on the amount of inductance shorted by the fault. This offset can be used for fault detection. It can be concluded from these observations that a higher sampling rate is required in the relay to observe such minute changes in the reactor impedance.

7.3. Curve Fitting and Simplified Illustration of $I0_{diff}$

In the earlier sections of this chapter, we observed that the data gathered from the tests in the lab has some noise as these are unfiltered raw data. Oscillations in the output and pickup element are also observed due the movement of the supply frequency when tests are performed. The system frequency is not fixed to an exact 60.0Hz, where some error or change in frequency is observed due to several factors caused by grid dynamics. Observing the pattern of the oscillations, the plot can be simplified to trace the mean and have clear illustrations from the pickup element.

Using the Matlab™ function called “fit”, the different cases of the faults seen in the previous section can be plotted as observed in Figure 7.23. The $I0_{diff}$ in the steady-state, or reference state, is set at 0, each line is the absolute value of $I0_{diff}$ calculated in each fault case in steps. The deviation of $I0_{diff}$ in each case is a clear indication of the magnitude of fault current. Figure 7.23 plots results only for the test results obtained from using the SEL-735 relay.

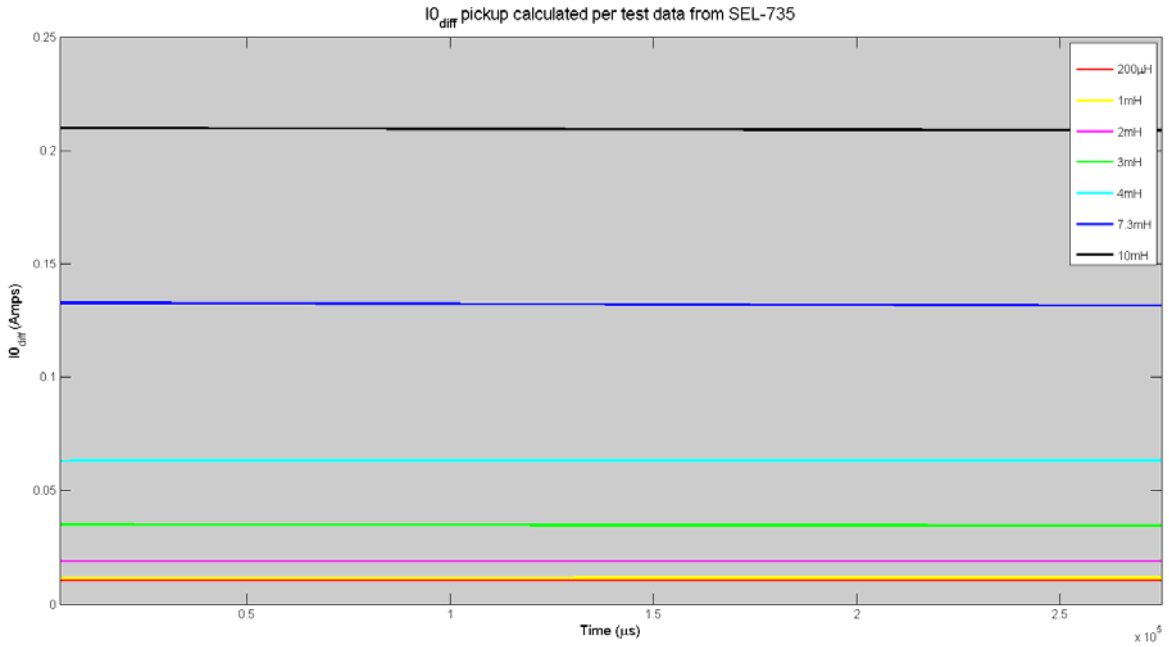

Figure 7.23. $I0_{diff}$ plotted for each test case and simplified with curve fitting

7.4. Comparing Hardware Test results with Simulation

The same observation can be made when faults are created in the Noxon ATP model. For simple comparison, only two faults in increasing steps are created and plotted in Matlab™ using the curve fitting function. Figure 7.24 shows the

offset of each plot from the reference abscissa. The simulation considering ideal conditions of the model has initial reference $I0_{diff}$ set at zero or the abscissa. The red plot shows I0diff pick up for 75mH of inductance shorted on phase A of reactor 1 in Noxon model. Similarly, the blue plot shows the offset for 150mH of inductance faulted on the reactor. The estimates are made based on primary current measurements.

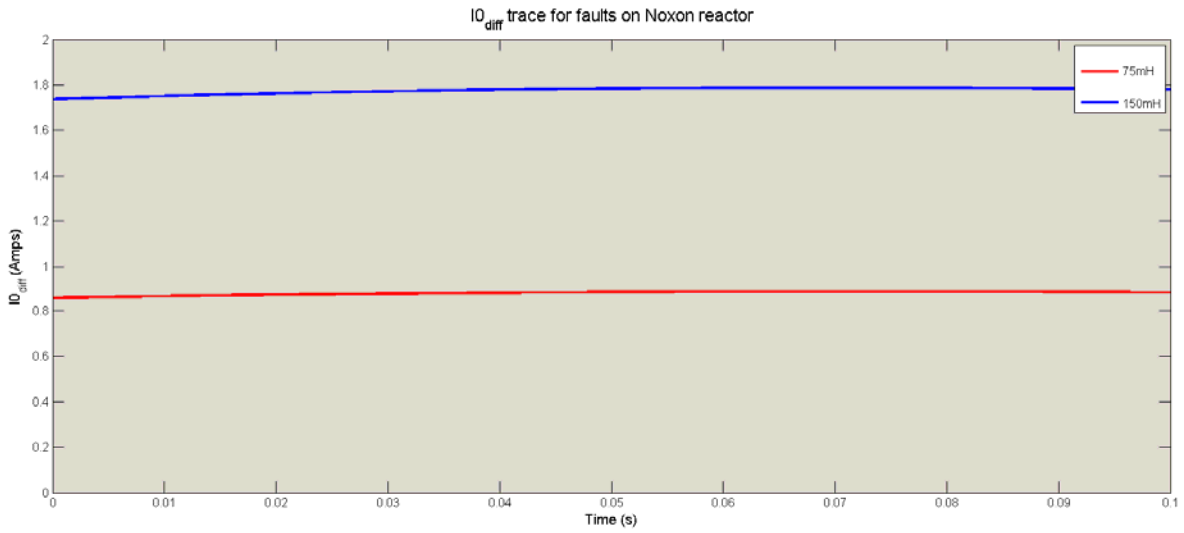

Figure 7.24. $I0_{diff}$ plotted for each faults on Noxon ATP model and simplified with curve fitting

7.5. Alternate Method- Comparing Zero Sequence Impedance of the Reactor

The scaling factor R_{Lim} can be viewed simply as the zero sequence impedance in an unfaulted condition of the reactor where only the magnitude is taken into consideration. In normal steady-state, the zero sequence voltage is small, while the zero sequence current is even smaller as observed in Figures 7.13 and 7.14 respectively. The factor R_{Lim} was calculated to be an average couple of ohms

in the case shown in Figure 7.15 without a fault, in normal operation. Subsequently, as the shorted coil on the phases is increased, the zero sequence current increases while the zero sequence voltage remains almost the same. The overall measured zero sequence impedance is reduced compared to R_{Lim}. Figure 7.25 shows the deviation of Z0 in each fault case from reference R_{Lim}. Based on the sensitivity of the relay measurements and system errors, the deviation of the mean of Z0 from the set reference of R_{Lim} (shown in dotted line) will provide the operating characteristic of the element. It can be observed that fault case shown with a solid red line is offset from the reference R_{Lim} in a direction opposite to the other fault cases. This is caused because the fault case of 200μH is very small and compensates the existing small imperfection or imbalance in the hardware set up. It shall also be noted that plots in Figure 7.25 are not absolute values unlike as shown in Figures 7.23 and 7.24. The operating characteristics of this method would be slightly different from the previous method as a fault of higher intensity reaches the abscissa regardless of position of reference R_{Lim}.

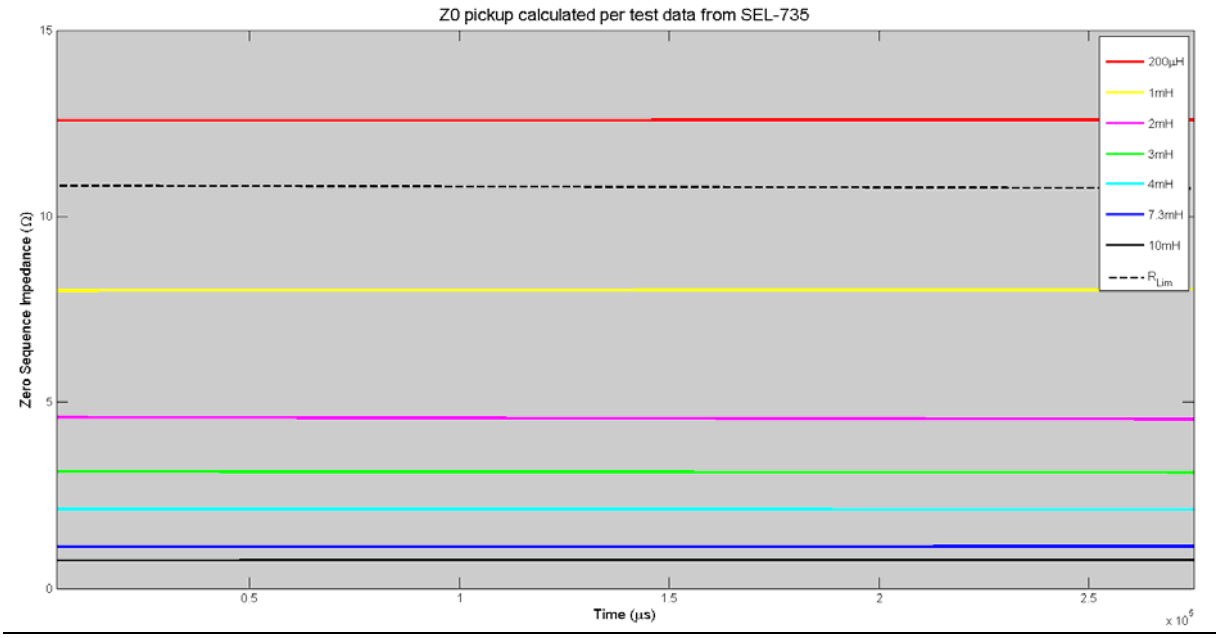

Figure 7.25: Z0 plotted after simplified curve fitting against the reference R_{Lim}

7.6. Summary

This chapter showed the application of the protection logic introduced in Chapter 4 on the real hardware setup and on the ATP model of the Noxon reactor. By creating greater turn-to-turn faults on the reactor, the change in the processed current element $I0_{diff}$ is evident. The higher sampling rate in the SEL 735 power meter helped in refining the observable change in the zero sequence current of the reactor during the turn-to-turn faults. Defining the reference quantity R_{Lim} has proven to be crucial in detecting such faults and comparison of R_{Lim} against the new measured zero sequence impedance serves as an alternate method.

8. SUMMARY, CONCLUSIONS AND FUTURE WORK

8.1. Summary

Advanced technologies in insulation materials and environmental concerns have increased demand for air core reactors. Being modular in design, the reactors also have the capability, like capacitor banks, for replacement of sections in case of damage. Most protection schemes isolate a fault and identify damage to the equipment. However, turn-to-turn faults in air core reactors need sensitive protection elements to detect faults shorting a small number of turns. In this research, some of the objectives of the project have been achieved over the course of the project.

Basic electrical theory has been used to identify turn-to-turn faults, where the neutral currents of two reactors connected in parallel to the same bus are compared. This is only feasible if two reactors are connected to the same bus. A more general option of comparing the bus zero sequence voltage with the neutral current of the reactor was proposed and tested, which serves as a solution for standalone operation of reactors. The calculations in Appendix-D show the how the pickup setting was designed considering errors in the measurement seen from instrument transformers, tolerance errors, standing imbalance and other likely challenges.

The study also yielded a solution to determine the faulted phase of the reactor efficiently through angle comparison with the negative sequence current of the

reactor. Finally, faulted phase and trip logic was proposed to identify a turn-to-turn fault on any phase of a reactor.

8.2. Conclusions

The simulation results in ATP and RTDS verified the concept of an element based on the differential current between two reactors connected on the same bus with a sensitivity down to 2.5 % of the reactor turns.

The hardware test setup was used to demonstrate a viable solution to apply for standalone reactors for detecting a turn-to-turn fault on one of its phases. The results in Chapter 7 show the scheme is viable down to faults with a small number of turns. However, a relay with higher sampling rate of at least 512 samples per cycle is necessary to observe such a small magnitude fault condition, thus improving detection of sensitive faults of magnitudes of 10%-15% limited by a ground overcurrent relay. Using the results observed in Chapter 7, the operating characteristics was defined as shown in Figure 8.1. The reference $I0_{diff\_ref}$ is shown as the bold line parallel to the time axis, with the restraint region (green) defined for standing errors and measurement sensitivity. The $I0_{diff\_ref}$ is set based on the standing unbalances and regular abnormalities in the system. For comparison, the plots in Section 7.3 have the $I0_{diff\_ref}$ set at 0.

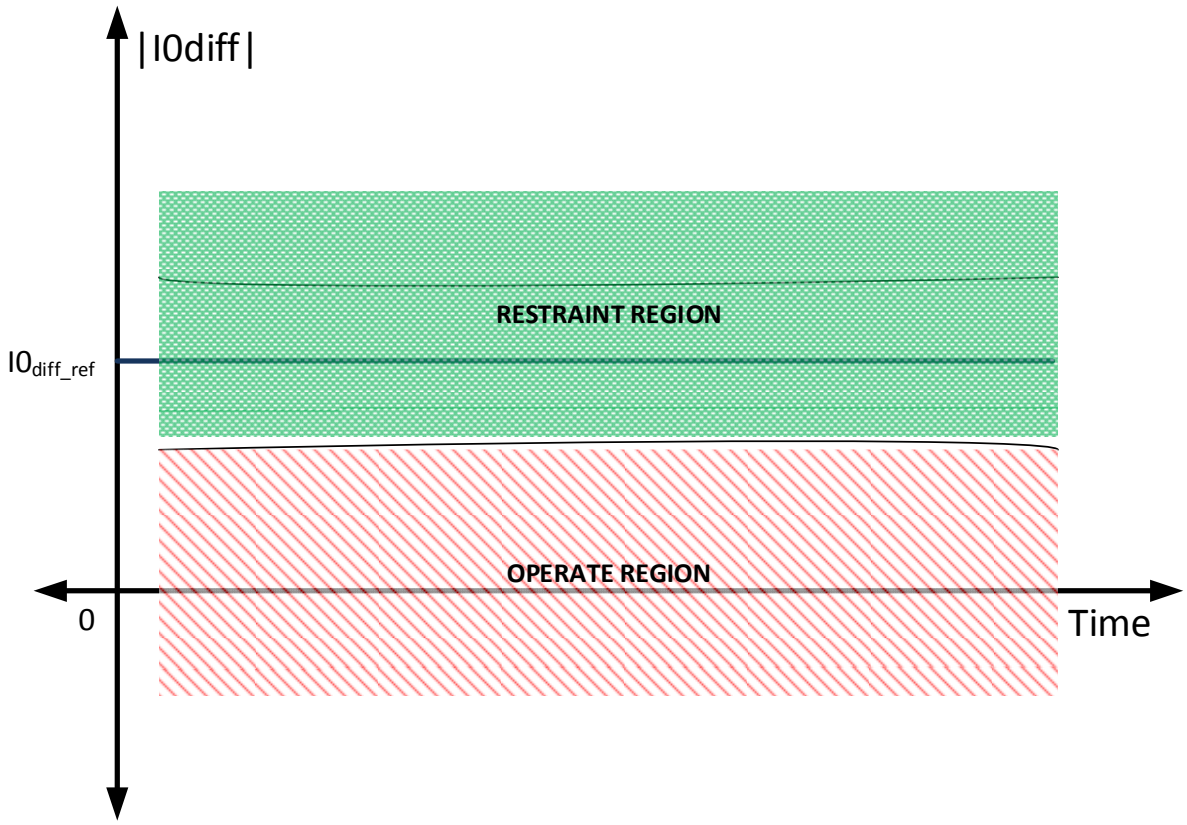

Figure 8.1. Operating Characteristics of the $I0_{diff}$ turn-to-turn fault protection element.

8.3. Future Work

Complete validation of the protection scheme requires implementing the scheme in a hardware device and testing in a real time digital simulator and then testing in the field. The following activities can be undertaken to validate and further strengthen the scheme:

i. Validate the hardware model setup with more tests with standing imbalance, external faults, and other cases with other protection functions such as restricted earth fault and reactor differential (87) in

service. Coordination with other protection elements present for the reactor protection needs to be justified in order to avoid misoperation. As mentioned in earlier chapters, the turn-to-turn fault protection takes less precedence over other critical protection functions.

ii. Extend trip logic to include more real-time functions, making it plausible to be implemented in field. The trip logic proposed in Chapter 5 is incomplete and ignores other functions in the trip logic such as other protection functions, device status, breaker gas pressure status etc.

iii. Estimate the magnitude of the fault current observed in the faulted winding based on the real construction of a reactor coil. All measurements made were from the terminals of the reactor and observed voltages and currents from a simplified view as shown in Figures 3.6 and 3.7. Estimation of the fault current in shorted turns requires study of the construction, geometry and mutual coupling between coils. Verification of simulations and calculations will also be required on a hardware test setup.

iv. Explore sizing characteristics of the software based limiting resistor based on the system imbalances and maximum zero sequence voltage observed. This exercise will be to find boundary conditions of the range over which it will be feasible to size the limiting resistor. Limiting factors include high standing zero sequence bus voltage, long-standing phase unbalances etc. The size of the limiting resistor will need to be

recalibrated in these cases to keep sensitive turn-to-turn fault identification operational.

v. Studying characteristics of a metering CT to determine if it can be used to observe shorted turn faults at lower currents. In addition, the response of CT should be observed at higher current levels in the linear region and with different CT ratios.

vi. Validate modifications on the present scheme with the hardware setup.

vii. Verify the parallel reactor current differential scheme with respect to another unfaulted reactor and include in logic. This verification will allow proof of more precise detection of fault on a reactor when compared with another reactor connected live on the same bus. Systems with this setup should be implemented with added protection. A hardware test setup can validate the simulations presented in chapter 5.

viii. Formulate a method to identify faulted section of the faulted phase. In a reactor coil with a series and parallel combination of coils, it will be hard to identify where the shorted turn is in the faulted phase.

BIBLIOGRAPHY

[1] Das, J.C..*Transients in Electrical Systems: Analysis, Recognition, and Mitigation.* McGraw-Hill Professional, 2010

[2] H. B. Brooks, Design of standards of inductance, and the proposed use of model reactors in the design of air-core iron-core reactors, *Bureau of Standards Journal of Research*, vol. 7, no. 2, p. 289, 1931.

[3] Sadiku, Matthew N. O. *Elements of Electromagnetics*. 4th ed. New York ; New Delhi: Oxford University Press, 2007.

[4] Papp, K., Sharp, M.R. & Peelo, "High Voltage Dry-Type Air-Core Shunt Reactors," D.F. Elektrotech. Inftech. (2014) 131: 349. doi:10.1007/s00502-014-0232-y

[5] *IEEE Guide for the Protection of Shunt Reactors*, IEEE Std C37.109-2006 (Revision of IEEE Std C37.109-1988) , pp.1-39, April 23 2007

[6] F. K. Basha and M. Thompson, "Practical EHV reactor protection," *2013 66th Annual Conference for Protective Relay Engineers*, College Station, TX, 2013, pp. 408-419.

[7] Z. Gajic, B. Hillstrom, F.Mekic "HV Shunt Reactor Secrets for Protection Engineer ," *30 Annual Western Protective Relay Conference*, Spokane, WA, October 21-23, 2003

[8] Kevin Damron, "Practical considerations and experiences protecting 230kV shunt air-core reactors banks," *43rd Annual Western Protective Relay Conference*, Spokane, WA, October 18-20, 2016.

[9] Y. Zhuang, Y. Wang and Q. Zhang, "Study on turn-to-turn insulation fault condition monitoring method for dry-type air-core reactor," *2015 IEEE 11th International*

Conference on the Properties and Applications of Dielectric Materials (ICPADM), Sydney, NSW, 2015, pp. 305-308.

[10] Ugur Arifoglu, *Design Algorithm of Air Core Multilayer Tapped Reactor*, http://www.isites.info/PastConferences/ISITES2015/ISITES2015/papers/A12-ISITES2015ID10.pdf (Accessed July 26, 2017).

[11] *Protection, Monitoring and control of Shunt Reactors*, CIGRE WG B5.37, 2012

Appendix- A

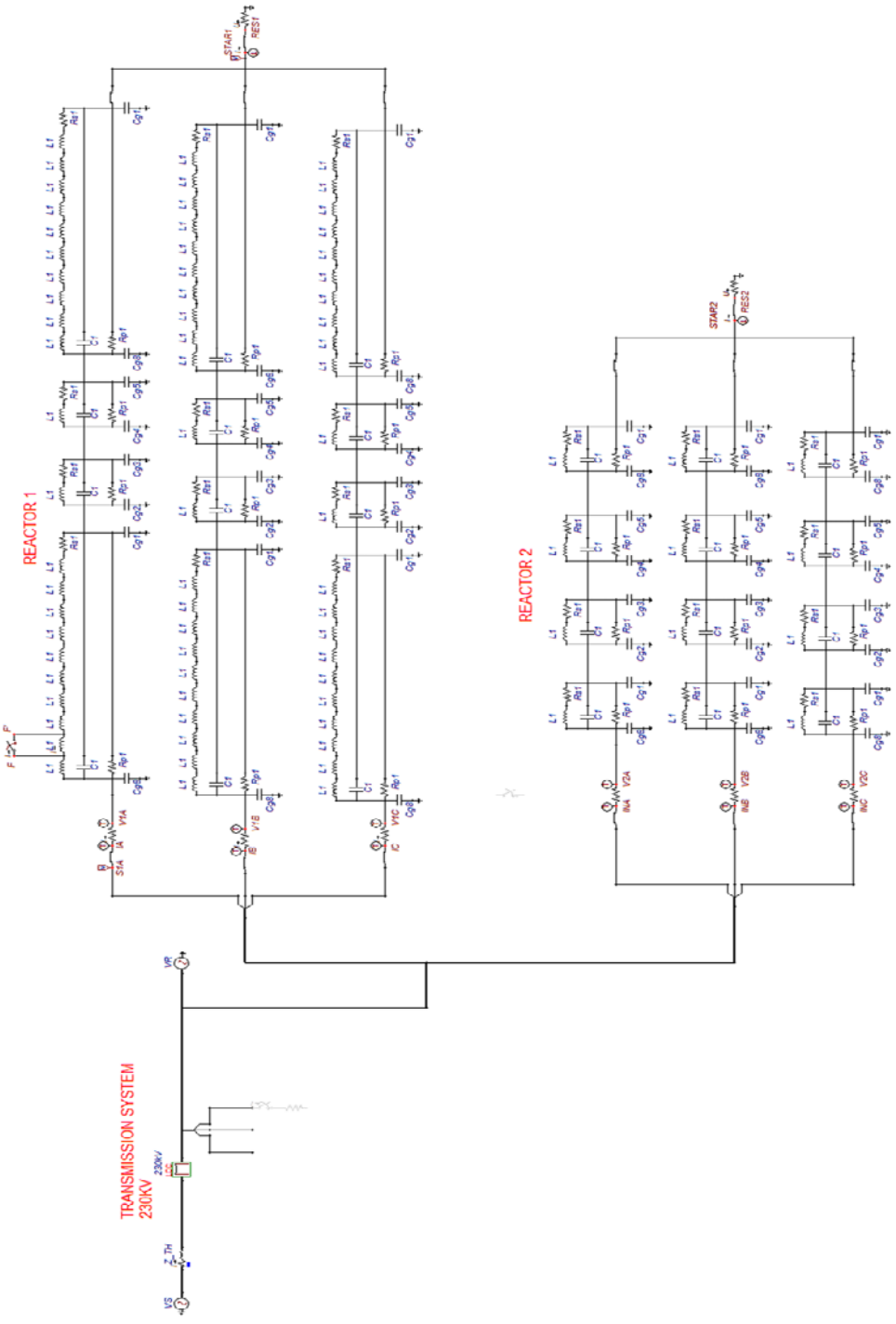

Figure A.1. ATPdraw model of two parallel three phase reactors

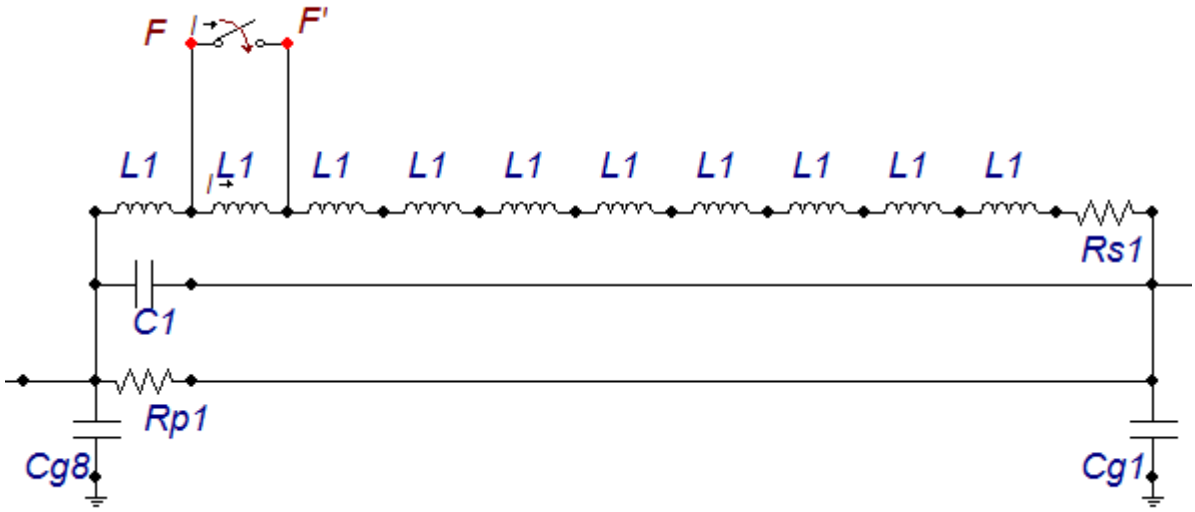

Figure A.2. Distributed equivalent circuit for a single section of a phase reactor, with a fault switch included.

Appendix-B

Inductance of parallel connected concentric coils

Estimating inductance of concentric conductors

$turns := 1$ innermost N1, Outermost N10

Data received from Avista about the reactor:

$N1 := 841\ turns$ [Turns on inner layer]

$N10 := 1285\ turns$ [Turns on outer layer]

$r1 := 1150\ mm$ [Radius of coil]

$A1 := \pi \cdot r1^2$ [Area of coil]

$l1 := 3391\ mm$ [length of one section of coil]

$layer := \left| \frac{N1 - N10}{10} \right| = 44.4\ turns$ [estimated difference of turns per layer]

Number of turns in each consecutive layer:

$N2 := N1 + layer$ $N3 := N2 + layer$ $N4 := N3 + layer$ $N5 := N4 + layer$

$N6 := N5 + layer$ $N7 := N6 + layer$ $N8 := N7 + layer$ $N9 := N8 + layer$

Inductance seen on each coil:

$L1 := \frac{N1^2 \cdot 10 \cdot \mu_0 \cdot A1}{l1} = 10.89\ H$ $L2 := \frac{N2^2 \cdot 9 \cdot \mu_0 \cdot A1}{l1} = 10.863\ H$

$L3 := \frac{N3^2 \cdot 8 \cdot \mu_0 \cdot A1}{l1} = 10.649\ H$ $L4 := \frac{N4^2 \cdot 7 \cdot \mu_0 \cdot A1}{l1} = 10.229\ H$

$L5 := \frac{N5^2 \cdot 6 \cdot \mu_0 \cdot A1}{l1} = 9.585\ H$ $L6 := \frac{N6^2 \cdot 5 \cdot \mu_0 \cdot A1}{l1} = 8.699\ H$

$L7 := \frac{N7^2 \cdot 4 \cdot \mu_0 \cdot A1}{l1} = 7.553\ H$ $L8 := \frac{N8^2 \cdot 3 \cdot \mu_0 \cdot A1}{l1} = 6.128\ H$

Non-Commercial Use Only

$$L9 := \frac{N9^2 \cdot 2 \cdot \mu_0 \cdot A1}{l1} = 4.406\ H \qquad L10 := \frac{N10^2 \cdot \mu_0 \cdot A1}{l1} = 2.542\ H$$

Resultant inductance of the coil

$$L_{res} := \left(L1^{-1} + L2^{-1} + L3^{-1} + L4^{-1} + L5^{-1} + L6^{-1} + L7^{-1} + L8^{-1} + L9^{-1} + L10^{-1}\right)^{-1} = 661.931\ mH$$

Inductance of one coil section:

$L_{nox} := 695\ mH$ [Actual inductance of one section received from reactor test report]

$$error := 1 - \frac{L_{res}}{L_{nox}} = 4.758\%$$

Inductance of hand wound multi layer coil:

$L_{inner} := 115\ \mu H$ $L_{middle} := 148\ \mu H$ $L_{outer} := 250\ \mu H$

$L_{parallel} := 119\ \mu H$ [measured]

$$L_{calc} := \left(L_{outer}^{-1} + \left(2 \cdot L_{middle}\right)^{-1} + \left(3 \cdot L_{inner}\right)^{-1}\right)^{-1} = 97.305\ \mu H$$

$$error := 1 - \frac{L_{calc}}{L_{parallel}} = 18.231\%$$

Non-Commercial Use Only

Appendix - C

Sizing Calculations for laboratory air core coil reactors

$j := \sqrt{-1}$ $f := 60\ Hz$ $\omega := 2 \cdot \pi \cdot f$

Source voltage: $V_{an} := 110\ V \angle 0\ deg$

Model power system current: $I_{ln} := 5\ A \angle -90\ deg = 5\mathrm{i}\ A$

Equivalent reactance: $X_{star} := \frac{V_{an}}{I_{ln}} = (22 \angle 90°)\ \Omega$

Rating of inductance per phase: $L_{star} := \frac{\mathrm{Im}\left\langle X_{star} \right\rangle}{\omega} = 58.357\ mH$

Desired inductance per coil: $10\ mH$

Based on the maximum current in the circuit, we can size the per phase inductance to be about 60mH.
Number of coils of 10mH required = (60mH/10mH)= ***6 Coils/Phase***

Assumptions:
1. Angle of voltage source set at 0deg.
2. The coils have negligible resistance.
3. Star configuration will be implemented.
4. Coils of 15AWG with inductance of 10mH each .

Non-Commercial Use Only

Appendix D

Calculations with Noxon Model

Graphing calculations for inter-turn fault detection on Air Core reactors

Constants:

$j := \sqrt{-1}$ $\quad a := 1 \cdot e^{j \cdot 120\ deg}$ $\quad f := 60\ Hz$ $\quad \omega := 2 \cdot \pi \cdot f$

$$A_{012} := \begin{bmatrix} 1 & 1 & 1 \\ 1 & a^2 & a \\ 1 & a & a^2 \end{bmatrix}$$

$$V_{abc} := 230\ kV \cdot \begin{bmatrix} 1 \\ a \\ a^2 \end{bmatrix} = \begin{bmatrix} 230\angle 0° \\ 230\angle 120° \\ 230\angle -120° \end{bmatrix} kV$$

$X\_R := 55$ [X/R ratio of Noxon reactors]

$X_{Lnox} := 283.21\ \Omega$ [Inductive reactance of one section of reactor per phase]

$R_{ph} := \frac{4 \cdot X_{Lnox}}{X\_R} = 20.597\ \Omega$ [Resistance of 4 sections of reactor per phase]

Select ratios of measuring instruments:

$CTRN := \frac{50\ A}{1\ A} = 50$ [Neutral CT of reactor]

$PTRB := \frac{230\ kV}{\sqrt{3} \cdot 115\ V} = 1154.701$ [Bus PT]

Non-Commercial Use Only

Tolerance in Inductances defined by manufacturer

Inductance of each reactor as per test report:

$L_{noxa} := 3011.57\ mH$ $L_{noxb} := 3006.41\ mH$ $L_{noxc} := 3008.92\ mH$

$tol := -2.5\%, -2\% .. 2.5\%$ [Range of tolerance]

$L_a(tol) := L_{noxa} \cdot (1 + tol)$ $L_b(tol) := L_{noxb} \cdot (1 + tol)$ $L_c(tol) := L_{noxc} \cdot (1 + tol)$

$$Z_{ph}(tol) := \begin{bmatrix} R_{ph} + j \cdot \omega \cdot L_a(tol) \\ R_{ph} + j \cdot \omega \cdot L_b(tol) \\ R_{ph} + j \cdot \omega \cdot L_c(tol) \end{bmatrix}$$

[Phase currents]

$$I_{abc}(tol) := \frac{V_{abc}}{\sqrt{3} \cdot Z_{ph}(tol)}$$

[Sequence currents in Unfaulted condition]

$I_{012}(tol) := A_{012} \cdot I_{abc}(tol)$

$|Z_{ph}(tol)_0|$ (Ω)

$|Z_{ph}(tol)_1|$ (Ω)

$|Z_{ph}(tol)_2|$ (Ω)

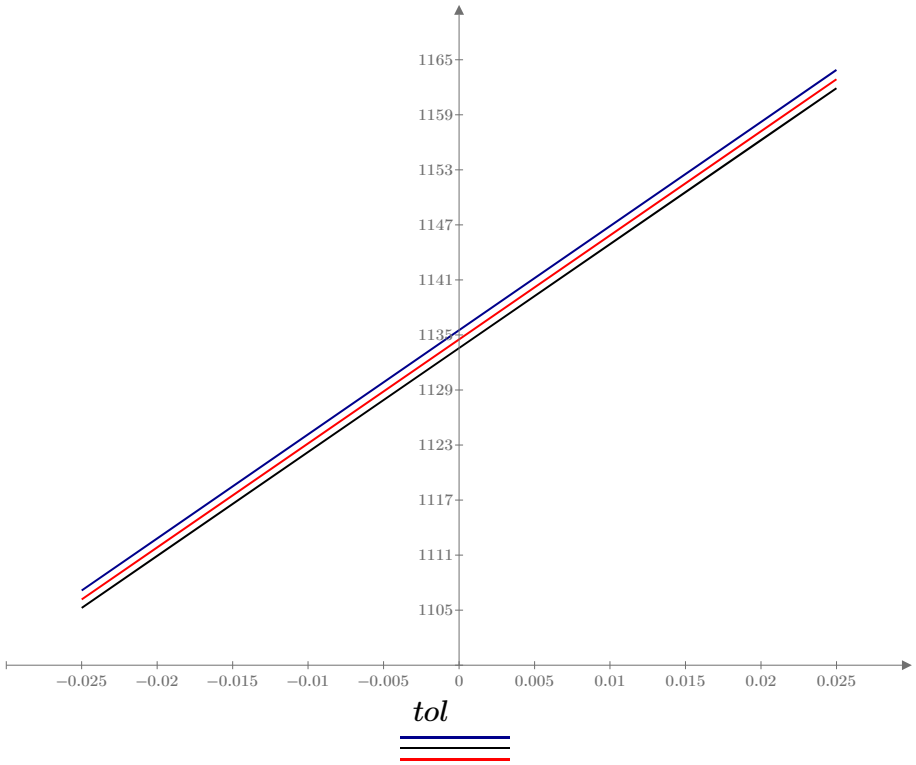

Variation of impedance with error tolerance

Non-Commercial Use Only

System unbalances

$K_{un} := 0.9, 0.91 .. 1.1$ [Range of unbalance]

$$V_{abc\_un}\langle K_{un}\rangle := \begin{bmatrix} K_{un} \cdot V_{abc_0} \\ V_{abc_1} \\ V_{abc_2} \end{bmatrix}$$ [Creating voltage unbalance]

$$I_{abc\_un}\langle K_{un}\rangle := \frac{V_{abc\_un}\langle K_{un}\rangle}{\sqrt{3} \cdot Z_{ph}(0)}$$ [Current imbalance with 0 tolerance error of impedance]

$$V0\langle K_{un}\rangle := \frac{V_{abc\_un}\langle K_{un}\rangle_0 + V_{abc\_un}\langle K_{un}\rangle_1 + V_{abc\_un}\langle K_{un}\rangle_2}{3}$$ [Zero sequence bus voltage]

$$I0\langle K_{un}\rangle := \frac{I_{abc\_un}\langle K_{un}\rangle_0 + I_{abc\_un}\langle K_{un}\rangle_1 + I_{abc\_un}\langle K_{un}\rangle_2}{3}$$ [Zero sequence current through neutral]

Sizing the limiting resistor:

$|V0(0.9)| = 7.667\ kV$ $|V0(1.1)| = 7.667\ kV$

$|I0(0.9)| = 3.949\ A$ $|I0(1.1)| = 3.847\ A$

$$R_{lim}\langle K_{un}\rangle := \frac{V0\langle K_{un}\rangle}{I0\langle K_{un}\rangle}$$ [Limiting resistor is dynamic and to be calculated in the relay]

Non-Commercial Use Only

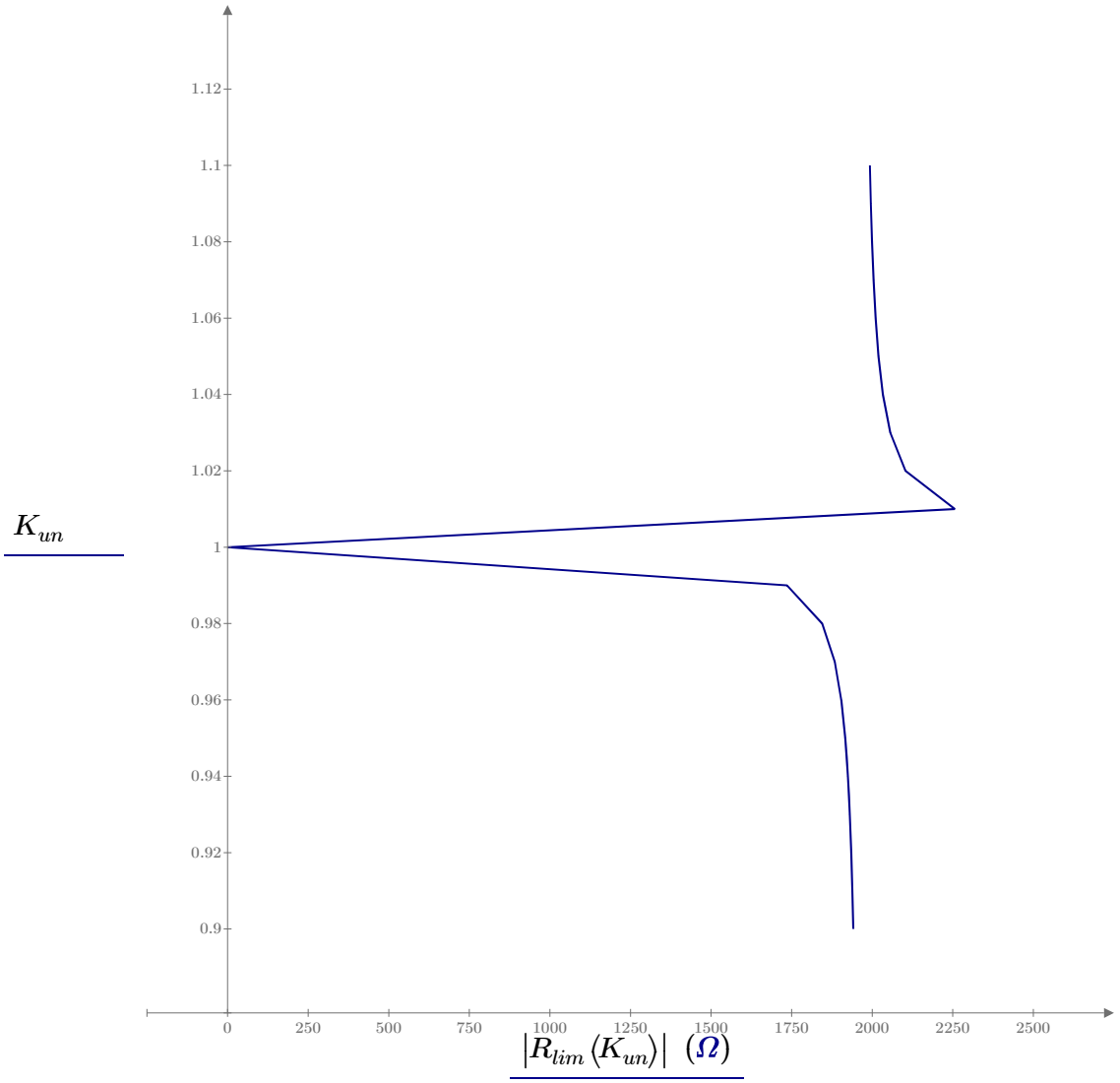

The limiting resistor calculation needs to be dynamic. As seen from the curve, based on the variation of zero sequence voltage, the limiting resistor needs to be recalculated to negate the effects of standing system imbalance.

Non-Commercial Use Only

Case With faulted turns on the winding A in A reference frame:

$im := 0.8, 0.81 .. 1$ [Amount of imbalance in the reactance]

$$Z_{fault}(im) := \begin{bmatrix} R_{ph} + j \cdot \omega \cdot L_{noxa} \cdot im \\ R_{ph} + j \cdot \omega \cdot L_{noxb} \\ R_{ph} + j \cdot \omega \cdot L_{noxc} \end{bmatrix}$$ [fault in Phase A]

$$I_{fault}(im) := \frac{V_{abc}}{\sqrt{3} \cdot Z_{fault}(im)}$$ [Phase currents when faulted]

$I_{012f}(im) := A_{012} \cdot I_{fault}(im)$ [Sequence Currents]

$\theta_{fault\_a}(im) := \arg\left(I_{012f}(im)_0\right) - \arg\left(I_{012f}(im)_2\right)$ [Angle difference in I0 and I2]

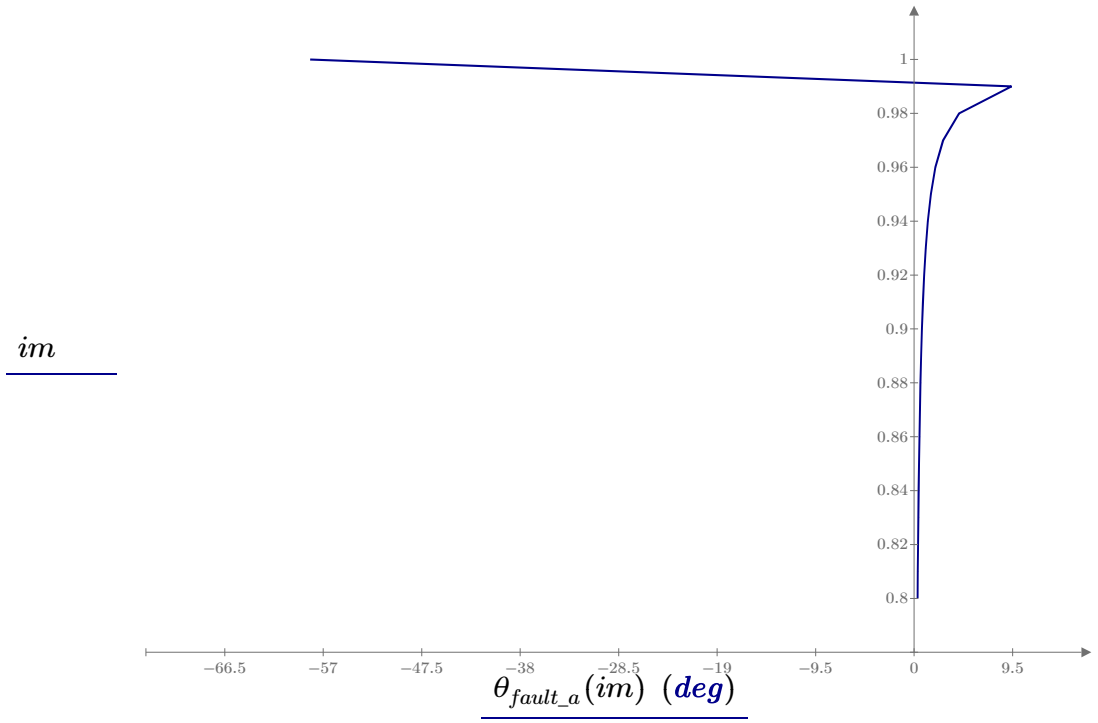

The angle difference is close to zero for up to 20% error in the reactance. Good measure of faulted phase.

Non-Commercial Use Only

Validation of protection logic:
Bus zero sequence voltage vs Reactor Neutral current

$$V_{0\_sec}\langle K_{un}\rangle := \frac{V0\langle K_{un}\rangle}{PTRB}$$ [Zero sequence voltage on secondary]

$$I0_{diffa}\langle K_{un}\rangle := \left| \frac{I_{012f}(0.975)_0}{CTRN} - \frac{V_{0\_sec}\langle K_{un}\rangle}{R_{lim}\langle K_{un}\rangle} \right|$$ [Differential current with 2.5% fault]

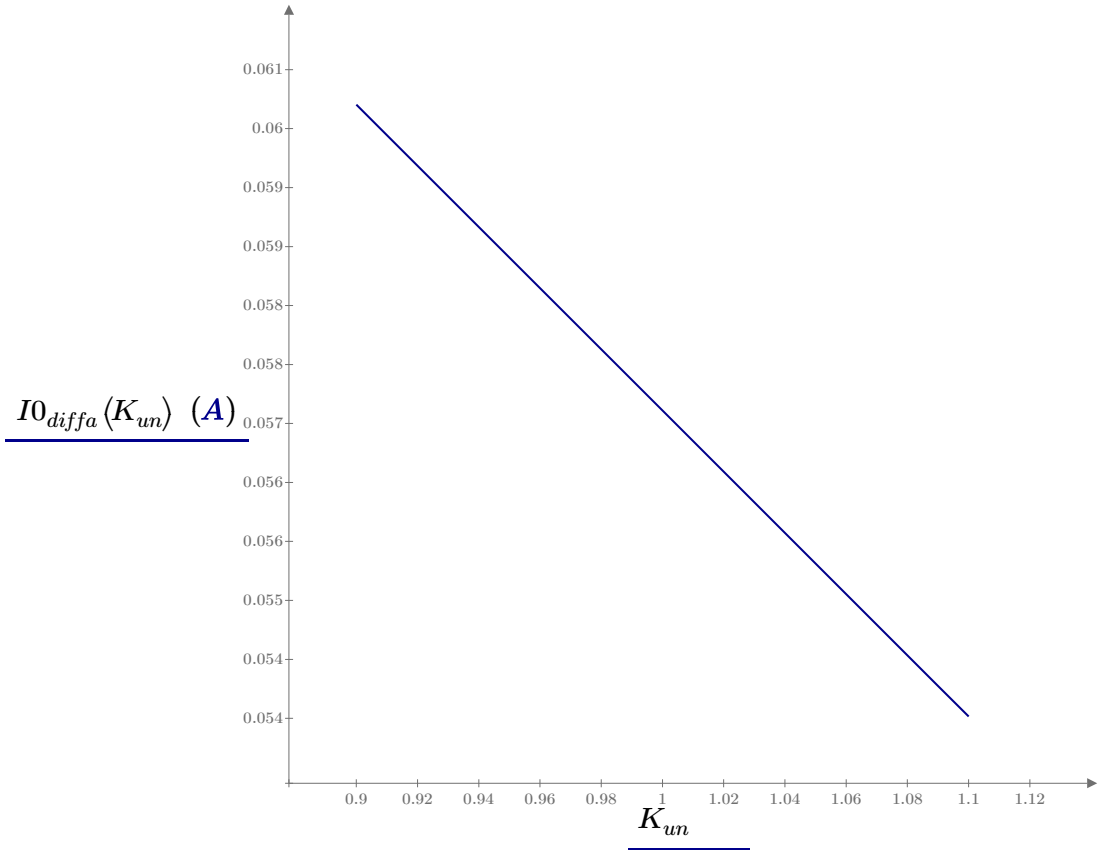

Variation of pickup currents on secondary side of CT with system unbalance

$I0_{diffa}(0.9) = 0.06\ A$ [Differential current with -10% system voltage imbalance]

$I0_{diffa}(1.1) = 0.054\ A$ [Differential current with +10% system voltage imbalance]

$I0_{diffa}(1) = 0.057\ A$ [Differential current with Balanced system]

Non-Commercial Use Only

Case With faulted turns on the winding B in A reference frame:

$$Z_{fault}(im) := \begin{bmatrix} R_{ph} + j \cdot \omega \cdot L_{noxa} \\ R_{ph} + j \cdot \omega \cdot L_{noxb} \cdot im \\ R_{ph} + j \cdot \omega \cdot L_{noxc} \end{bmatrix}$$

$$I_{fault}(im) := \frac{V_{abc}}{\sqrt{3} \cdot Z_{fault}(im)}$$

$$I_{012f}(im) := A_{012} \cdot I_{fault}(im)$$

$$\theta_{fault\_b}(im) := \arg\left(I_{012f}(im)_0\right) - \arg\left(I_{012f}(im)_2\right)$$

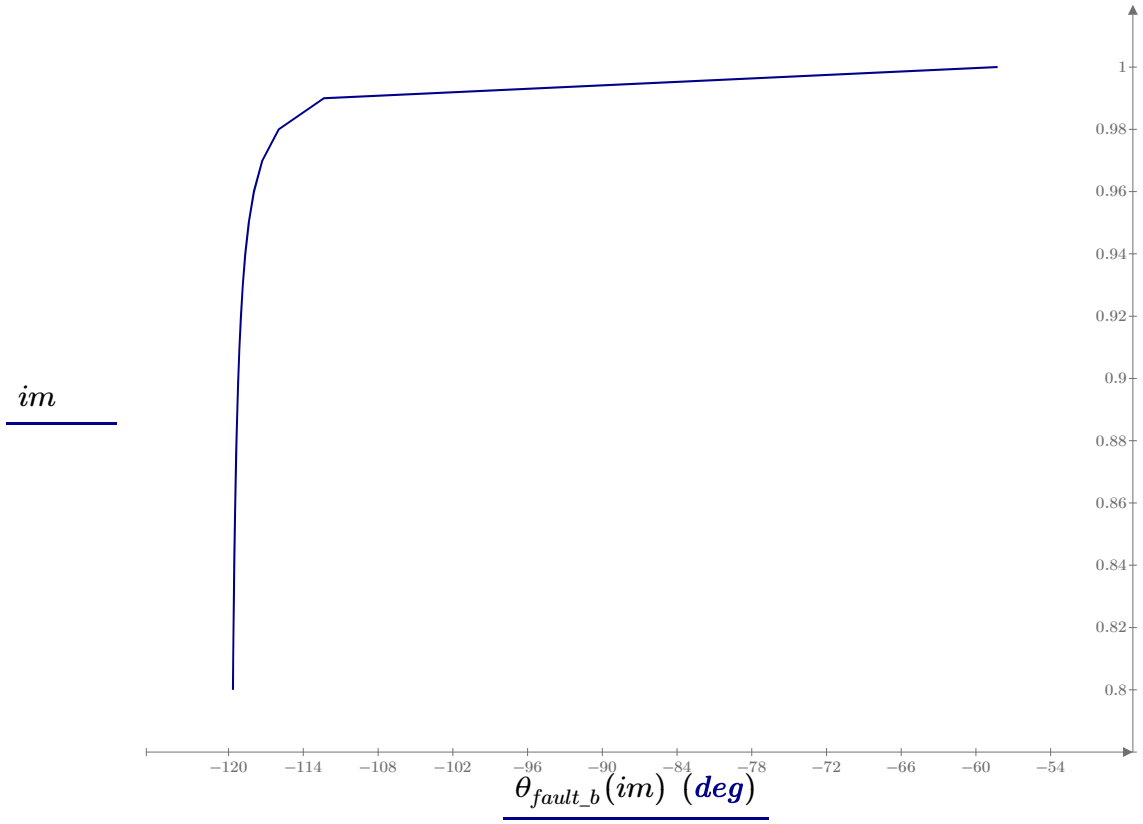

The angle difference is close to -120deg for upto 20% error in the reactance. Good identification of faulted phase.

Non-Commercial Use Only

Case With faulted turns on the winding B in A reference frame:

$$Z_{fault}(im) := \begin{bmatrix} R_{ph} + j \cdot \omega \cdot L_{noxa} \\ R_{ph} + j \cdot \omega \cdot L_{noxb} \\ R_{ph} + j \cdot \omega \cdot L_{noxc} \cdot im \end{bmatrix}$$

$$I_{fault}(im) := \frac{V_{abc}}{\sqrt{3} \cdot Z_{fault}(im)}$$

$$I_{012f}(im) := A_{012} \cdot I_{fault}(im)$$

$$\theta_{fault\_c}(im) := \arg\left(I_{012f}(im)_0\right) - \arg\left(I_{012f}(im)_2\right)$$

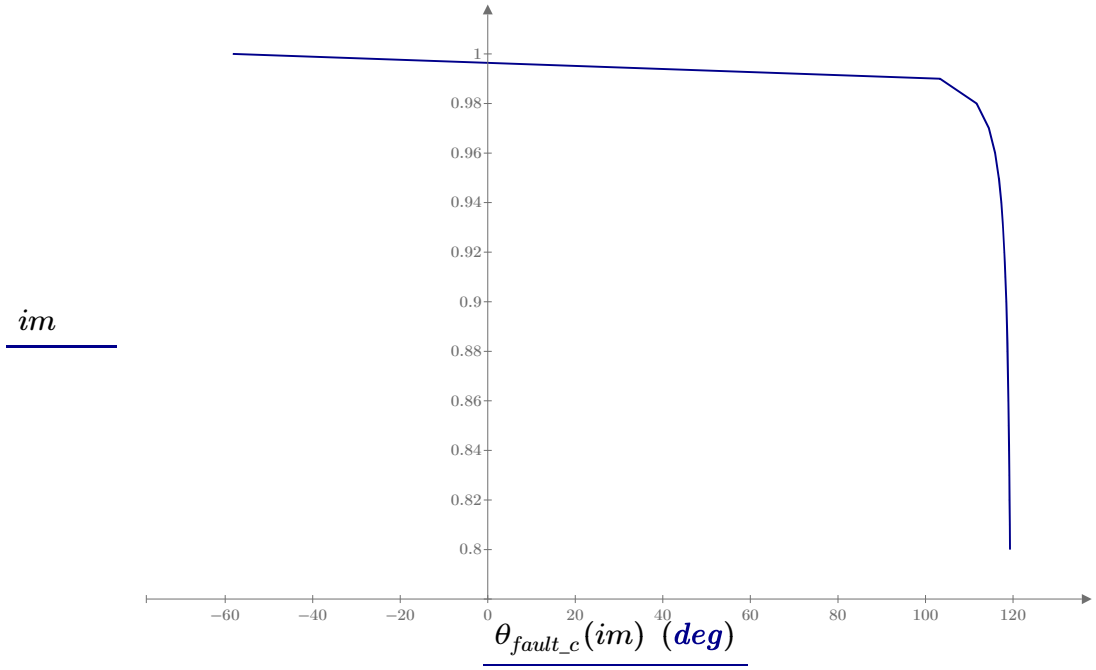

The angle difference is close to +120deg for upto 20% error in the reactance. Good measure of faulted phase.

Non-Commercial Use Only

Comparitive comparison of fault in A phase and angle comparison in other reference frame.

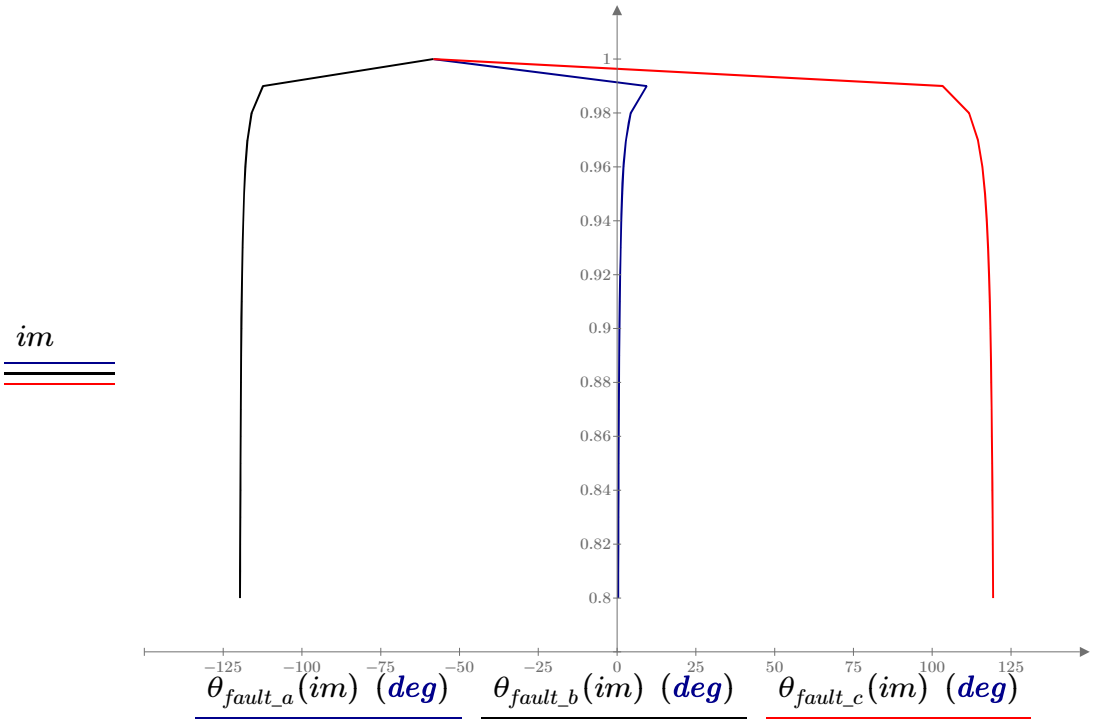

Non-Commercial Use Only

Appendix E

Tests with 411L

Graphing calculations for Inter-turn fault detection on Air Core reactors - Lab Model

Calibration of Rlim:

$test10239 := \text{READFILE}(\text{".\040617\_tests\_411L\10239\_Reference.csv"}, \text{"delimited"})$

$time := test10239^{\langle 1 \rangle}\ ms$

$IAW := test10239^{\langle 2 \rangle}\ A$ $IBW := test10239^{\langle 3 \rangle}\ A$ $ICW := test10239^{\langle 4 \rangle}\ A$

$VAY := test10239^{\langle 5 \rangle}\ V$ $VBY := test10239^{\langle 6 \rangle}\ V$ $VCY := test10239^{\langle 7 \rangle}\ V$

$I0W_{ref} := test10239^{\langle 8 \rangle}\ A$ $I2W_{ref} := test10239^{\langle 9 \rangle}\ A$ $V0Y_{ref} := test10239^{\langle 10 \rangle}\ V$ $R_{Lim} := \frac{V0Y_{ref}}{I0W_{ref}}$

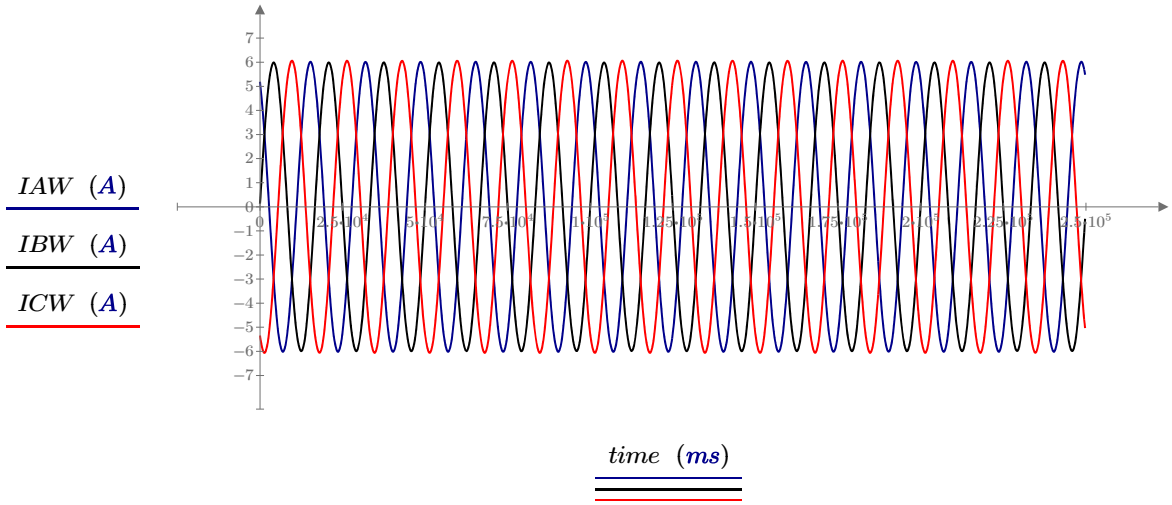

Steady state phase currents recorded by relay

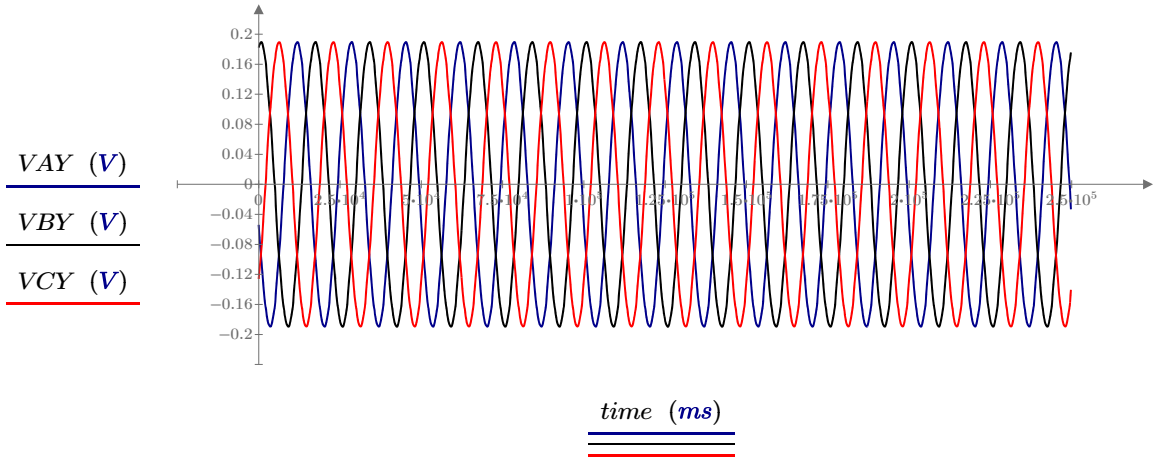

Non-Commercial Use Only

Steady state phase voltages recorded by relay

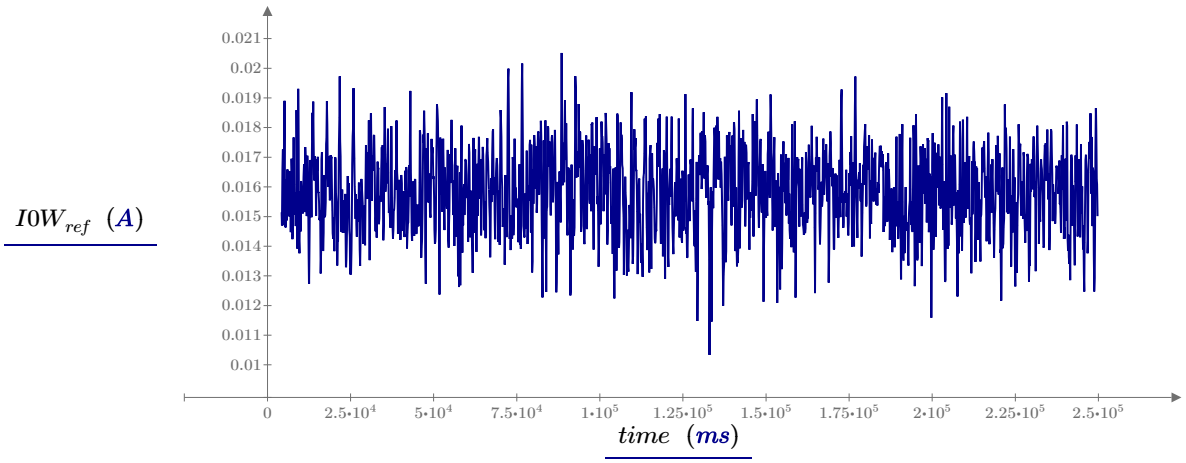

Zero sequence reference current measured by relay

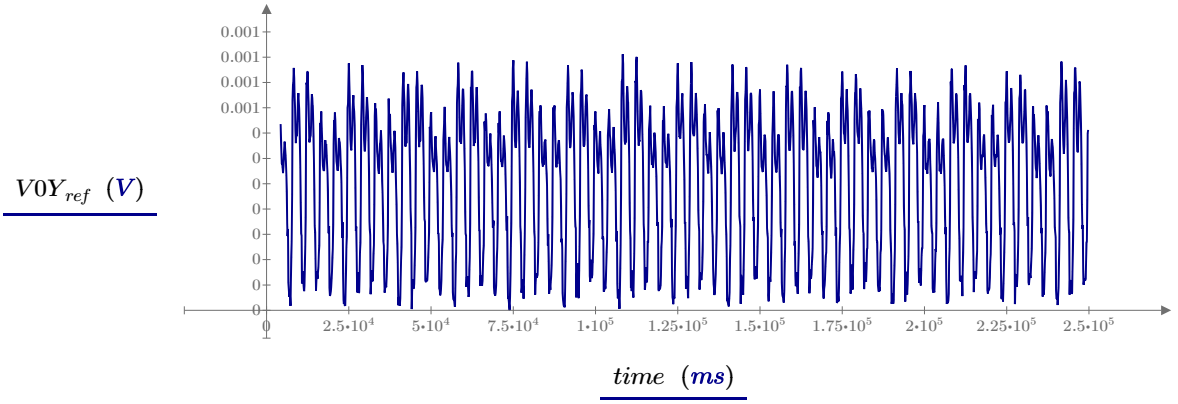

Zero sequence reference voltage measured by relay

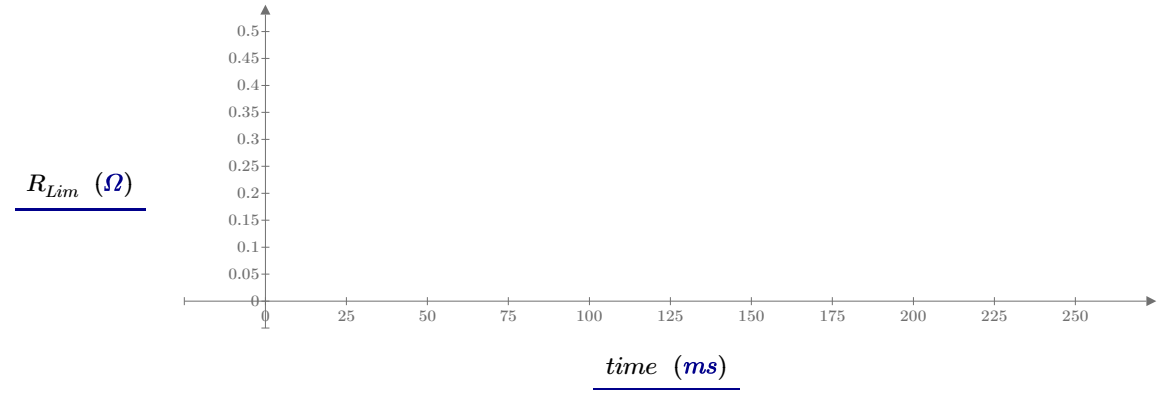

Non-Commercial Use Only

Reference quantity Rlim for utilization in identifying fault conditions

$$I0diff_{steady} := \frac{V0Y_{ref}}{R_{Lim}} - I0W_{ref}$$

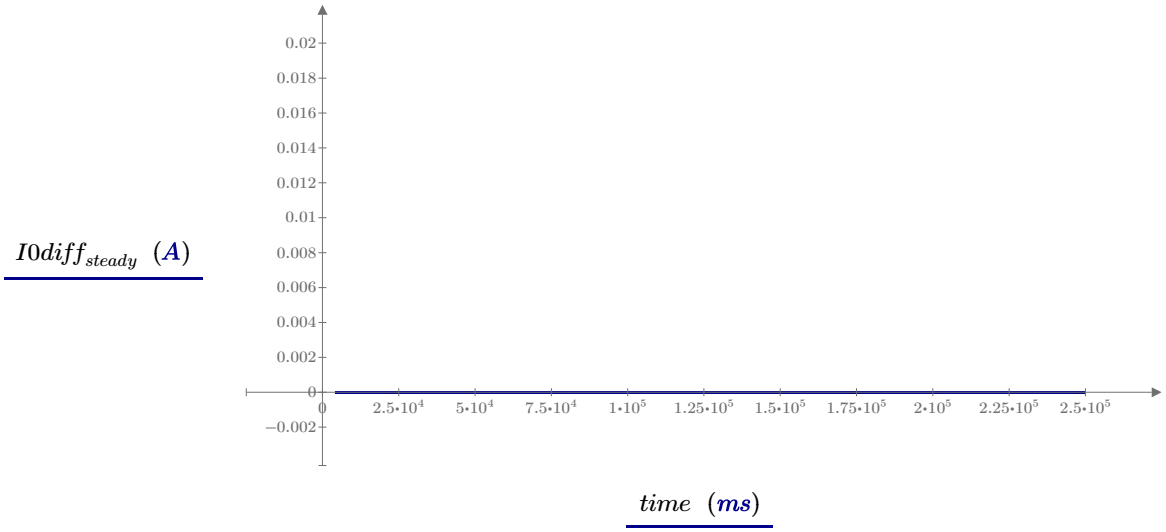

Verifying that the pick up current I0diff is zero for steady state condition

Non-Commercial Use Only

3mH inductance shorted on test coils in lab setup

$test10242 := \text{READFILE}(\text{".\040617\_tests\_411L\10242.csv"}, \text{"delimited"})$

$time := test10242^{\langle 1 \rangle}\ ms$

$I0W := test10242^{\langle 8 \rangle}\ A$ $I2W := test10242^{\langle 9 \rangle}\ A$ $V0Y := test10242^{\langle 10 \rangle}\ V$

$$I0diff := \frac{V0Y}{R_{Lim}} - I0W$$

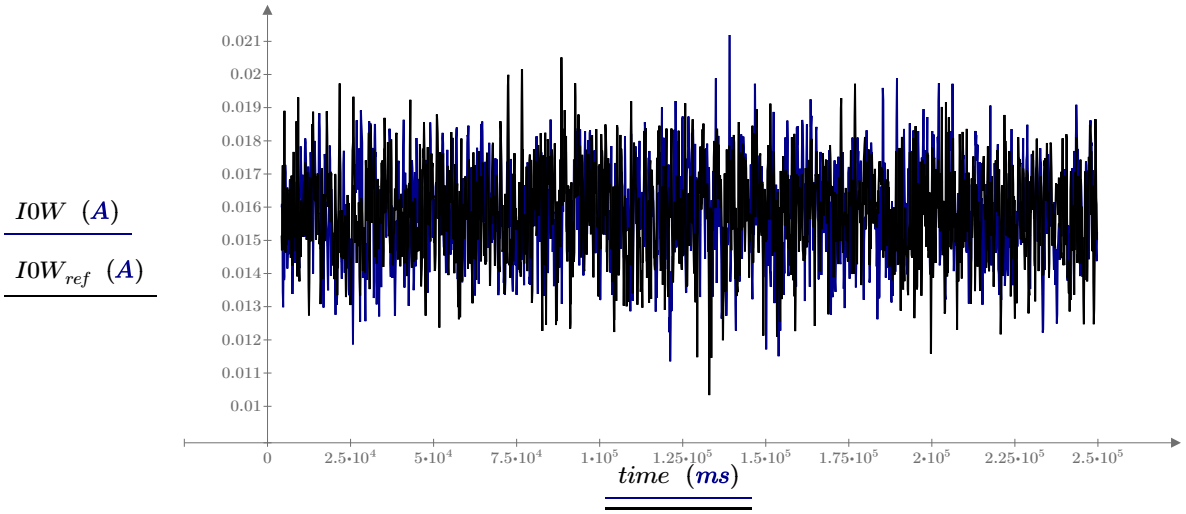

Comparing I0W in faulted case vs I0Wref in steady state

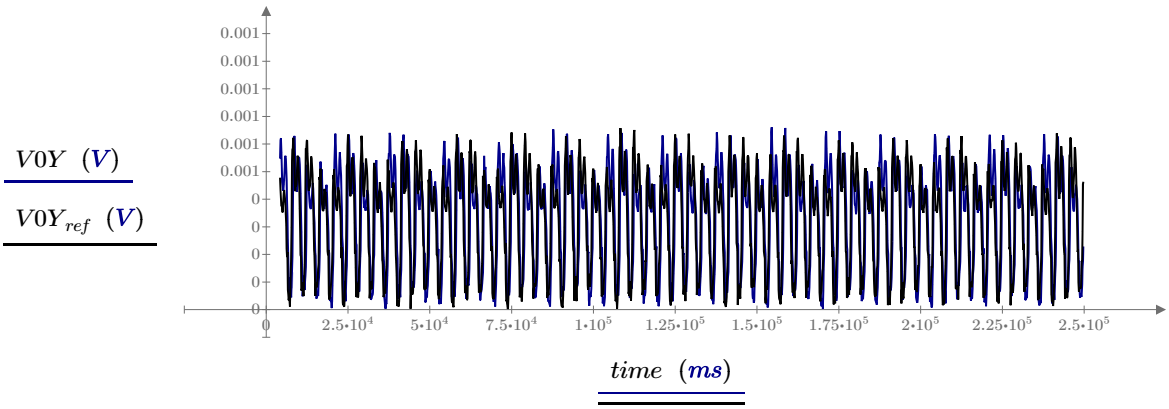

Non-Commercial Use Only

Comparing V0Y in faulted case vs V0Yref in steady state

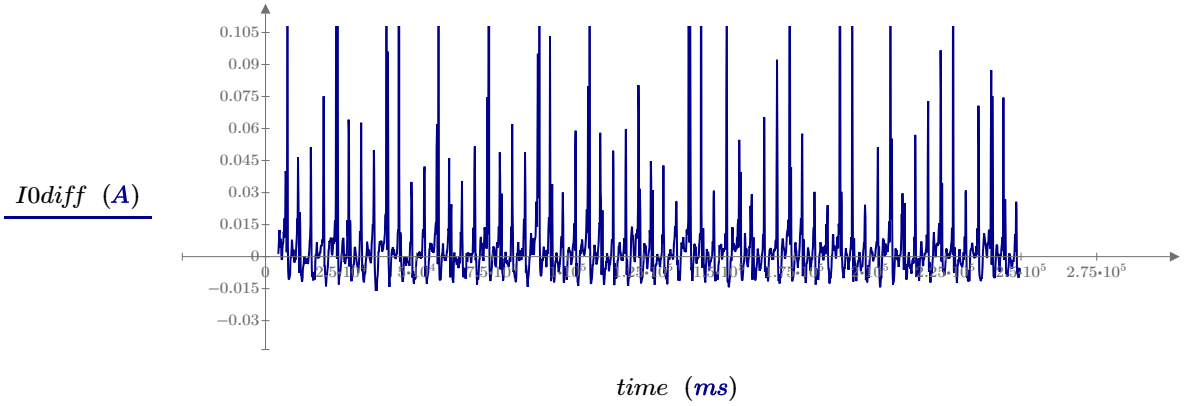

Plot of I0diff pick up current in faulted case

3.3mH inductance shorted on test coils in lab setup

$test10244 := \text{READFILE}(\text{".\040617\_tests\_411L\10244.csv"}, \text{"delimited"})$

$time := test10244^{\langle 1 \rangle}\ ms$

$I0W := test10244^{\langle 8 \rangle}\ A$ $I2W := test10244^{\langle 9 \rangle}\ A$ $V0Y := test10244^{\langle 10 \rangle}\ V$

$$I0diff := \frac{V0Y}{R_{Lim}} - I0W$$

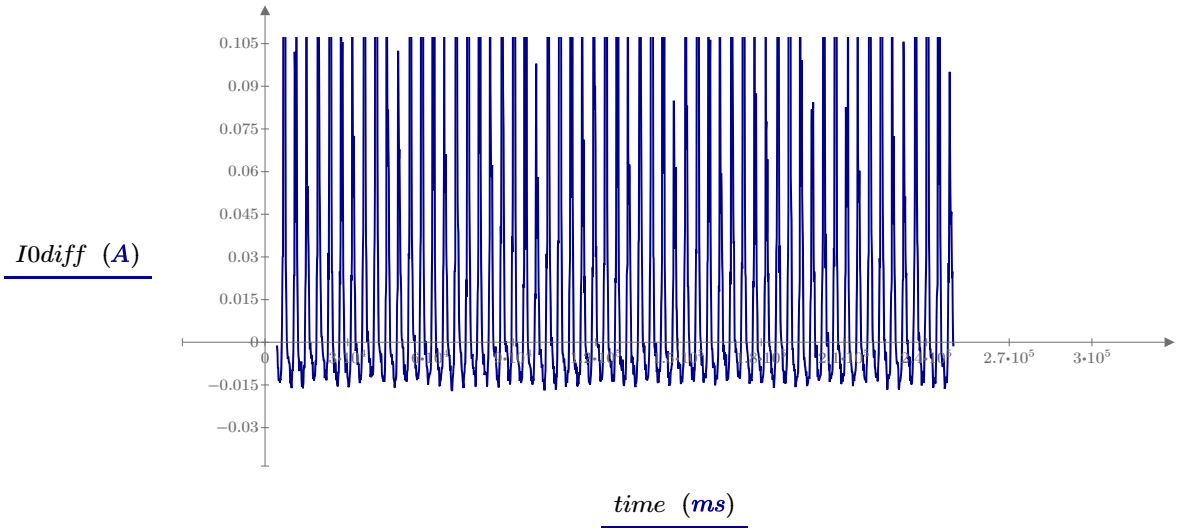

Non-Commercial Use Only

Plot of I0diff pick up current in faulted case

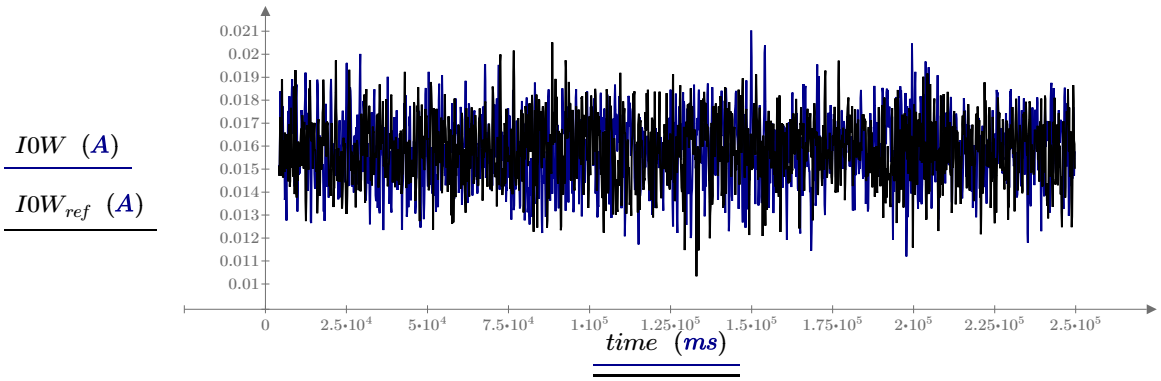

Comparing I0W in faulted case vs I0Wref in steady state

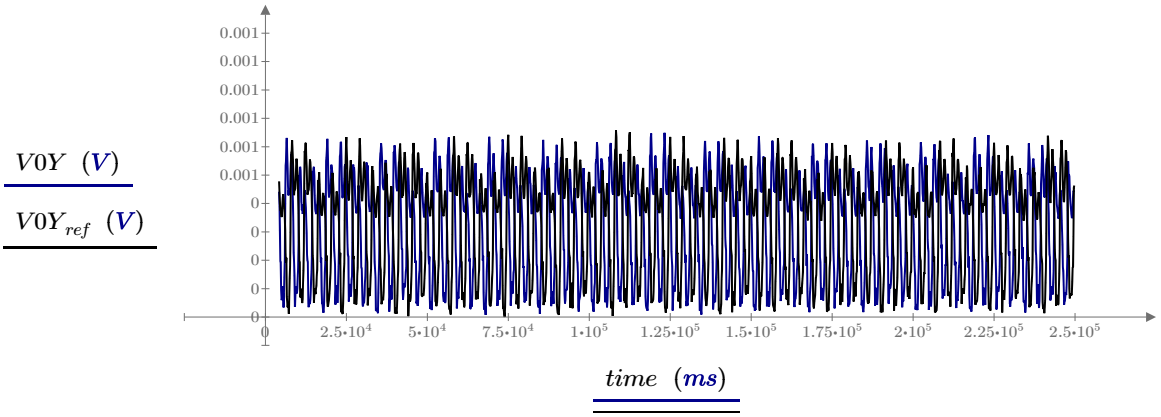

Comparing V0Y in faulted case vs V0Yref in steady state

Non-Commercial Use Only

3.5mH inductance shorted on test coils in lab setup

$test10246 := \text{READFILE}(\text{".\040617\_tests\_411L\10246.csv"}, \text{"delimited"})$

$time := test10246^{\langle 1 \rangle}\ ms$

$I0W := test10246^{\langle 8 \rangle}\ A$ $I2W := test10246^{\langle 9 \rangle}\ A$ $V0Y := test10246^{\langle 10 \rangle}\ V$

$$I0diff := \frac{V0Y}{R_{Lim}} - I0W$$

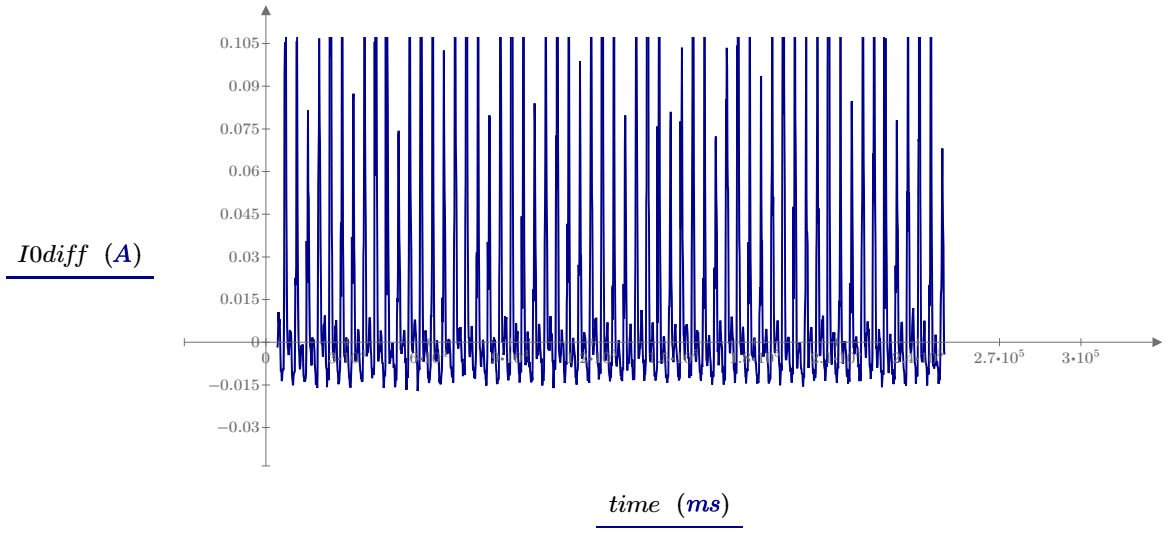

Plot of I0diff pick up current in faulted case

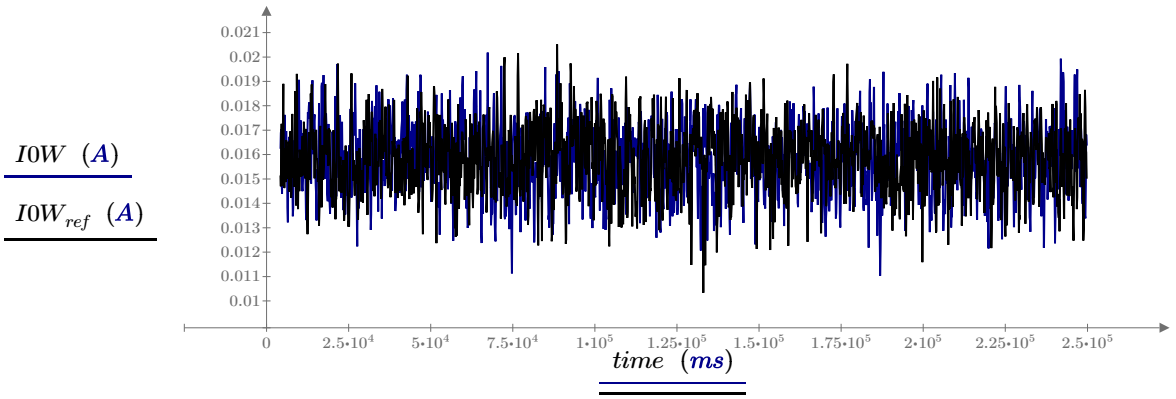

Non-Commercial Use Only

Comparing I0W in faulted case vs I0Wref in steady state

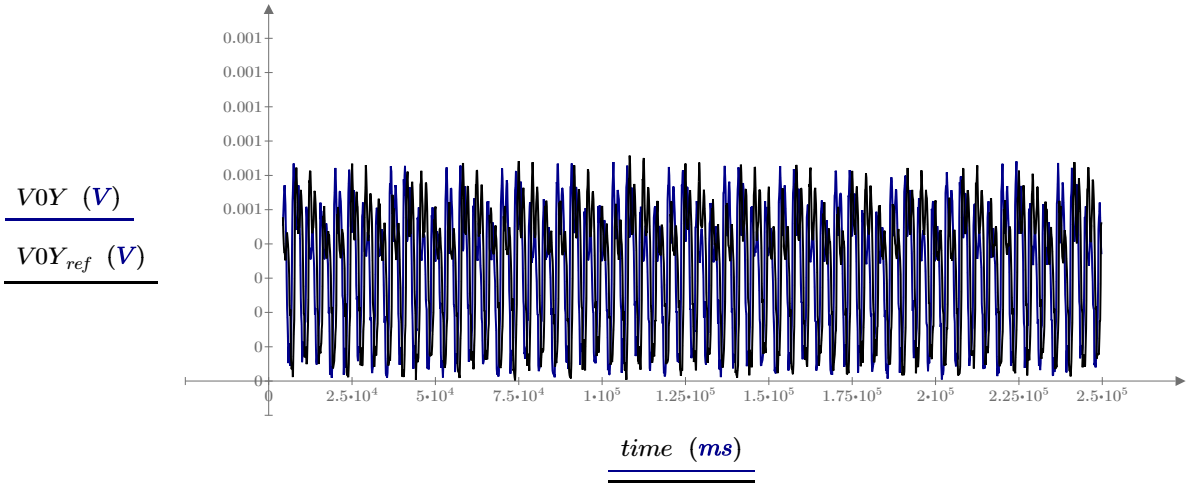

Comparing V0Y in faulted case vs V0Yref in steady state

4mH inductance shorted on test coils in lab setup

$test10248 := \text{READFILE}(\text{".\040617\_tests\_411L\10248.csv"}, \text{"delimited"})$

$time := test10248^{\langle 1 \rangle}\ ms$

$I0W := test10248^{\langle 8 \rangle}\ A$ $I2W := test10248^{\langle 9 \rangle}\ A$ $V0Y := test10248^{\langle 10 \rangle}\ V$

$$I0diff := \frac{V0Y}{R_{Lim}} - I0W$$

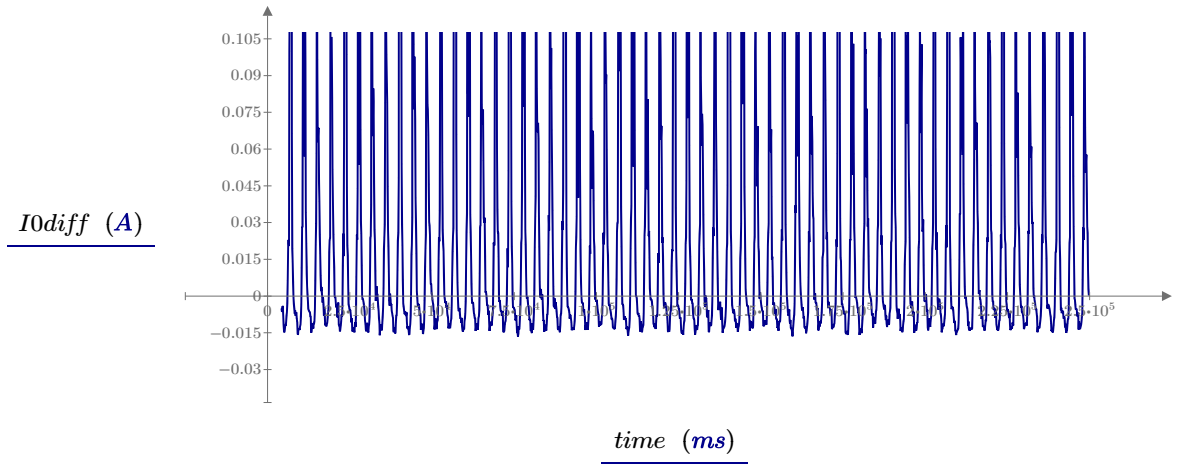

Non-Commercial Use Only

Plot of I0diff pick up current in faulted case

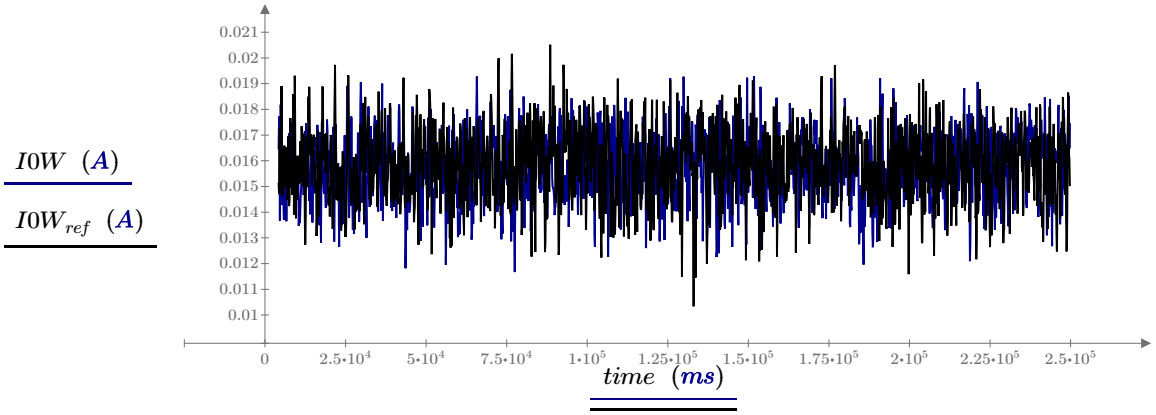

Comparing I0W in faulted case vs I0Wref in steady state

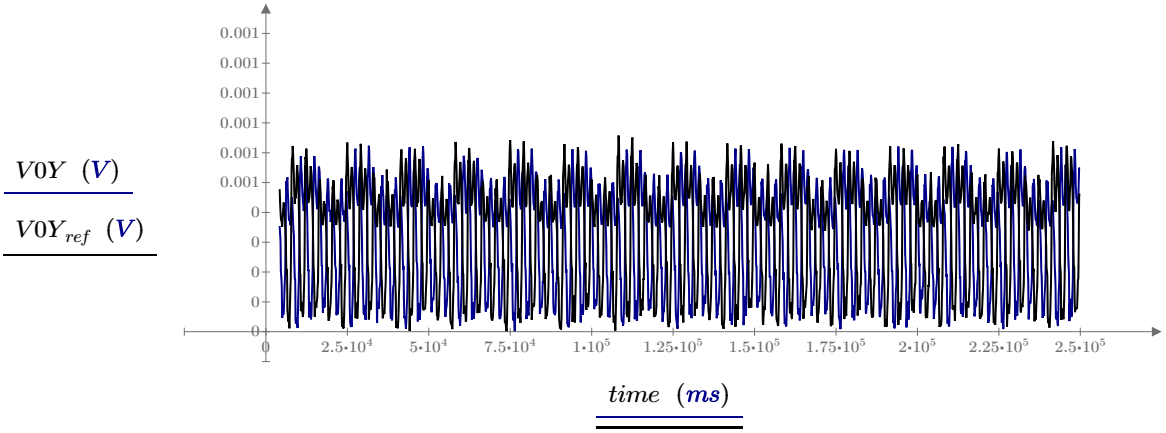

Comparing V0Y in faulted case vs V0Yref in steady state

Non-Commercial Use Only

7.3mH inductance shorted on test coils in lab setup

$test10250 := \text{READFILE}(\text{".\040617\_tests\_411L\10250\_ReactorTest1.csv"}, \text{"delimited"})$

$time := test10250^{\langle 1 \rangle}\ ms$

$I0W := test10250^{\langle 8 \rangle}\ A$ $I2W := test10250^{\langle 9 \rangle}\ A$ $V0Y := test10250^{\langle 10 \rangle}\ V$

$$I0diff := \frac{V0Y}{R_{Lim}} - I0W$$

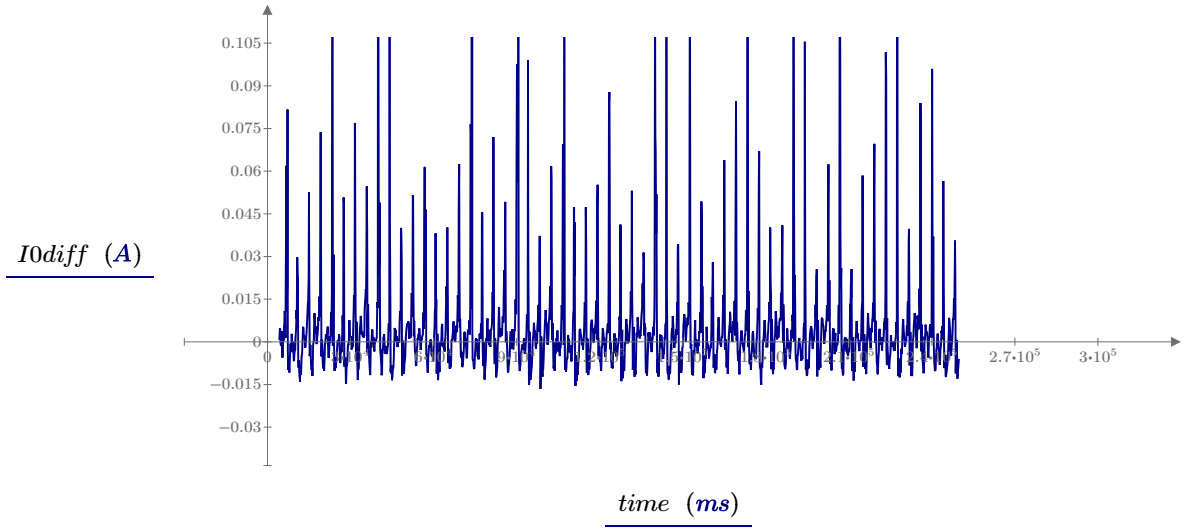

Plot of I0diff pick up current in faulted case

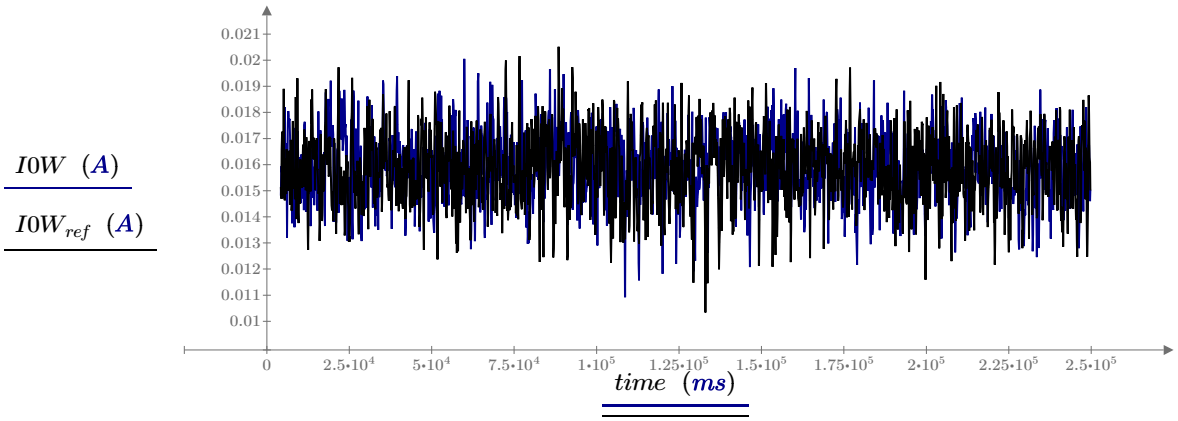

Non-Commercial Use Only

Comparing I0W in faulted case vs I0Wref in steady state

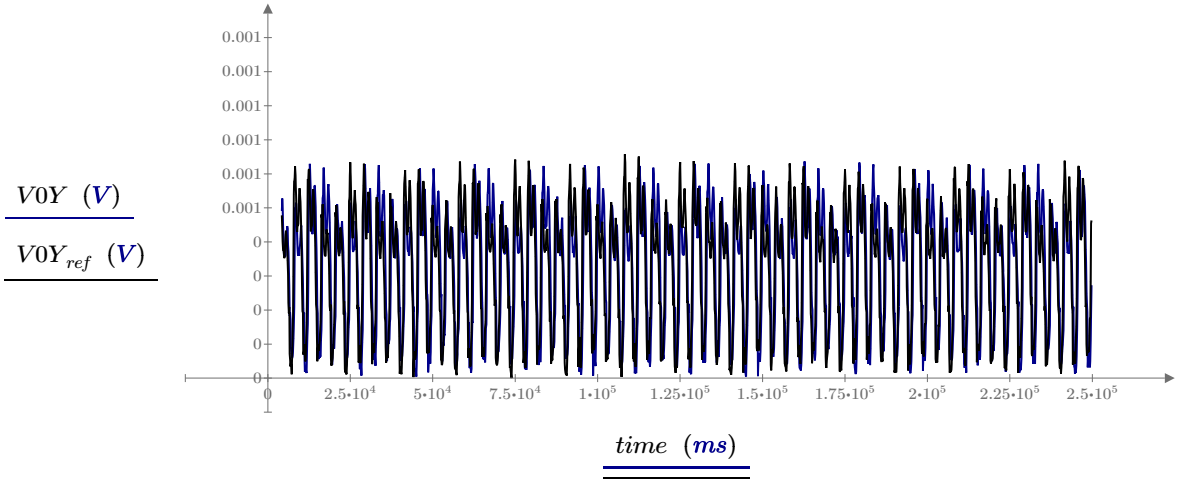

Comparing V0Y in faulted case vs V0Yref in steady state

10mH inductance shorted on test coils in lab setup

$test10252 := \text{READFILE}(\text{".\040617\_tests\_411L\10252\_lasttest.csv"}, \text{"delimited"})$

$time := test10252^{\langle 1 \rangle}\ ms$

$I0W := test10252^{\langle 8 \rangle}\ A$ $I2W := test10252^{\langle 9 \rangle}\ A$ $V0Y := test10252^{\langle 10 \rangle}\ V$

$I0diff := \frac{V0Y}{R_{Lim}} - I0W$

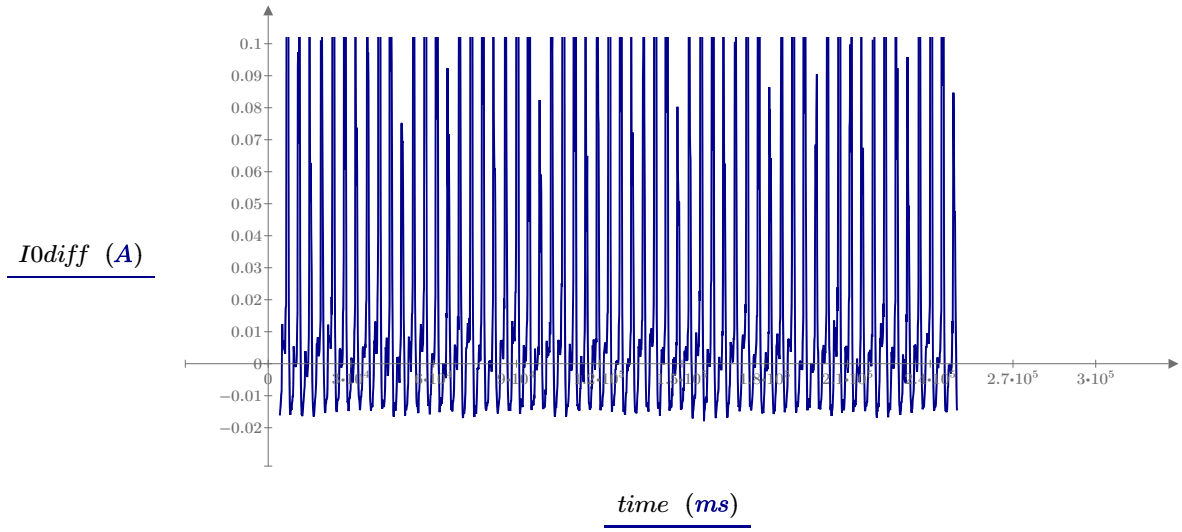

Non-Commercial Use Only

Plot of I0diff pick up current in faulted case

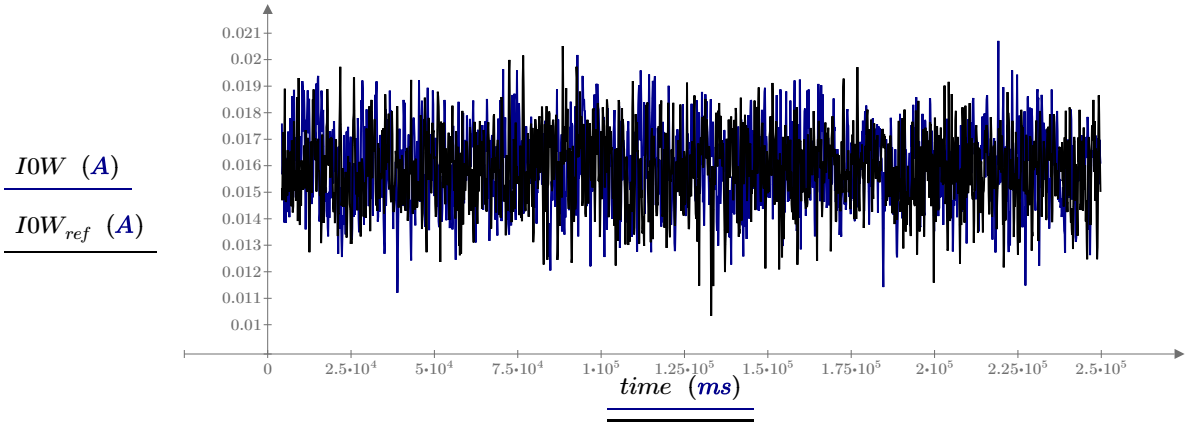

Comparing I0W in faulted case vs I0Wref in steady state

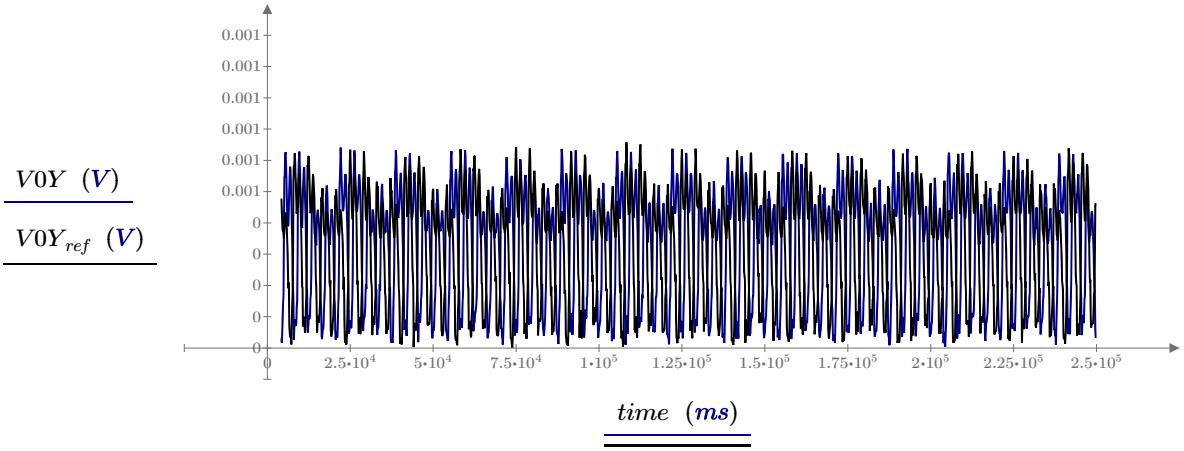

Comparing V0Y in faulted case vs V0Yref in steady state

Non-Commercial Use Only

Tests with SEL-735

Graphing calculations for Inter-turn fault detection on Air Core reactors- Lab model

Calibration of Rlim:

$test00 := \text{READFILE}(\text{".\040917\_735\_w\_neutral\Event0.csv"}, \text{"delimited"})$

$time := test00^{\langle 1 \rangle}\ ms$

$IAW := test00^{\langle 2 \rangle}\ A$ $IBW := test00^{\langle 3 \rangle}\ A$ $ICW := test00^{\langle 4 \rangle}\ A$

$VAY := test00^{\langle 5 \rangle}\ V$ $VBY := test00^{\langle 6 \rangle}\ V$ $VCY := test00^{\langle 7 \rangle}\ V$

$I0W_{ref} := test00^{\langle 8 \rangle}\ A$ $I2W_{ref} := test00^{\langle 9 \rangle}\ A$ $V0Y_{ref} := test00^{\langle 10 \rangle}\ V$

$$R_{Lim} := \frac{V0Y_{ref}}{I0W_{ref}}$$

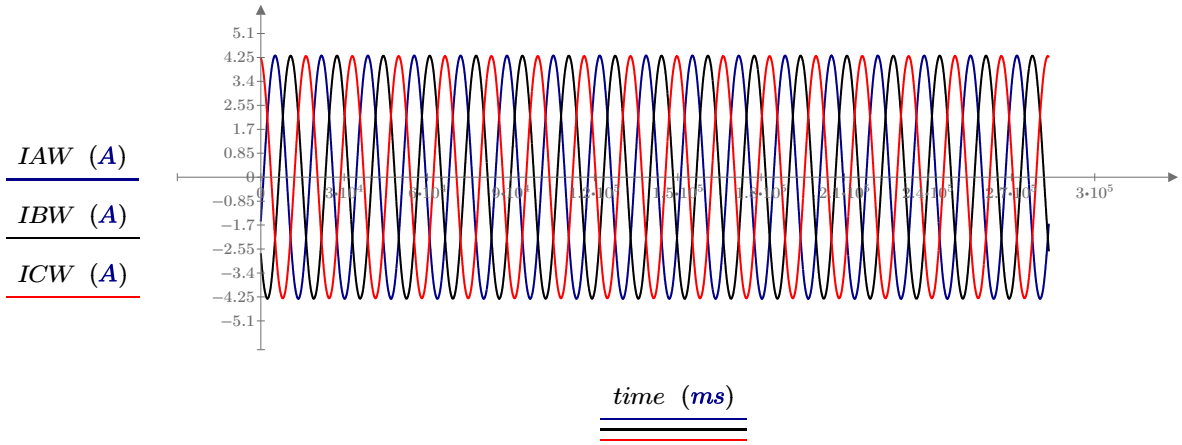

Steady state phase currents recorded by relay

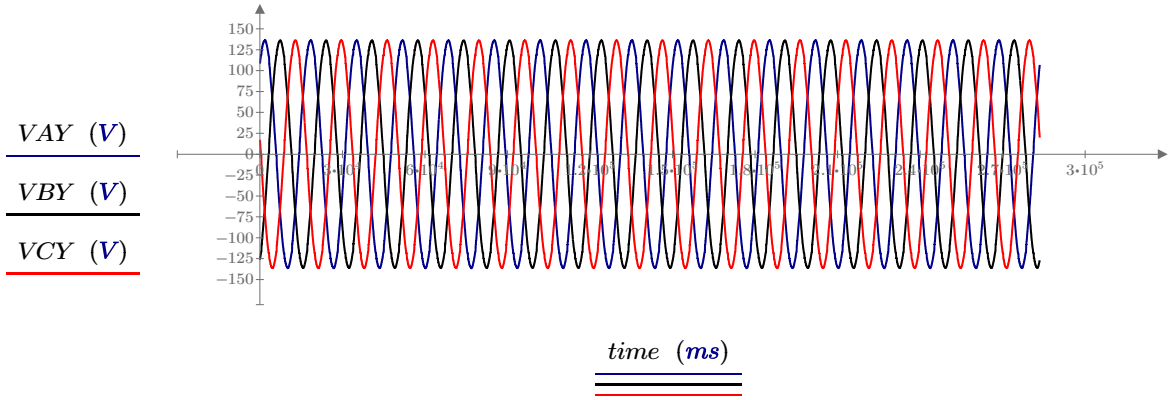

Non-Commercial Use Only

Steady state phase voltages recorded by relay

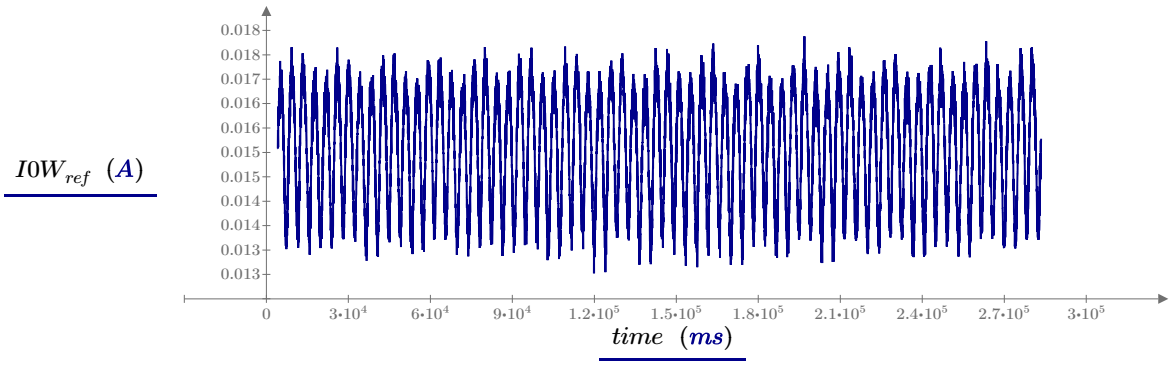

Zero sequence reference current measured by relay

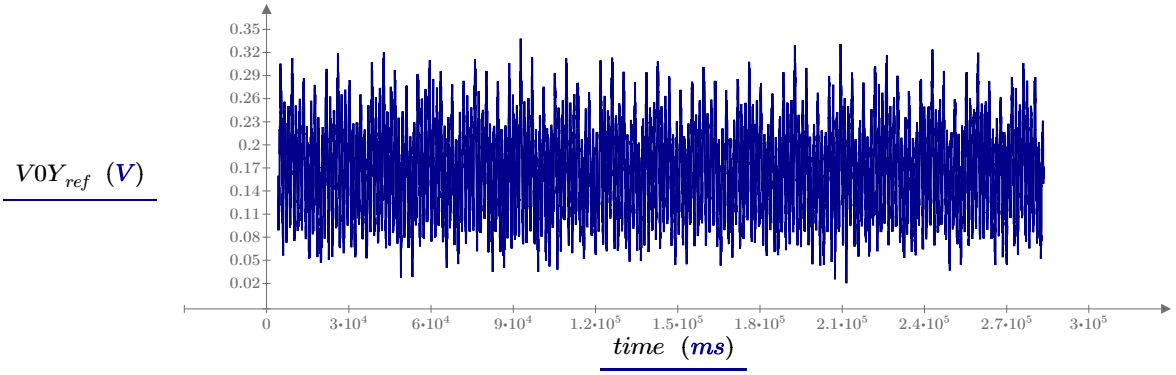

Zero sequence reference voltage measured by relay

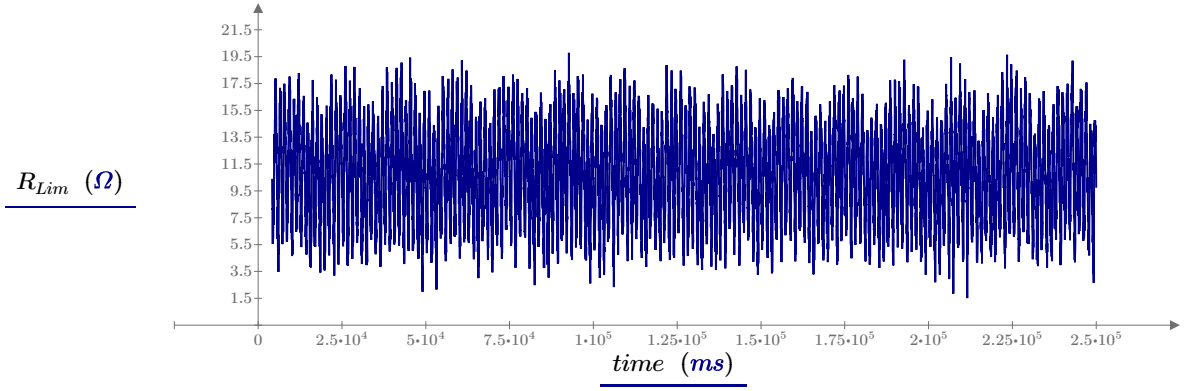

Non-Commercial Use Only

Reference quantity Rlim for utilization in identifying fault conditions

$I0diff_{steady} := \frac{V0Y_{ref}}{R_{Lim}} - I0W_{ref}$ [Pickup current in steady state]

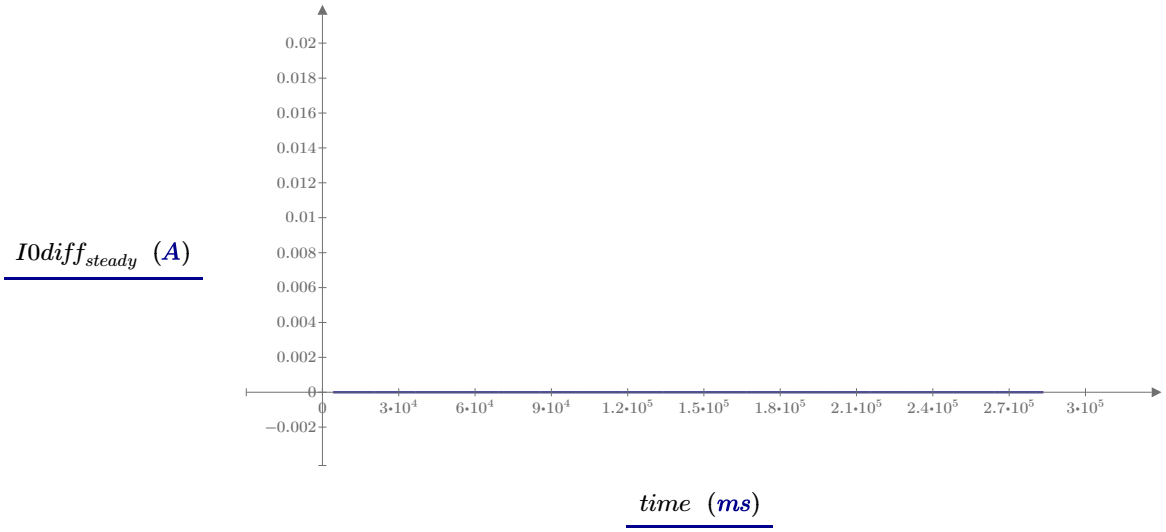

200uH inductance shorted on test coils in lab setup

$test01 := READFILE(".\040917_735_w_neutral\Event01.csv", "delimited")$

$time := test01^{\langle 1 \rangle}\ ms$

$I0W := test01^{\langle 8 \rangle}\ A$ $I2W := test01^{\langle 9 \rangle}\ A$ $V0Y := test01^{\langle 10 \rangle}\ V$

$I0diff := \frac{V0Y}{R_{Lim}} - I0W$ $Z0 := \frac{V0Y}{I0W}$

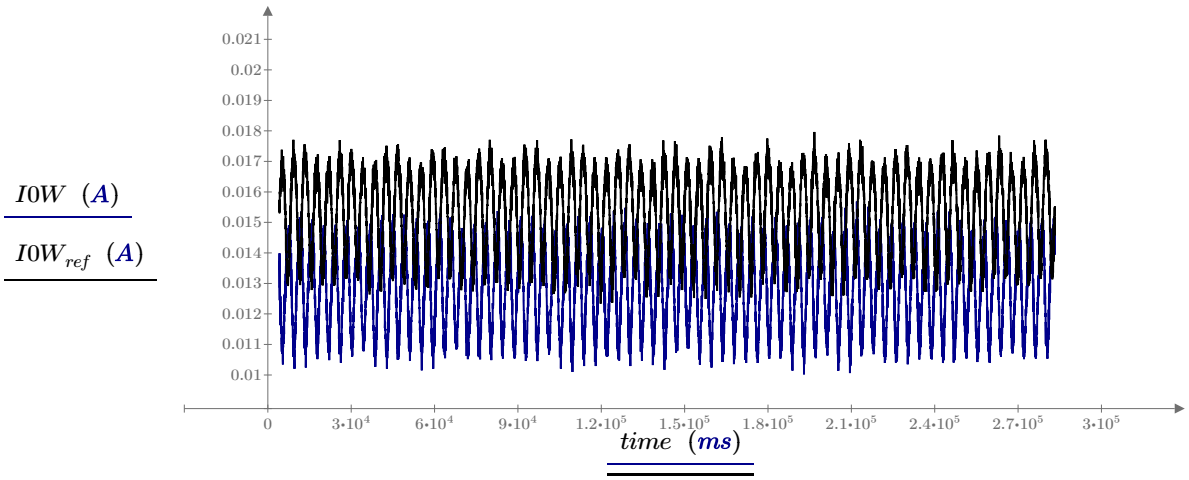

Non-Commercial Use Only

Comparing I0W in faulted case vs I0Wref in steady state

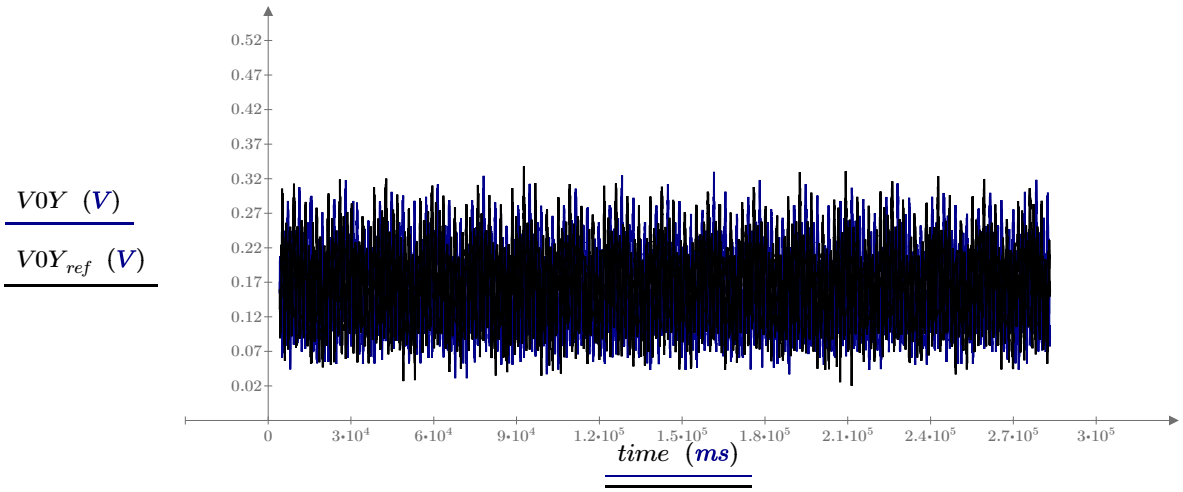

Comparing V0Y in faulted case vs V0Yref in steady state

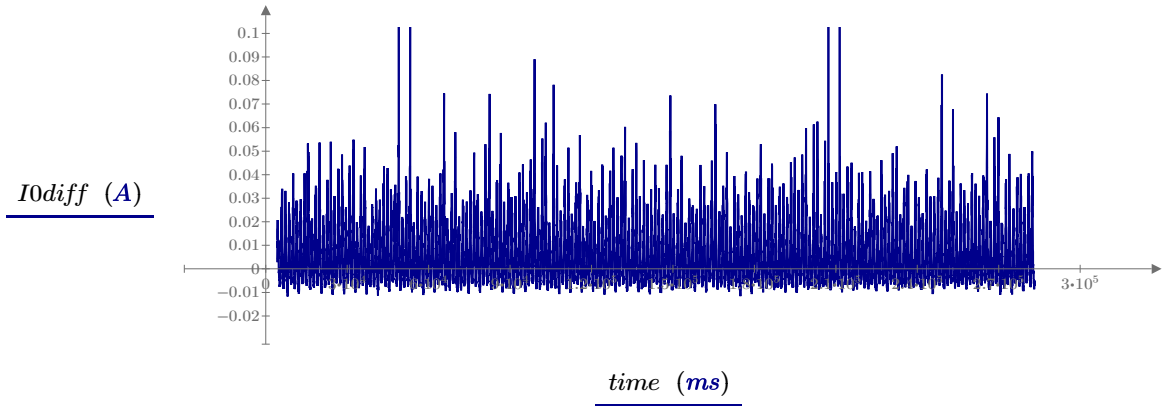

Plot of I0diff pick up current in faulted case

Non-Commercial Use Only

1mH inductance shorted on test coils in lab setup

$test04 := \text{READFILE}(\text{".\040917\_735\_w\_neutral\Event04.csv"}, \text{"delimited"})$

$time := test04^{\langle 1 \rangle}\ ms$ $\quad I0W := test04^{\langle 8 \rangle}\ A$ $\quad V0Y := test04^{\langle 10 \rangle}\ V$

$I0diff := \frac{V0Y}{R_{Lim}} - I0W$ $\quad Z0 := \frac{V0Y}{I0W}$

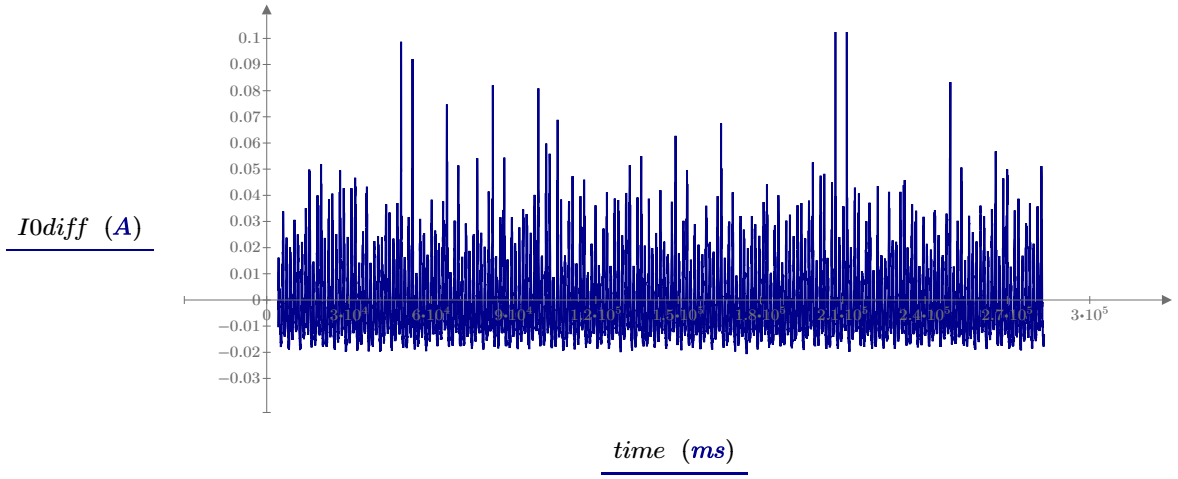

Plot of I0diff pick up current in faulted case

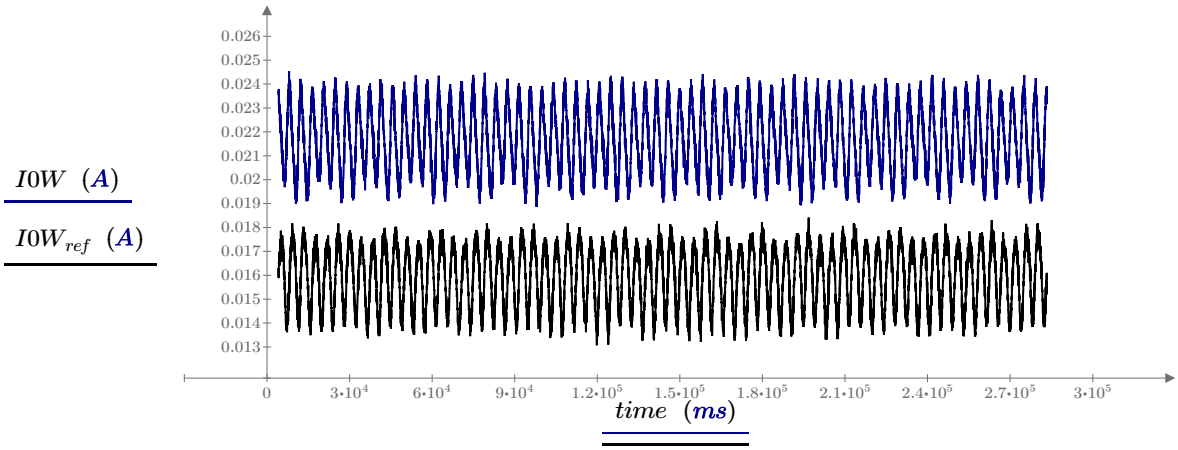

Comparing I0W in faulted case vs I0Wref in steady state

Non-Commercial Use Only

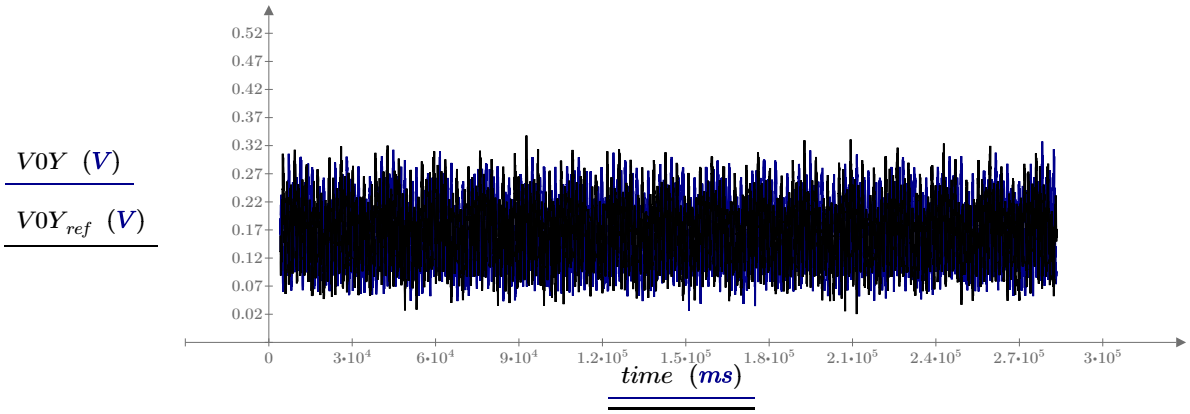

Comparing V0Y in faulted case vs V0Yref in steady state

2mH inductance shorted on test coils in lab setup

$test02 := \text{READFILE}(\text{".\040917\_735\_w\_neutral\Event02.csv"}, \text{"delimited"})$

$time := test02^{\langle 1 \rangle}\ ms$

$I0W := test02^{\langle 8 \rangle}\ A$ $I2W := test02^{\langle 9 \rangle}\ A$ $V0Y := test02^{\langle 10 \rangle}\ V$

$I0diff := \frac{V0Y}{R_{Lim}} - I0W$ $Z0 := \frac{V0Y}{I0W}$

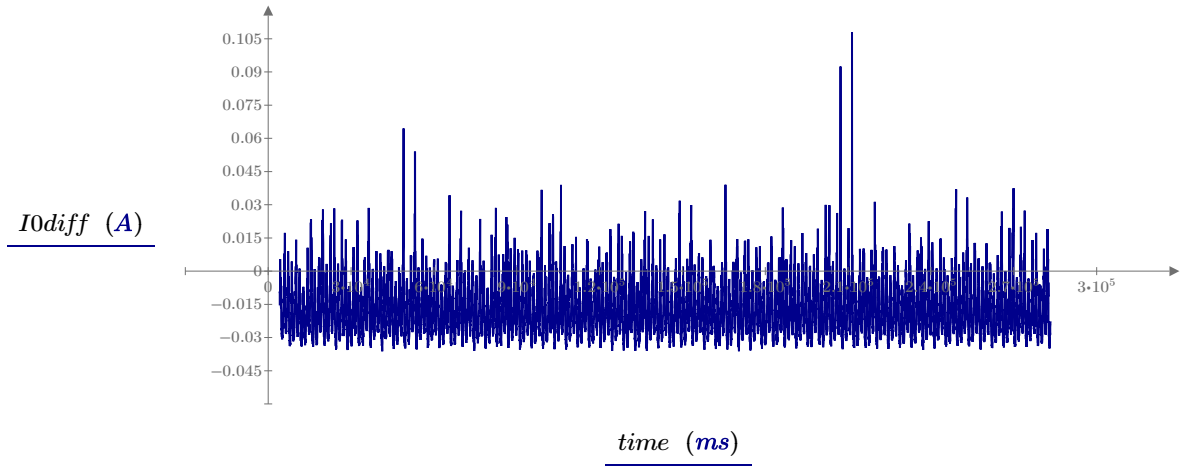

Plot of I0diff pick up current in faulted case

Non-Commercial Use Only

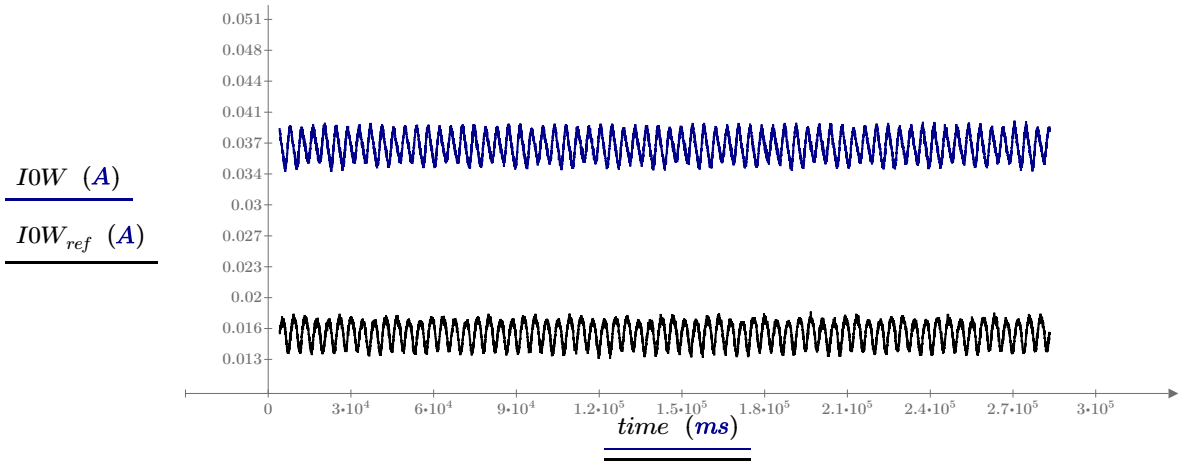

Comparing I0W in faulted case vs I0Wref in steady state

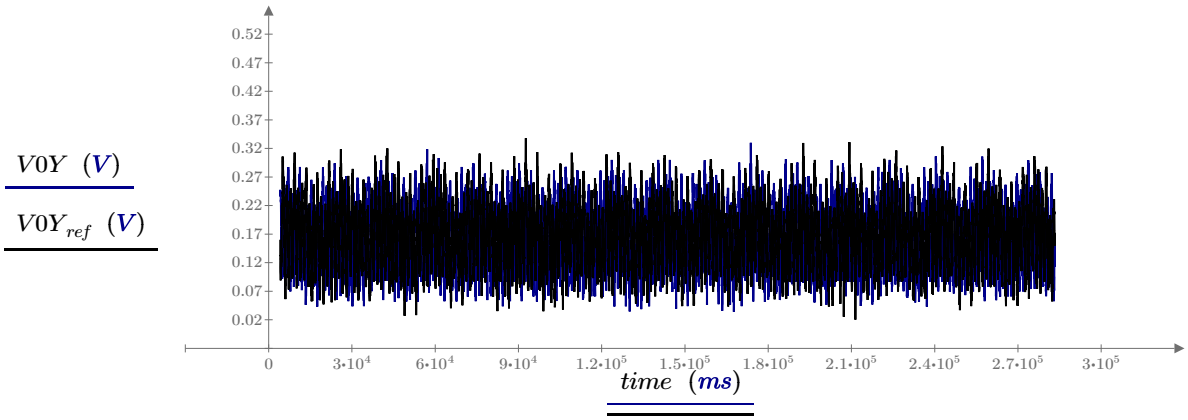

Comparing V0Y in faulted case vs V0Yref in steady state

Non-Commercial Use Only

3mH inductance shorted on test coils in lab setup

$test03 := \text{READFILE}(\text{".\040917\_735\_w\_neutral\Event03.csv"}, \text{"delimited"})$

$time := test03^{\langle 1 \rangle}\ ms$

$I0W := test03^{\langle 8 \rangle}\ A$ $I2W := test03^{\langle 9 \rangle}\ A$ $V0Y := test03^{\langle 10 \rangle}\ V$

$I0diff := \frac{V0Y}{R_{Lim}} - I0W$ $Z0 := \frac{V0Y}{I0W}$

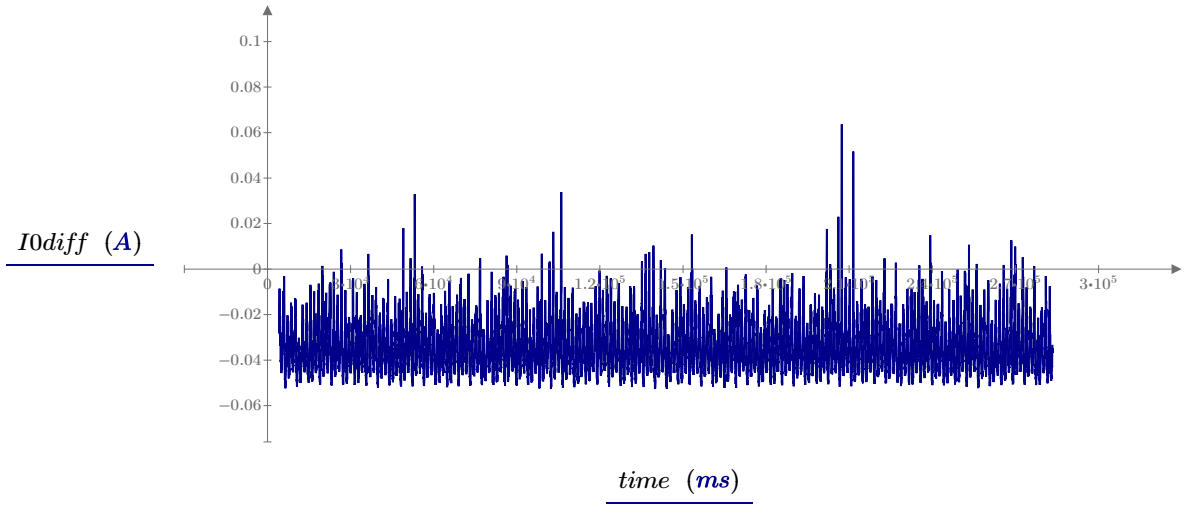

Plot of I0diff pick up current in faulted case

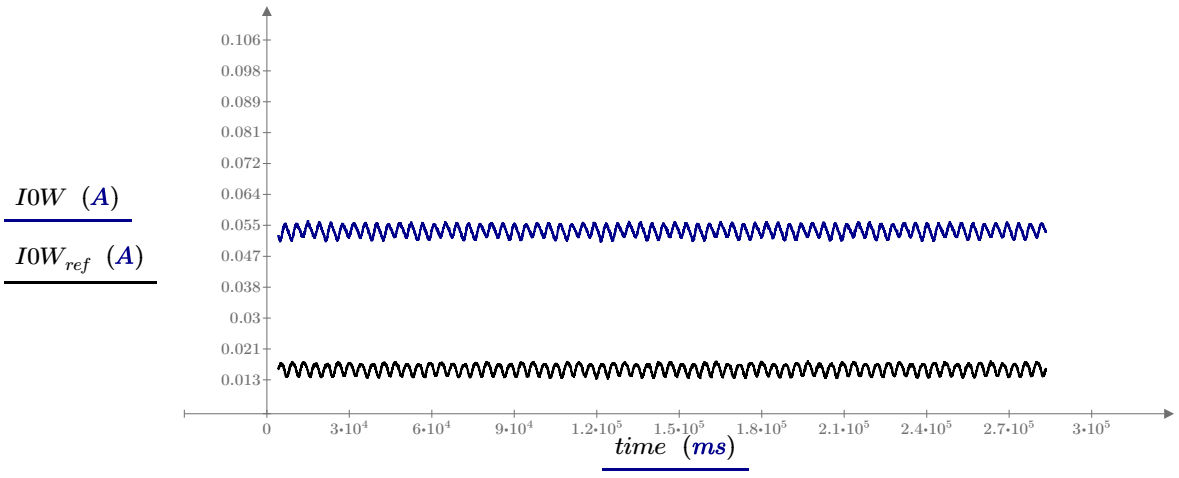

Comparing I0W in faulted case vs I0Wref in steady state

Non-Commercial Use Only

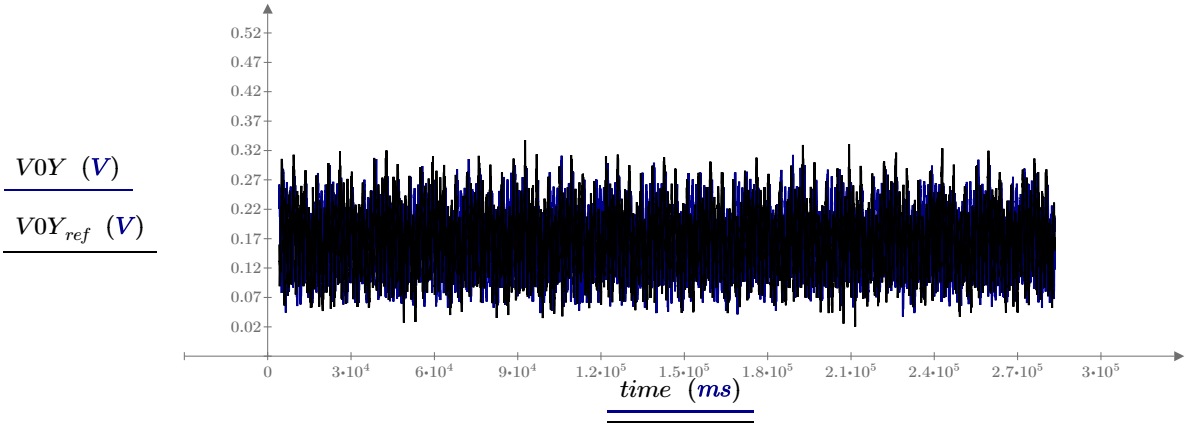

Comparing V0Y in faulted case vs V0Yref in steady state

4mH inductance shorted on test coils in lab setup

$test05 := \text{READFILE}(\text{".\040917\_735\_w\_neutral\Event05.csv"}, \text{"delimited"})$

$time := test05^{\langle 1 \rangle}\ ms$

$I0W := test05^{\langle 8 \rangle}\ A$ $I2W := test05^{\langle 9 \rangle}\ A$ $V0Y := test05^{\langle 10 \rangle}\ V$

$$I0diff := \frac{V0Y}{R_{Lim}} - I0W \qquad Z0 := \frac{V0Y}{I0W}$$

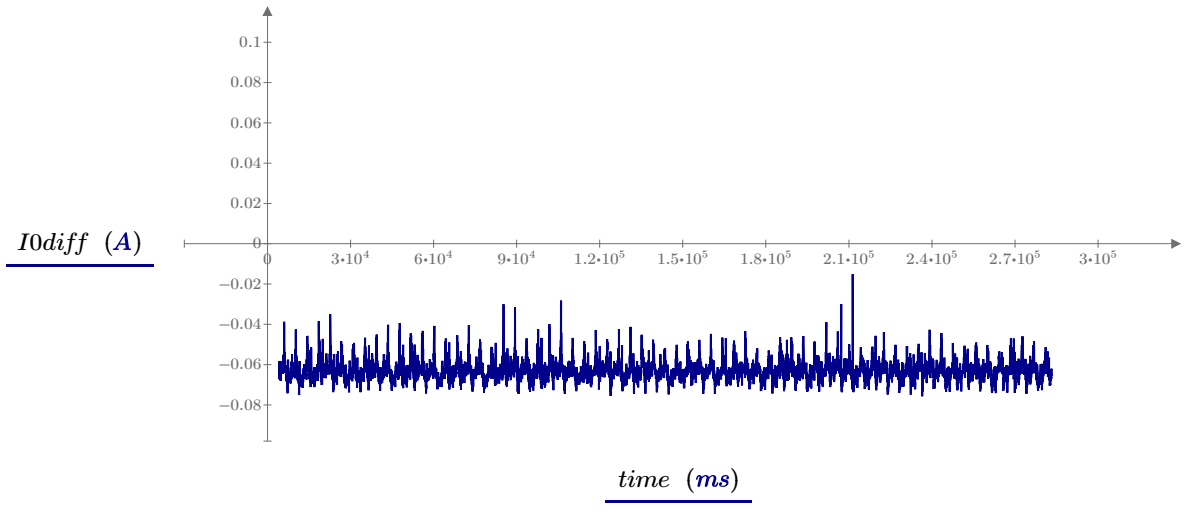

Plot of I0diff pick up current in faulted case

Non-Commercial Use Only

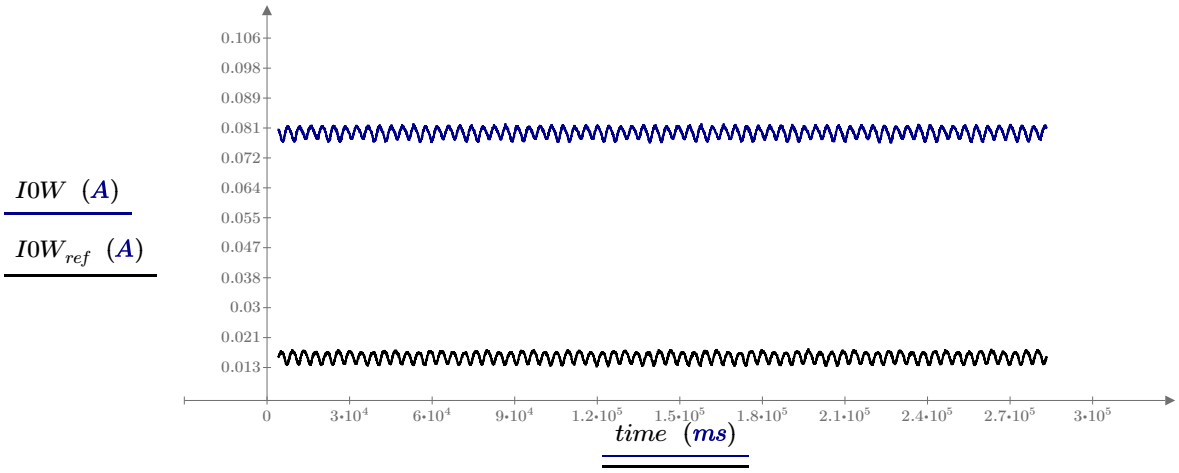

Comparing I0W in faulted case vs I0Wref in steady state

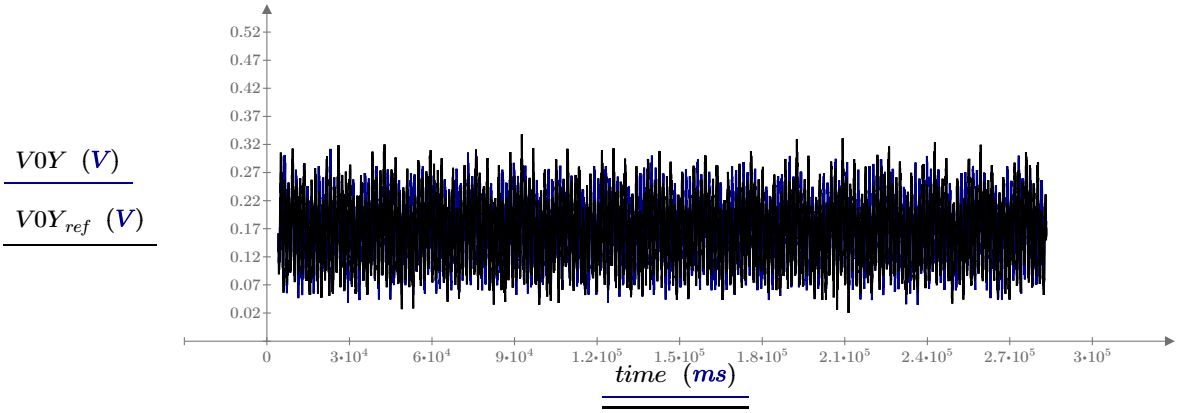

Comparing V0Y in faulted case vs V0Yref in steady state

Non-Commercial Use Only

7.3mH inductance shorted on test coils in lab setup

$test06 := \text{READFILE}(\text{".\040917\_735\_w\_neutral\Event06.csv"}, \text{"delimited"})$

$time := test06^{\langle 1 \rangle}\ ms$ $I0W := test06^{\langle 8 \rangle}\ A$ $I2W := test06^{\langle 9 \rangle}\ A$ $V0Y := test06^{\langle 10 \rangle}\ V$

$I0diff := \frac{V0Y}{R_{Lim}} - I0W$ $Z0 := \frac{V0Y}{I0W}$

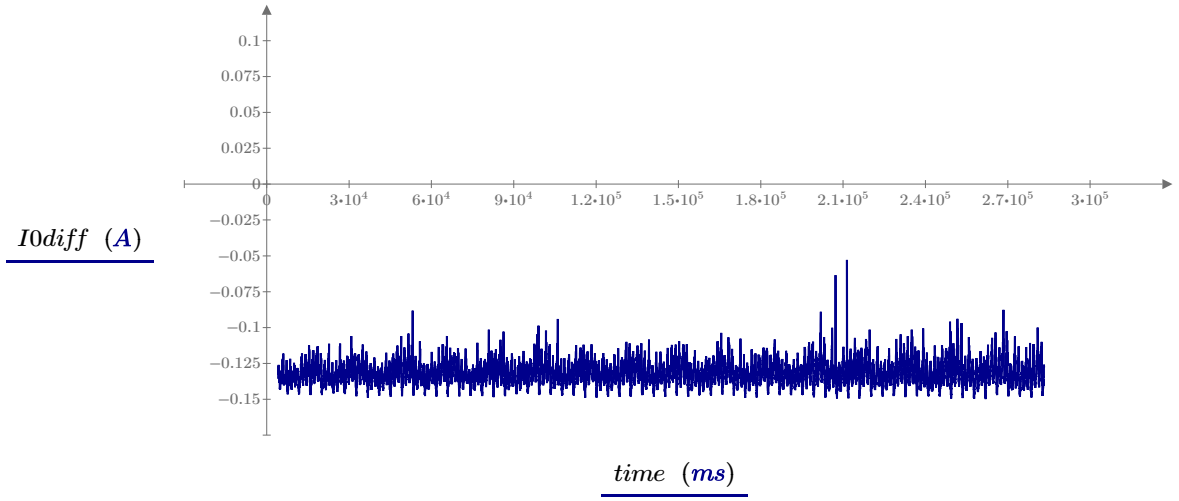

Plot of I0diff pick up current in faulted case

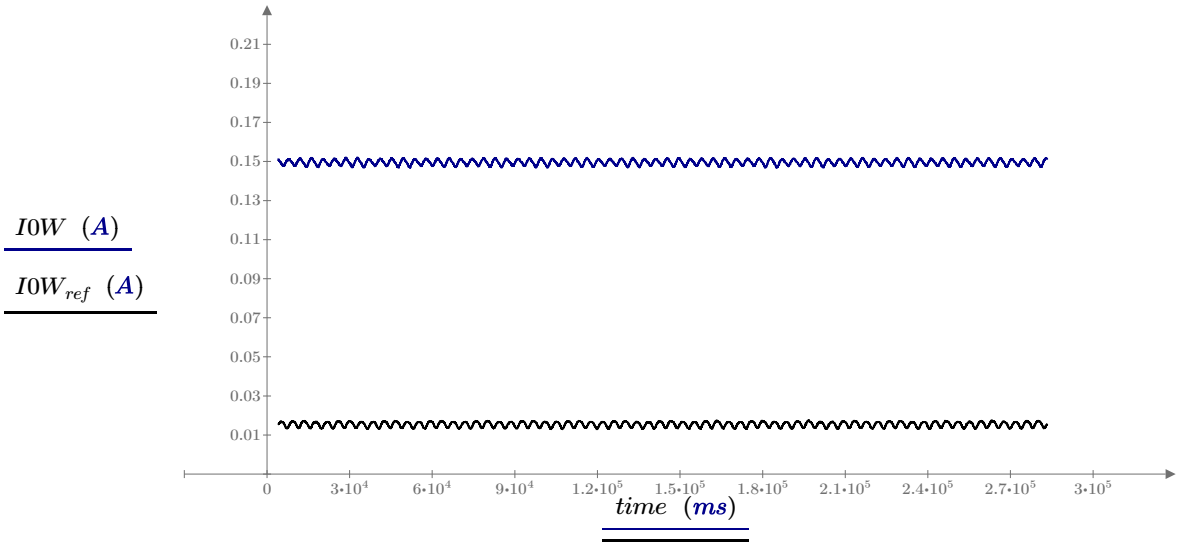

Comparing I0W in faulted case vs I0Wref in steady state

Non-Commercial Use Only

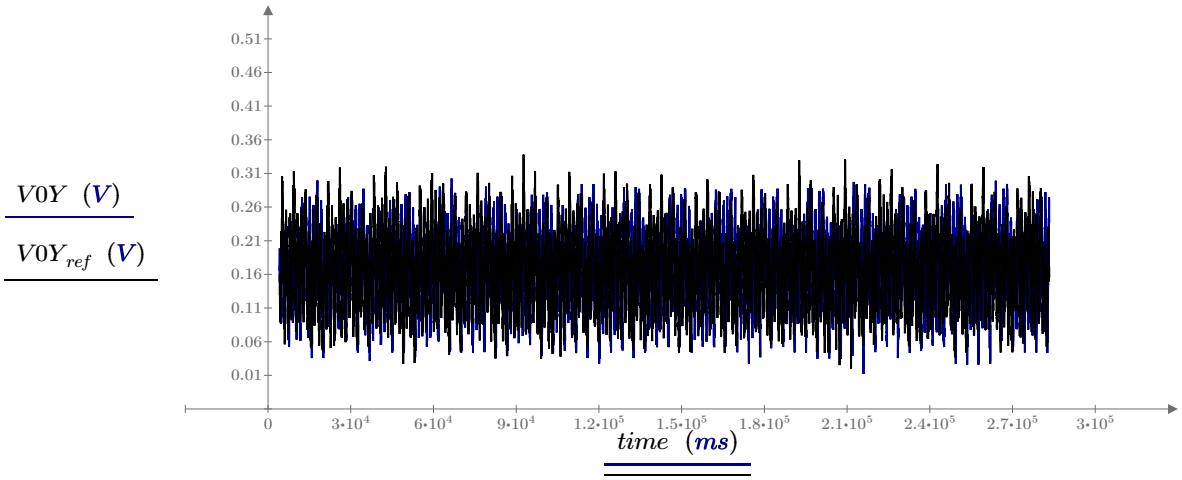

Comparing V0Y in faulted case vs V0Yref in steady state

With 10mH Shorted

$test07 := \text{READFILE}(\text{".\040917\_735\_w\_neutral\Event07.csv"}, \text{"delimited"})$

$time := test07^{\langle 1 \rangle}\ ms$ $I0W := test07^{\langle 8 \rangle}\ A$ $I2W := test07^{\langle 9 \rangle}\ A$ $V0Y := test07^{\langle 10 \rangle}\ V$

$I0diff := \frac{V0Y}{R_{Lim}} - I0W$ $Z0 := \frac{V0Y}{I0W}$

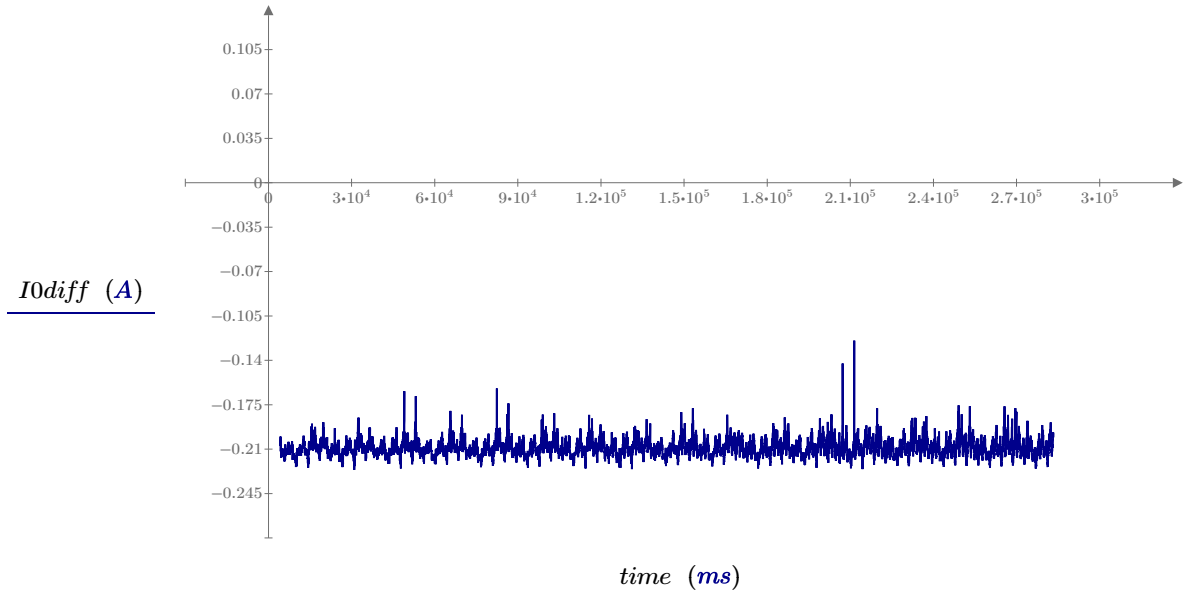

Plot of I0diff pick up current in faulted case

Non-Commercial Use Only

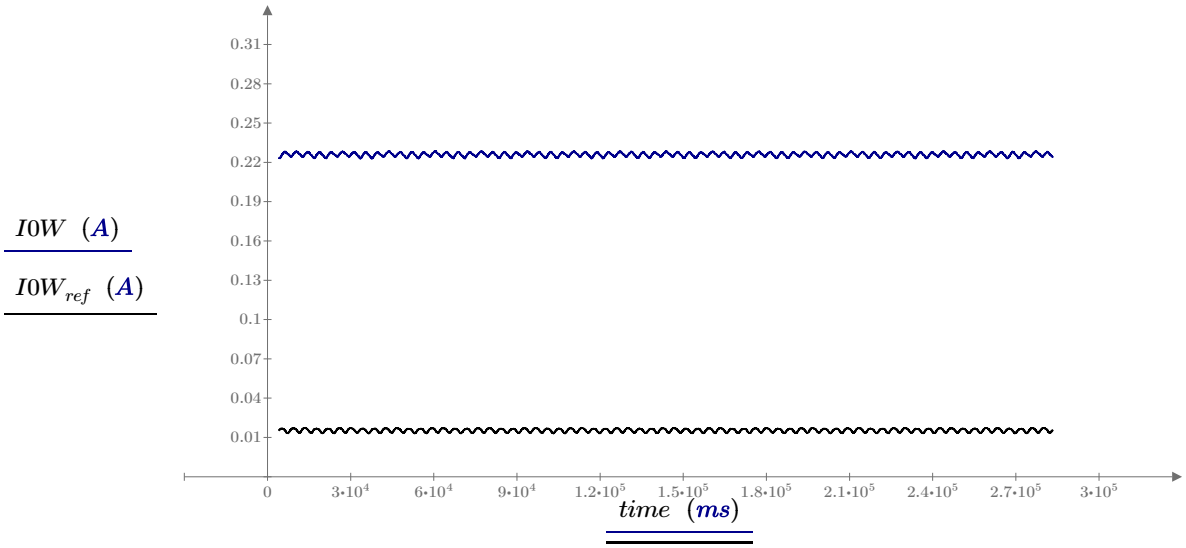

Comparing I0W in faulted case vs I0Wref in steady state

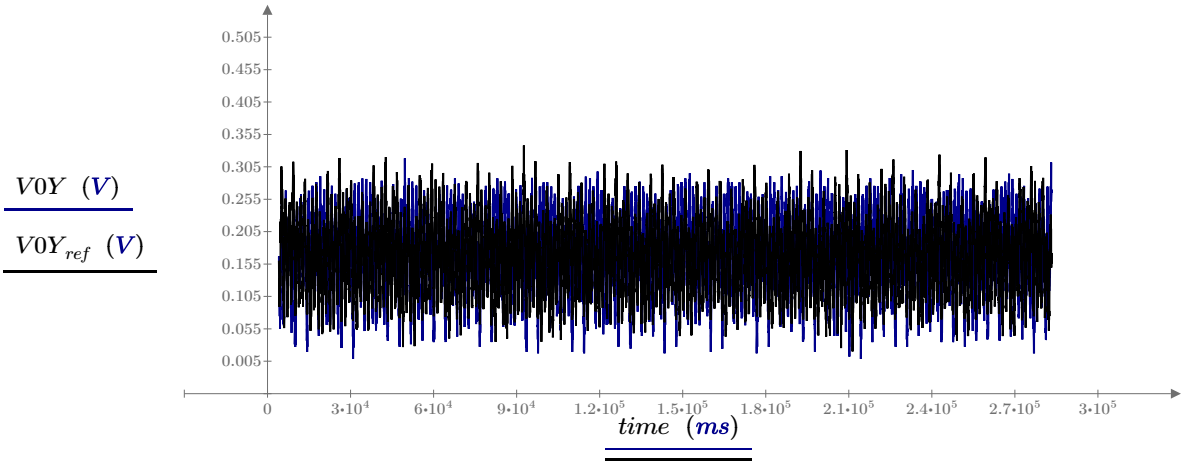

Comparing V0Y in faulted case vs V0Yref in steady state

Non-Commercial Use Only